

CREMINO Containment Data Report

T. Stubbs
R. Heinle

August 1998



Lawrence
Livermore
National
Laboratory

This is an informal report intended primarily for internal or limited external distribution. The opinions and conclusions stated are those of the author and may or may not be those of the Laboratory.

Work performed under the auspices of the U.S. Department of Energy by the Lawrence Livermore National Laboratory under Contract W-7405-ENG-48.

DISCLAIMER

This document was prepared as an account of work sponsored by an agency of the United States Government. Neither the United States Government nor the University of California nor any of their employees, makes any warranty, express or implied, or assumes any legal liability or responsibility for the accuracy, completeness, or usefulness of any information, apparatus, product, or process disclosed, or represents that its use would not infringe privately owned rights. Reference herein to any specific commercial products, process, or service by trade name, trademark, manufacturer, or otherwise, does not necessarily constitute or imply its endorsement, recommendation, or favoring by the United States Government or the University of California. The views and opinions of authors expressed herein do not necessarily state or reflect those of the United States Government or the University of California, and shall not be used for advertising or product endorsement purposes.

This report has been reproduced
directly from the best available copy.

Available to DOE and DOE contractors from the
Office of Scientific and Technical Information
P.O. Box 62, Oak Ridge, TN 37831
Prices available from (615) 576-8401, FTS 626-8401

Available to the public from the
National Technical Information Service
U.S. Department of Commerce
5285 Port Royal Road
Springfield, VA 22161

CREMINO Instrumentation Summary

| Instrumentation | Fielded on this Event | Data Return | Present in this Report |
|--|-----------------------|-------------|------------------------|
| <u>Plug Emplacement</u> ^(a) | yes | no | - |
| <u>Radiation</u> | yes | yes | yes |
| <u>Pressure</u> | | | |
| Stemming | yes | yes | yes |
| Challenge | no | - | - |
| Cavity | no | - | - |
| Atmospheric | no | - | - |
| <u>Motion</u> | | | |
| Free Field | yes | yes | yes |
| Surface | yes | yes | yes |
| Plug | yes | yes | yes |
| Stemming | no | - | - |
| Surface Casing | yes | yes | yes |
| Emplacement Pipe | yes | yes | yes |
| <u>Hydroyield</u> ^(b) | yes | yes | no |
| <u>Collapse</u> ^(c) | yes | yes | yes |
| <u>Stress</u> | yes | yes | no |
| <u>Strain</u> ^(d) | yes | no | no |
| <u>Other Measurements</u> ^(e) | yes | yes | yes |

- (a) Description only.
- (b) SLIFER in emplacement hole.
- (c) CLIPER in emplacement and satellite holes.
- (d) Emplacement pipe load.
- (e) In and on emplacement pipe (PINEX experiment).

Event Personnel

Containment Physics

B. Hudson LLNL
 J. Kalinowski EG&G/AVO
 T. Stubbs EG&G/AVO

Instrumentation

L. Starrh LLNL
 A. Bruns EG&G/AVO
 W. Webb EG&G/NVO.
 R. Sievert EG&G/NVO

Contents

| | | |
|-----|--|-----|
| 1. | Event Description | |
| 1.1 | Site | 1 |
| 1.2 | Emplacement | 1 |
| 1.2 | Instrumentation | 2 |
| 2. | Stemming Behavior | |
| 2.1 | Pressure and Radiation | 9 |
| 2.2 | Motion | 10 |
| 3. | Emplacement Pipe Measurements | |
| 3.1 | Pressure, Temperature and Radiation | 37 |
| 3.2 | Motion | 38 |
| 4. | Measurements During Collapse | |
| 4.1 | Motion | 53 |
| 4.2 | Pressure and Radiation | 54 |
| 5. | Measurements in the Satellite Hole | 74 |
| | References | 99 |
| | Appendix A. High Resolution Pressure and Temperature in Emplacement Pipe | 100 |

1. Event Description

1.1 Site

The CREMINO event was detonated in hole U8e of the Nevada Test Site as indicated in figure 1.1. The device had a depth-of-burial (DOB) of 210 m in the Alluvium of area 8, about 365 m above the standing water level and about 500 m above the Paleozoic formation, as shown in figure 1.2⁽¹⁾. The companion experiment, "CAERPHILLY", was simultaneously executed at a depth of 408 m in the same hole. Stemming of the 2.18 m diameter emplacement hole followed the plan shown in figure 1.4. A log of the stemming operations was maintained by Holmes & Narver⁽²⁾.

Detonation time was 09:30:00 PDT on September 27, 1978, and about 30 minutes later a sub-surface collapse terminated at a depth of about 80 m.

No radiation arrivals were detected above ground and the containment of these events was considered successful.

1.2 Emplacement

One strain station (86) was fielded on the emplacement pipe near its top and another station (81) on the emplacement pipe just below the device canister of CREMINO to monitor the load during installation and stemming. During these procedures, outputs of these stations were recorded by hand in the stemming log maintained by Holmes & Narver⁽²⁾.

The three stemming plugs were composed of coal-tar epoxy (LAE 59, denoted CTE). The deepest plug was about 10 m thick encompassing the position of the pressure plate of a PINEX experiment in the emplacement pipe. The emplacement pipe was constrained to move with the geologic formation at this point by the inclusion of drag rings on the pipe making this a formation-coupling plug. A 5.5 m thick CTE plug (the stemming platform) was fielded midway between the bottom and top plugs. The top plug (within the surface casing) consisted of a 5.5 m thick layer of CTE, topped by a 1.7 m thick layer of foam cubes and sand and a 2.7 m thick layer of soft coal tar and aggregate (LAE 59Y). Above the diagnostics canister of CREMINO, stemming between the plugs consisted of layers of LLL mix. The top of the hole (above the top soft plug) was filled with LLL mix and fly-ash backfill to within about 3 m of the surface. See figure 1.3.

Two rigid plugs of thickness 15.2 and 19.8 m were emplaced in the satellite hole with the remainder of the hole being filled with rock-matching grout except for the top 1.5 m which was left open. See figure 1.5.

This experiment included a mechanical PINEX experiment as part of the device diagnostics and, for this, the emplacement pipe was left open and evacuated above the detector plate (at a depth of 118.3 m) which was extracted to a receptacle above the ball valve closure on the top of the pipe. This receptacle was detached from the pipe shortly after the detonation and pulled to a location beyond the expected extent of the resulting crater. Between the detector plate and the diagnostics canister, the pipe was sealed with a series of two pressure plates and two pressure domes.

1.3 Instrumentation

Figure 1.4 is a schematic layout of the instrumentation designed to monitor the emplacement procedures and performance of the CREMINO event. Figure 1.5 is a schematic layout of the instrumentation designed to monitor the free-field motion and stress associated with the CREMINO event in the satellite hole Ue8e. Sandia collected the data from the soil stress gauges shown in figure 1.5.

Nine pressure and radiation stations were fielded in the stemming of the emplacement hole as well as six stations monitoring the pressure, temperature, and radiation within the emplacement pipe which was used as a conduit for a mechanical PINEX experiment. Vertical motion of each of the three rigid plugs, the ground surface, and the recording trailer was measured along with the vertical motion of the emplacement pipe at five locations corresponding to significant structures within the pipe.

Vertical motion was monitored at nine stations in the satellite hole, 60.9 m from the emplacement hole. The deepest two motion stations included triaxial measurements while each of the five deepest included supplemental "low-range" transducers. Being in the satellite hole and grouted in place with "rock-matching" grout, the data from these stations are considered free-field measurements

D-cable information was used for quality assurance during the stemming operations and was recorded post-shot to monitor cavity collapse as were the outputs of CLIPER gauges in the stemming of the hole and on the emplacement pipe. Two CLIPER gauges were also mounted in the satellite hole.

Data from the pressure, radiation, temperature, motion transducers, and D-cables were transmitted to the recording trailer by an analog system and recorded on magnetic tape.

Results of the yield measurements are reported elsewhere⁽³⁾.

A history of the fielding operations of the instrumentation is outlined in reference 4. Details of the instrumentation are given in reference 5.

CREMINO

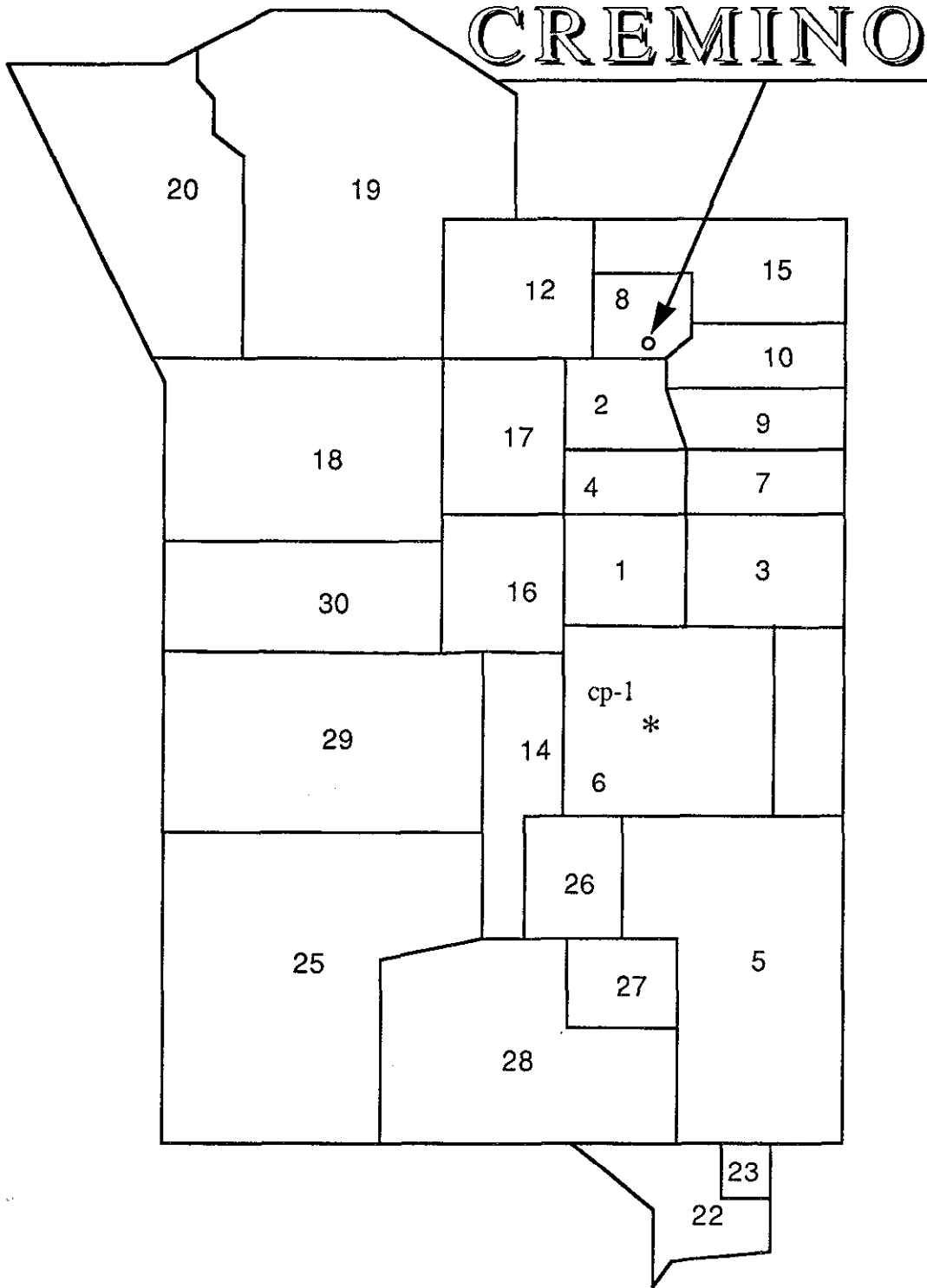


Figure 1.1 Map of the Nevada Test Site indicating the location of hole U8e.

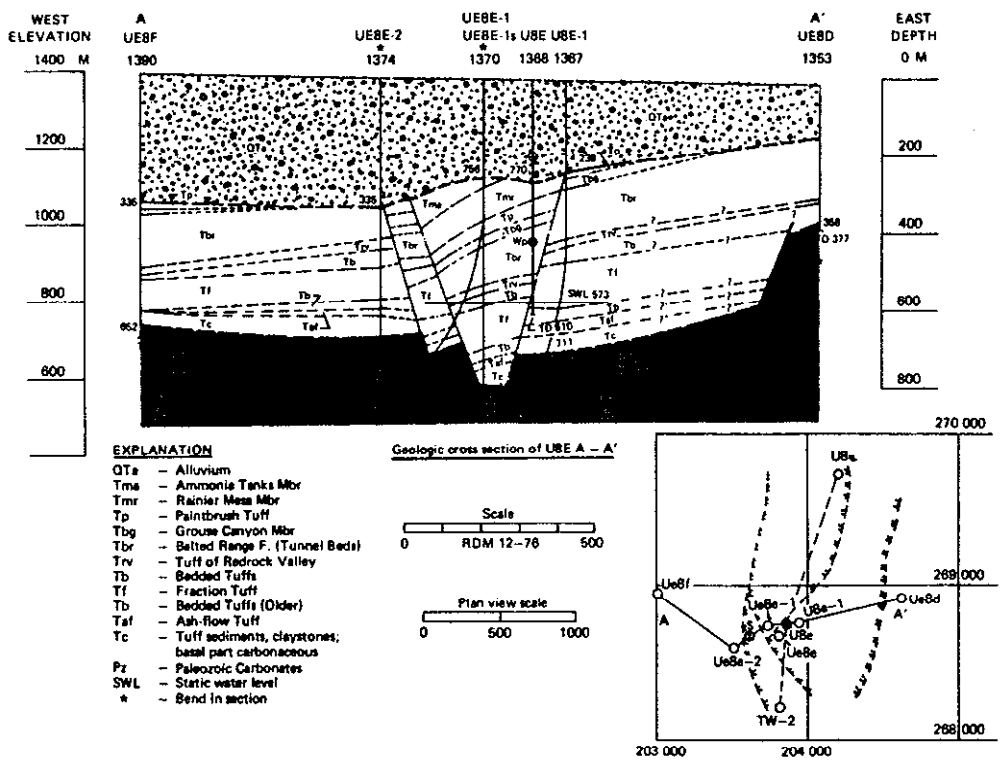


Figure 1.2 East-West geologic cross sections through hole U8e.

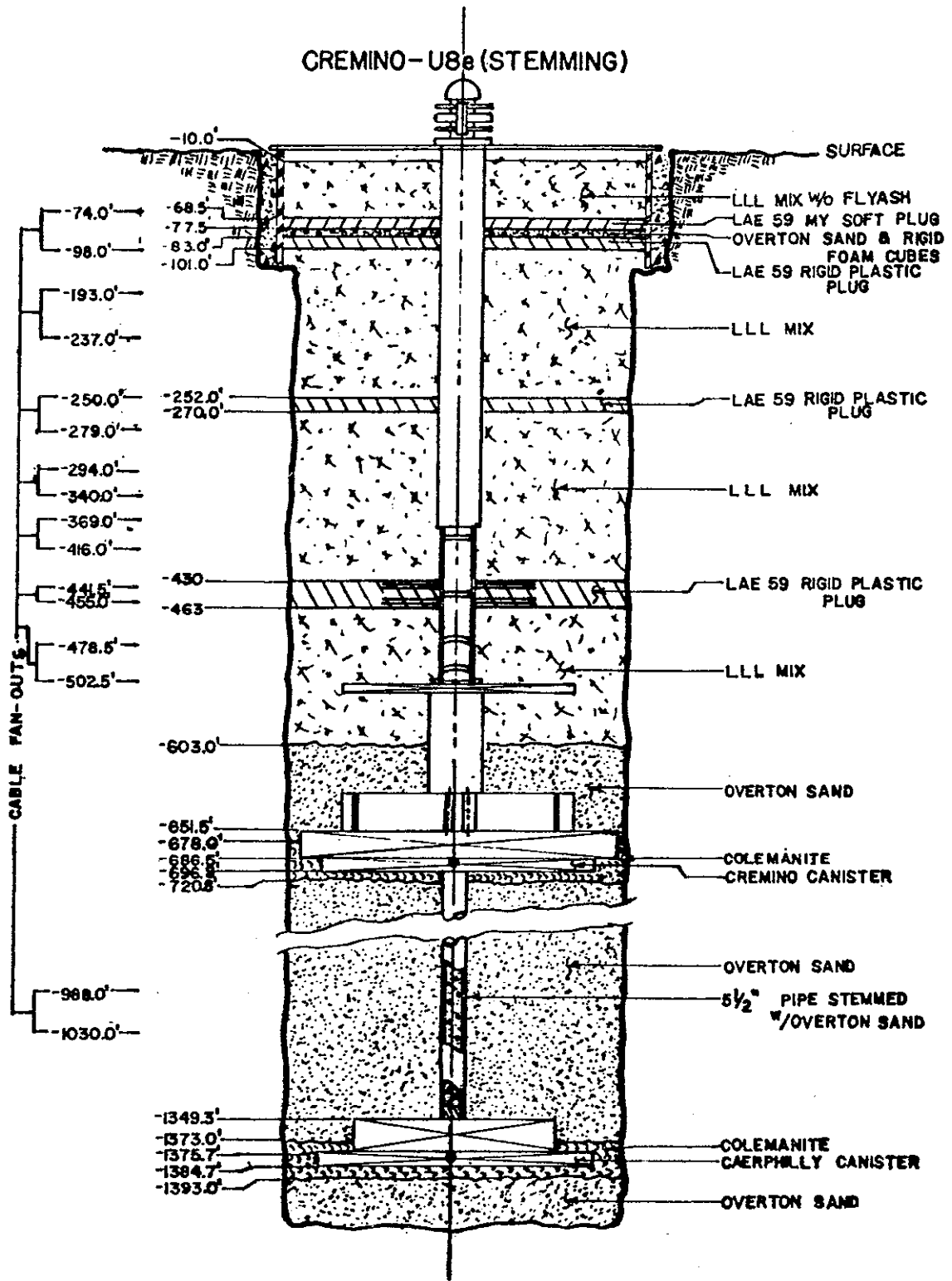


Figure 1.3 As-built stemming plan for the event CREMINO in Hole U8e.

2. Stemming Behavior

2.1 Pressure and Radiation

Stemming pressure and radiation were monitored at the nine locations indicated in figure 1.4 and the wave forms received from each station during the first 2000 s are shown in figures 2.1 - 2.9. All stations with the exception of the deepest, station 32, and station 40, just below the top plug, were lost due to cable breakage at collapse at about 1800 s.

Station 32 (figure 2.1) was apparently lost at early time; the radiation wave form after zero time is unreasonably stable over nearly the entire period displayed and is thus discounted. Late radiation arrivals are seen in all three of the stations below the formation coupling plug (figures 2.2 - 2.4) and are given in the following table:

| Station | Radiation Arrival Time |
|---------|------------------------|
| 33 | 130, 370 |
| 34 | 75, 185, 400, 630 |
| 35 | 100, 570 |

The arrival at station 34 before that of the deeper station 33 suggests that the integrity of the emplacement pipe was compromised in the region between stations 33 and 35. This is also suggested by the multiple arrivals at station 34 in the absence of driving pressure arrivals. Above the formation coupling plug there are no significant radiation arrivals before collapse (figures 2.5 - 2.9). Pressures at all stations but 33 and 34 (figures 2.2 and 2.3) can be explained as the result of ground or stemming motion. That of station 33, with a pressure arrival at about 200 s may be caused by the cavity gasses in addition to the motion-induced compression. The pressure wave form of station 34 is suggestive of compression, but it will require a computational effort to verify this.

The first 60 s of the radiation and pressure data are shown in figures 2.10 - 2.18 for greater time definition. Again, station 32 is shown to be lost at early time (figure 2.10). Radiation transducers at the three stations at or above the intermediate plug (figures 2.16 - 2.18) suffered from signal saturation and temporary loss from EMP as did that of station 35 (figure 2.13). All other sensors registered prompt radiation "shine" from the emplacement pipe. No other radiation sources are seen above the formation coupling plug before collapse. This plug serves as an effective barrier to migration of radioactive gasses up the stemming column, at least until collapse engulfs the plug.

2.2 Motion

Vertical motion in the stemming column was monitored in each of the three rigid plugs and wave forms of the data received are shown in figures 2.19 - 2.21. Similar records from a station in the ground surface 15.2 m from SGZ are shown in figure 2.22 and the vertical motion of the recording trailer is given in figure 2.23. Each of the figures displays the data for a total of 3.0 s. Remarkably close agreement between the integrated accelerometer and velocimeter records is shown in figures 2.19 - 2.21. Characteristics of the transducers and the motion wave forms are given in Tables 2.1 -2.3.

Drag rings in the formation coupling plug influenced the early acceleration and interfered with the ground motion experienced at station 21 (figure 2.19). The emplacement pipe was "greased" with hydroseal at the locations of the two rigid plugs above the formation coupling plug and the motion data at these locations (stations 22 and 23) were relatively uninfluenced by the early motion of the emplacement pipe (figures 2.20 and 2.21).

The motion data are otherwise unremarkable.

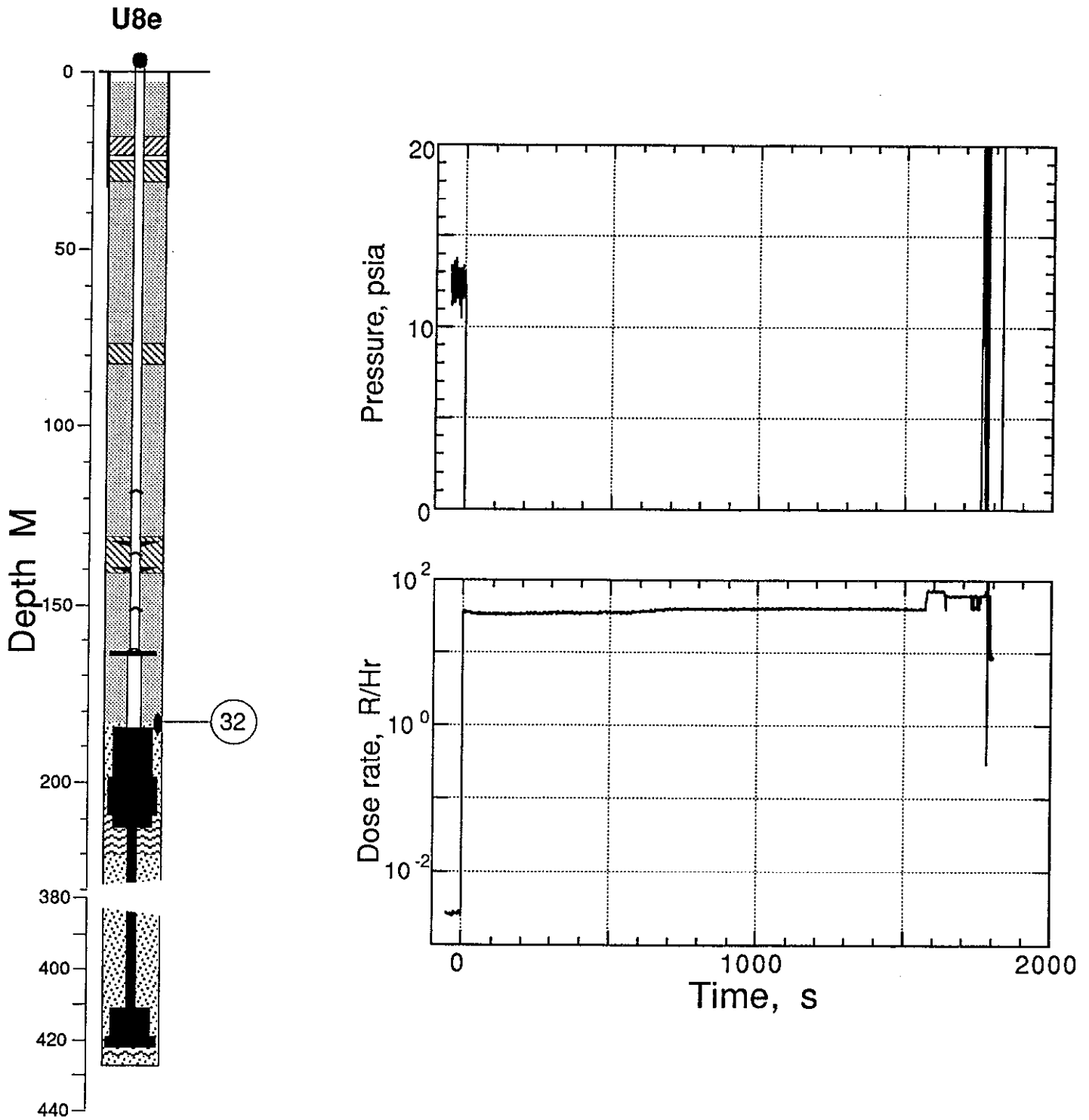


Figure 2.1 Pressure and radiation measured at station 32 (depth 184.7 m). This station was apparently lost close to time zero.

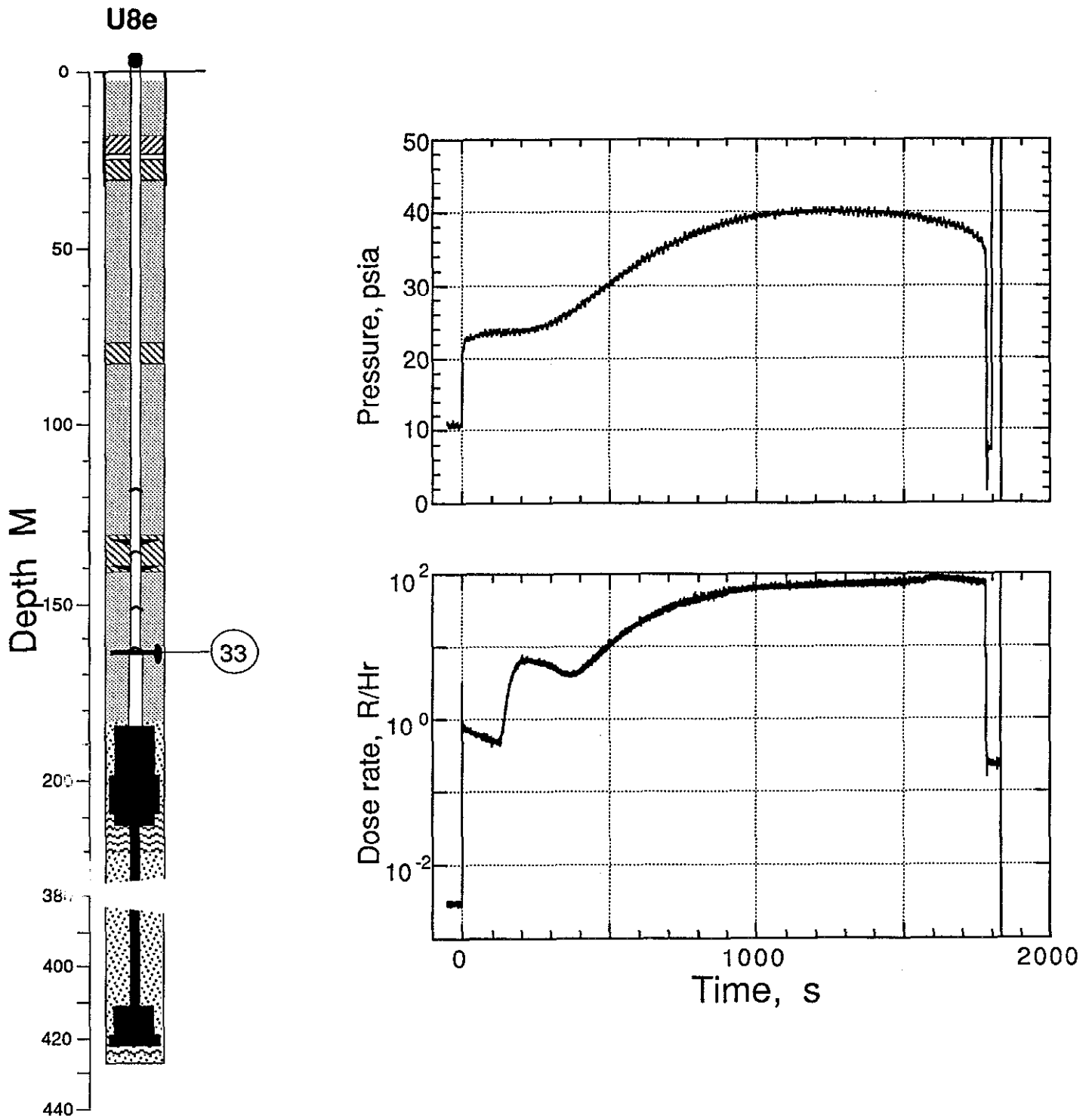


Figure 2.2 Pressure and radiation measured at station 33 (depth 163.6 m), near the first pressure dome, above the tau can.

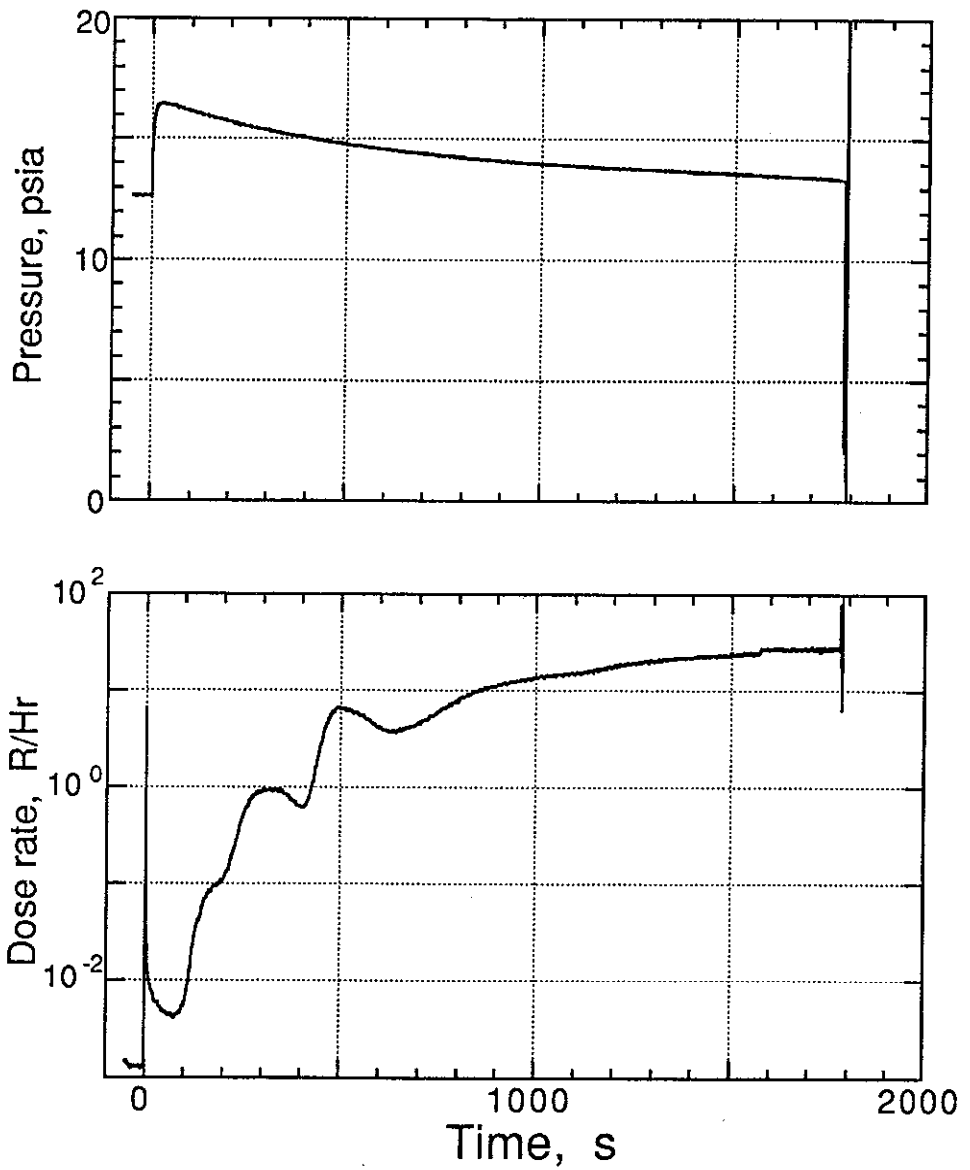
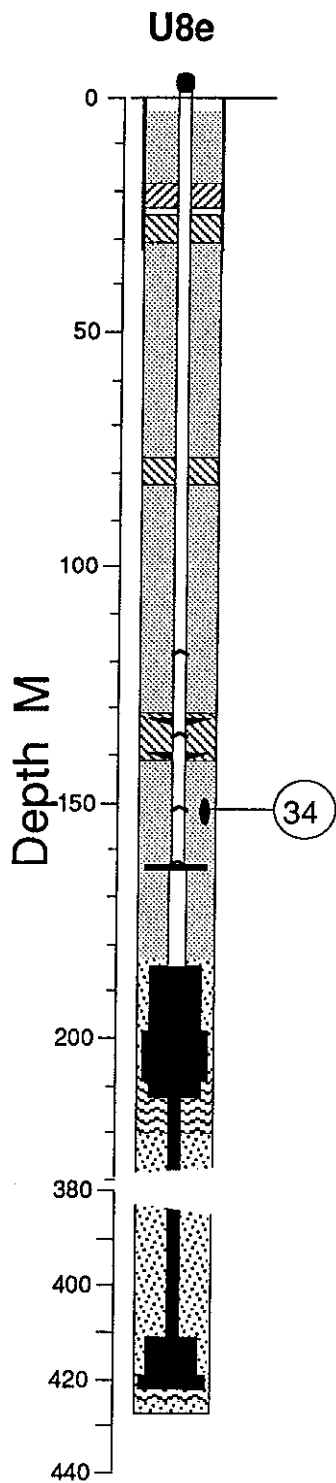


Figure 2.3 Pressure and radiation measured at station 34 (depth 151.5), near the second pressure dome.

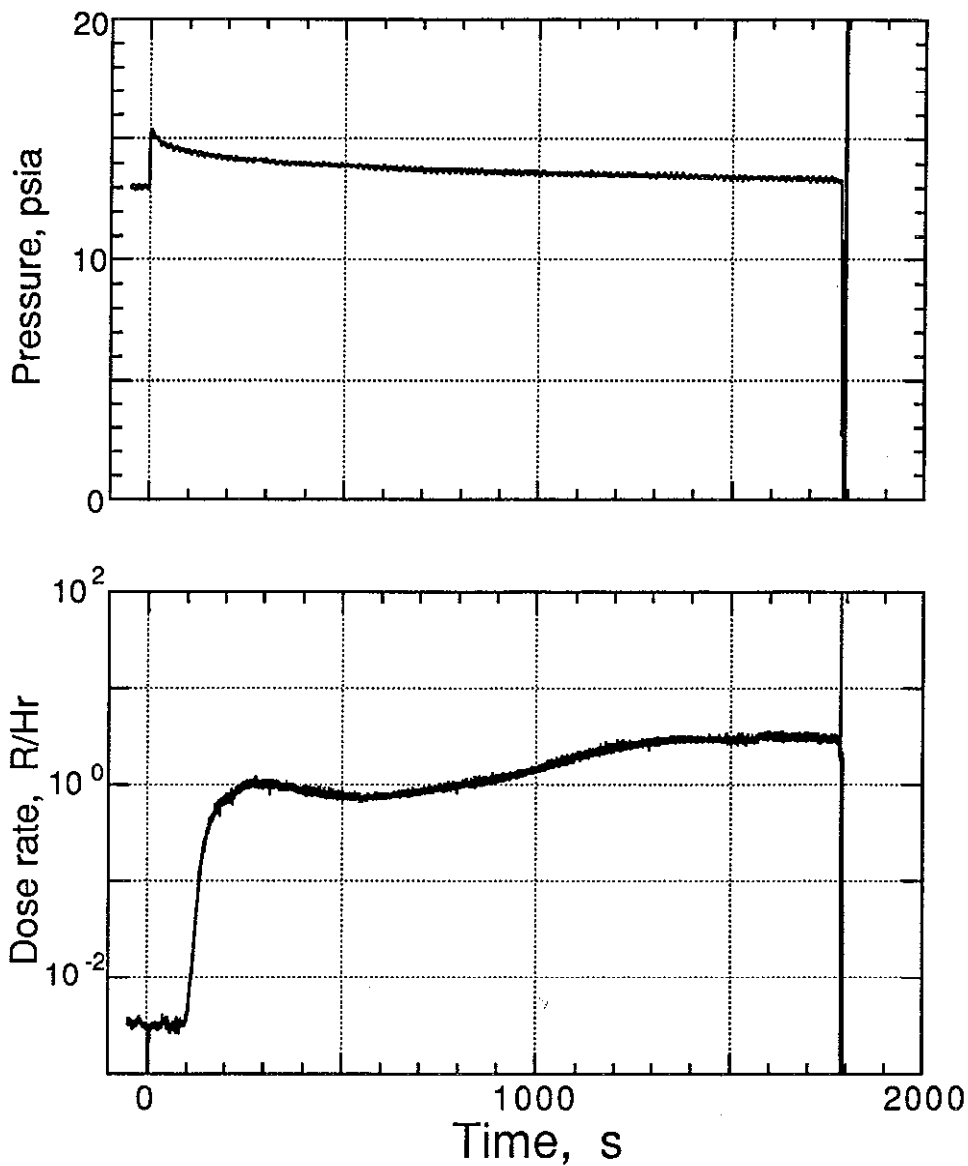
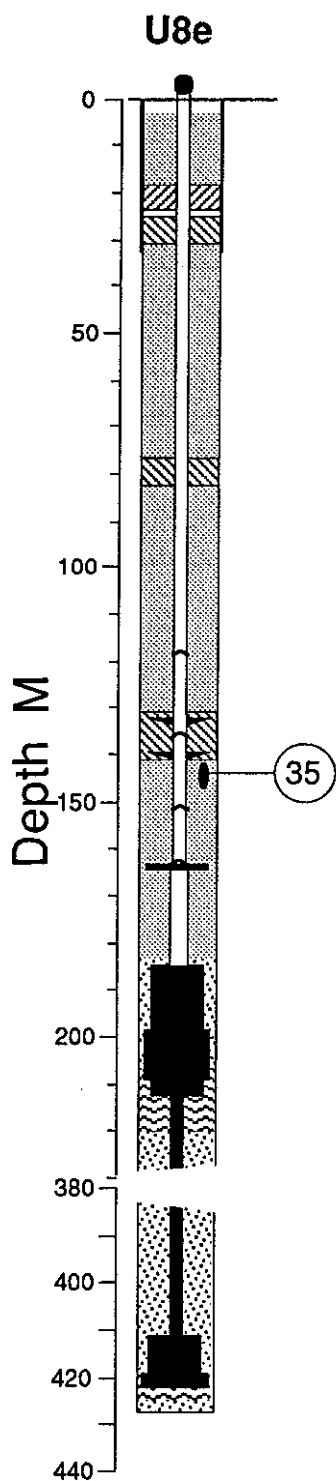


Figure 2.4 Pressure and radiation measured at station 35 (depth 143.9 m), below the formation coupling plug.

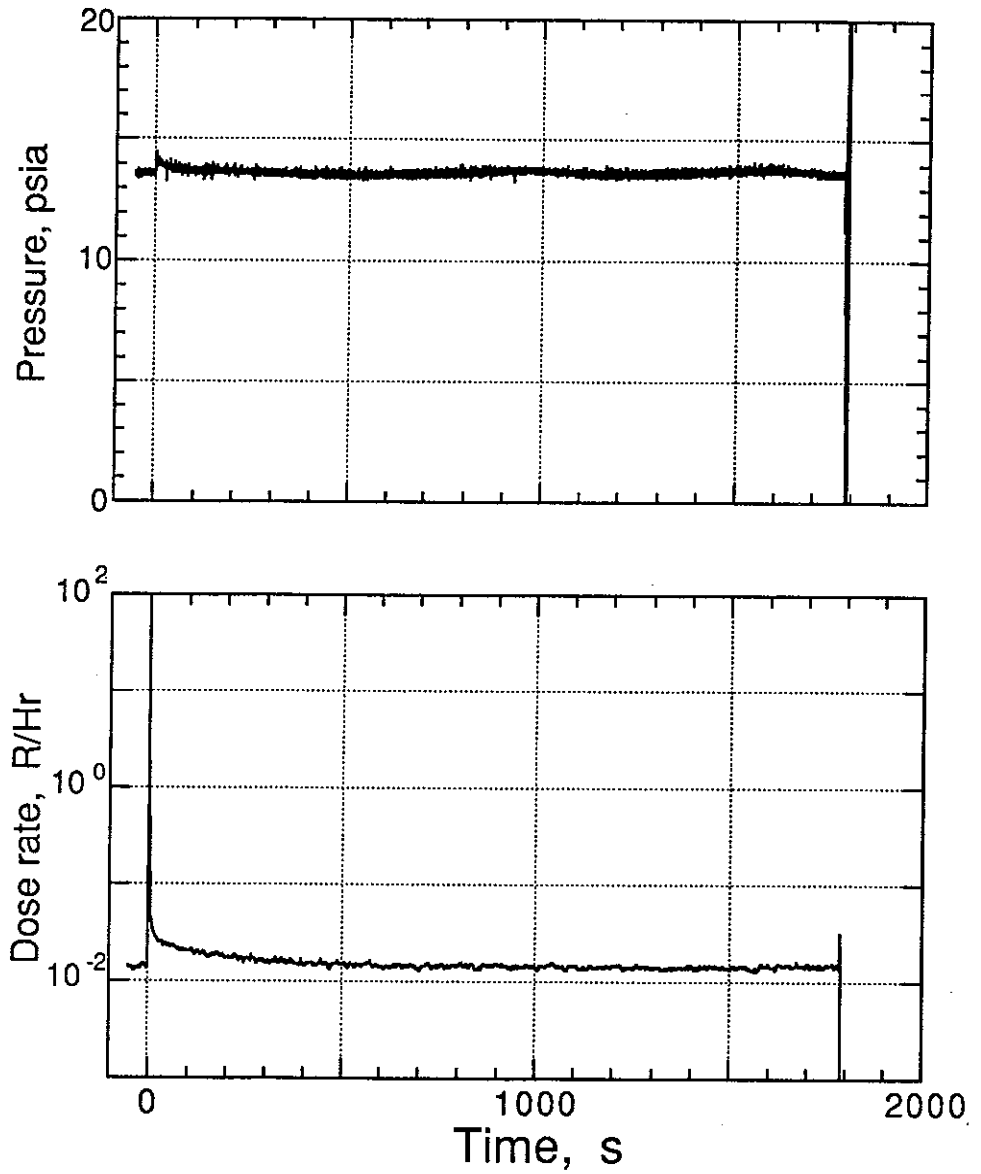
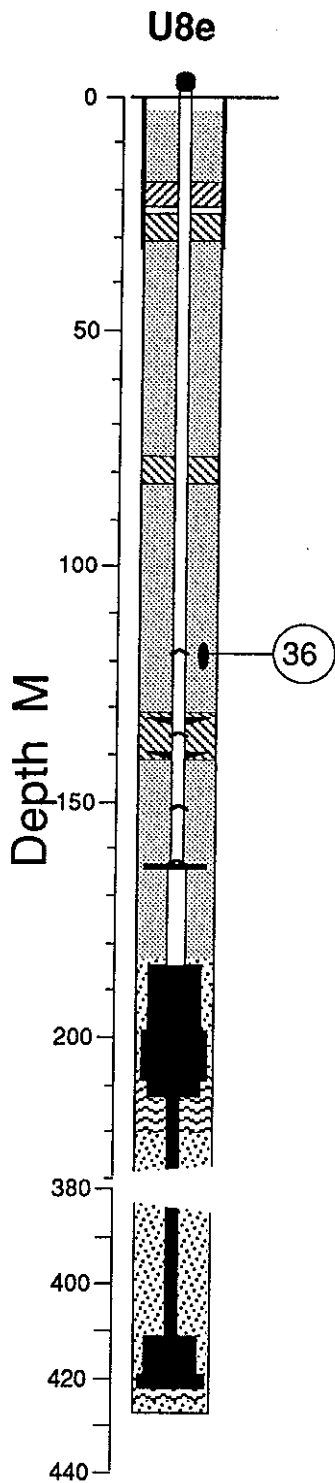


Figure 2.5 Pressure and radiation measured at station 36 (depth 118.4 m), near the detector plate, above the formation coupling plug.

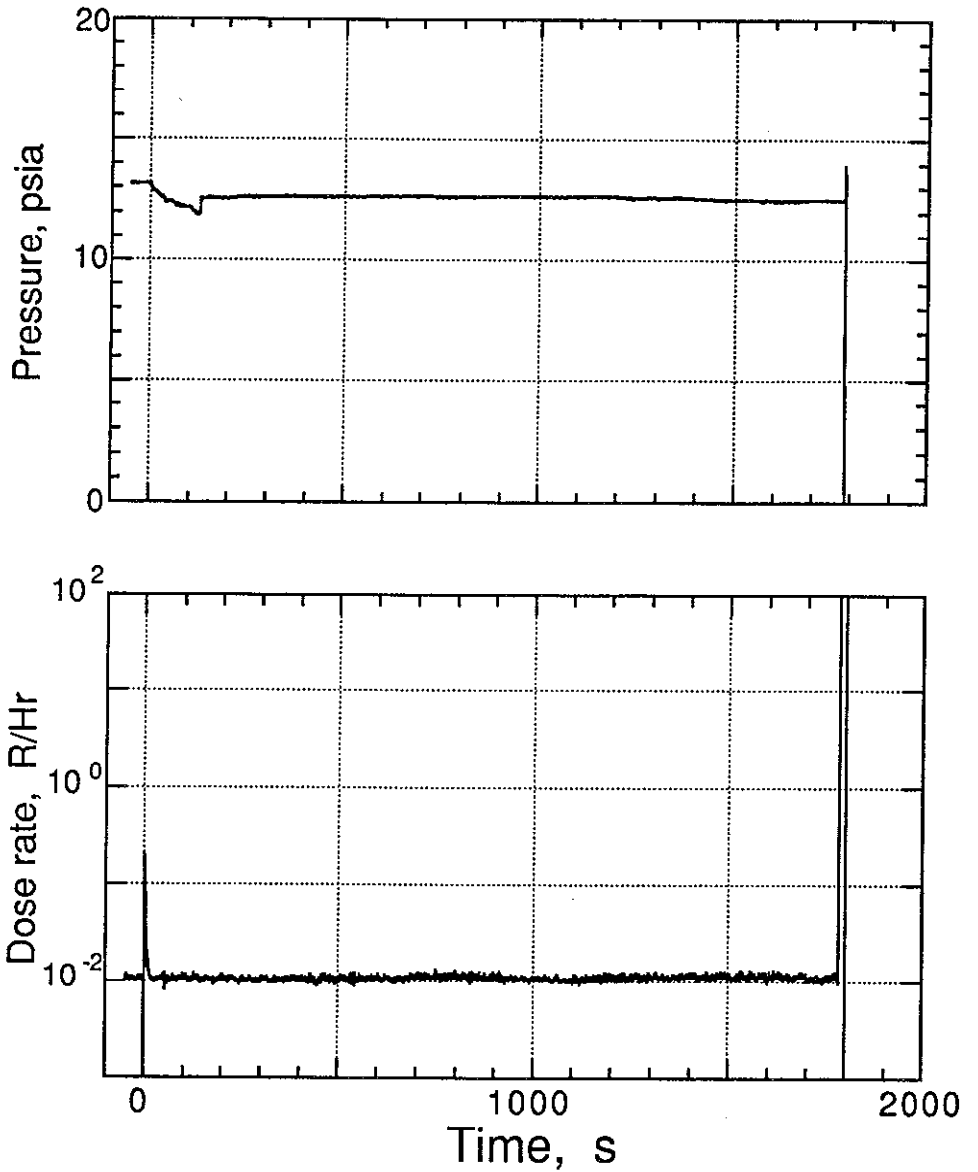
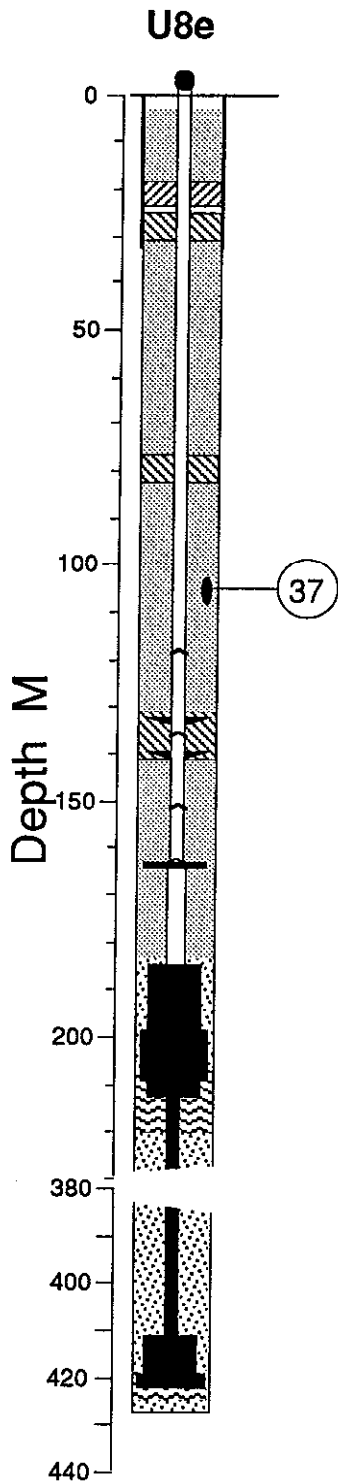


Figure 2.6 Pressure and radiation measured at station 37 (depth 104.7), midway between the formation coupling plug and the stemming platform.

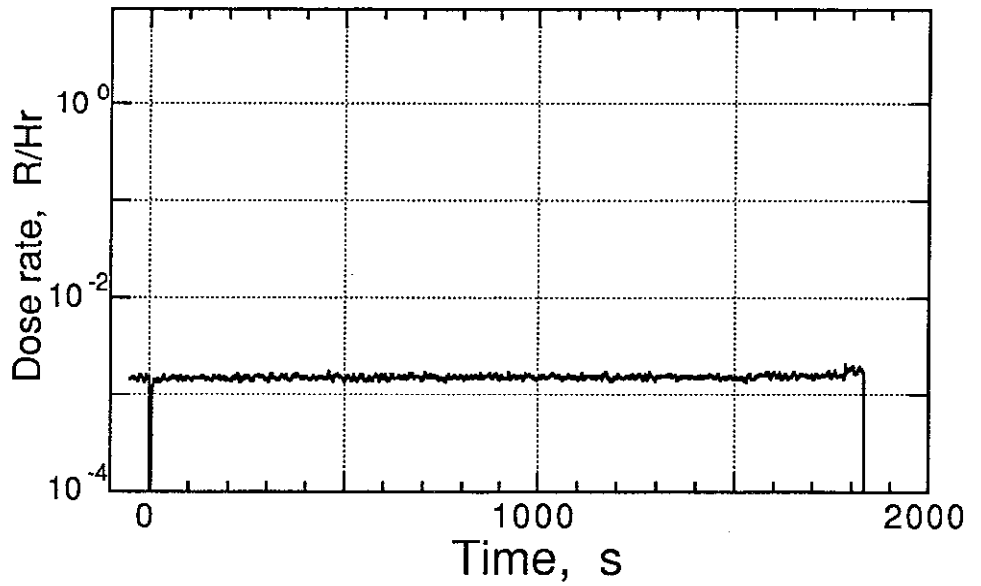
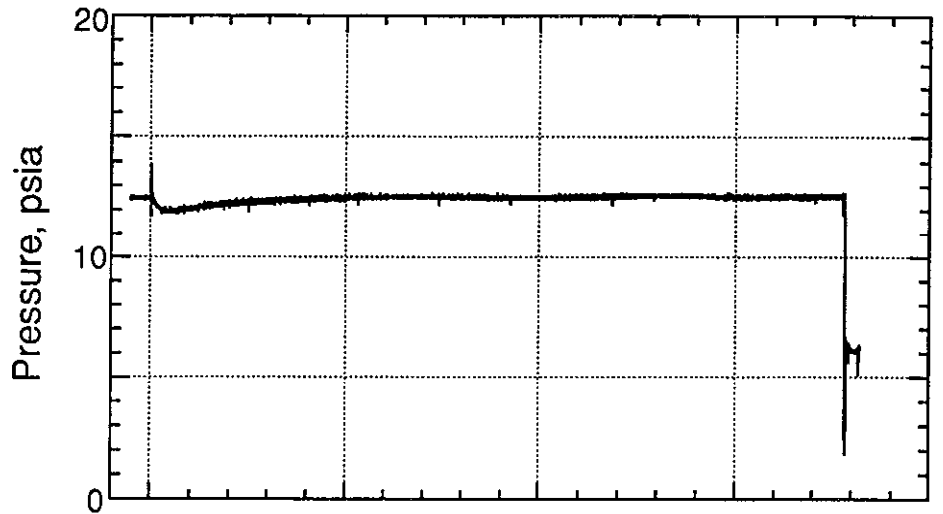
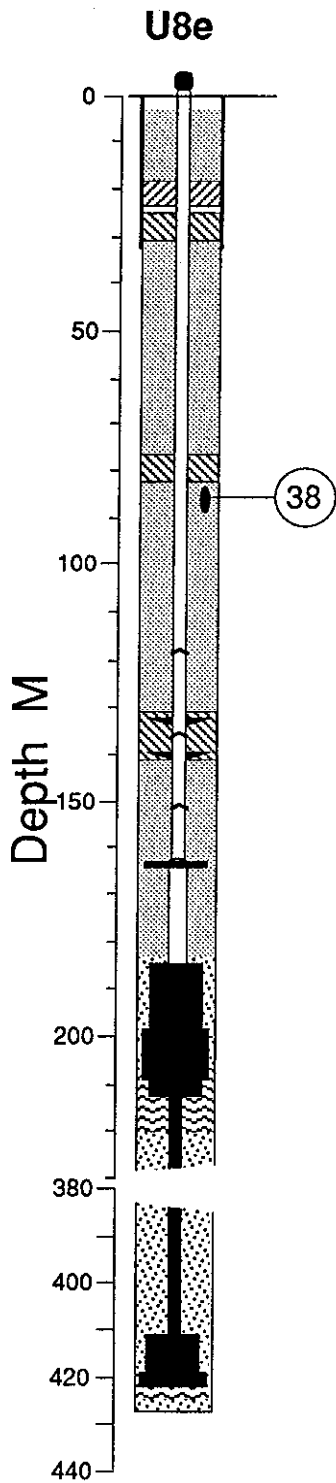


Figure 2.7 Pressure and radiation measured at station 38 (depth 85.7 m), below the stemming platform.

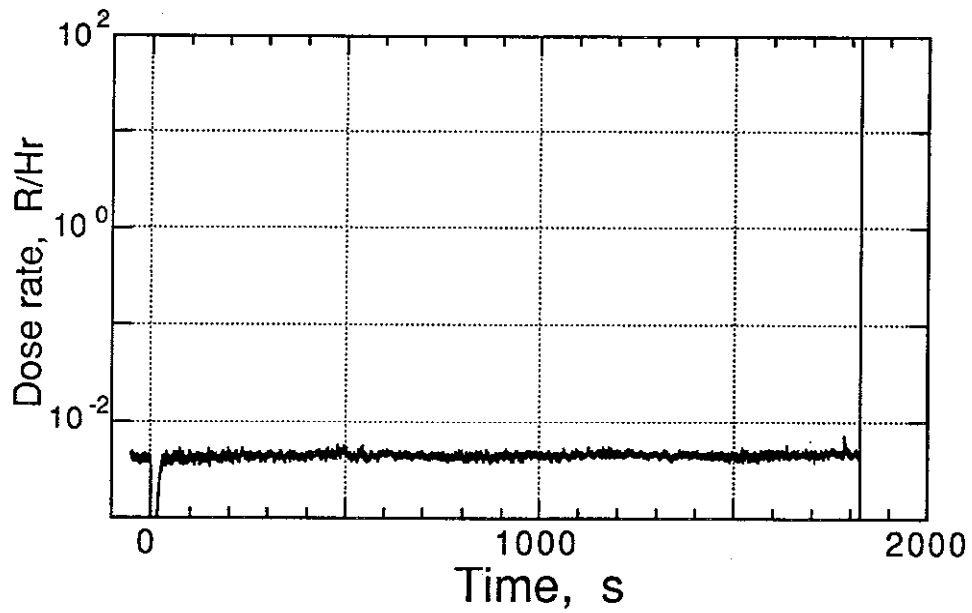
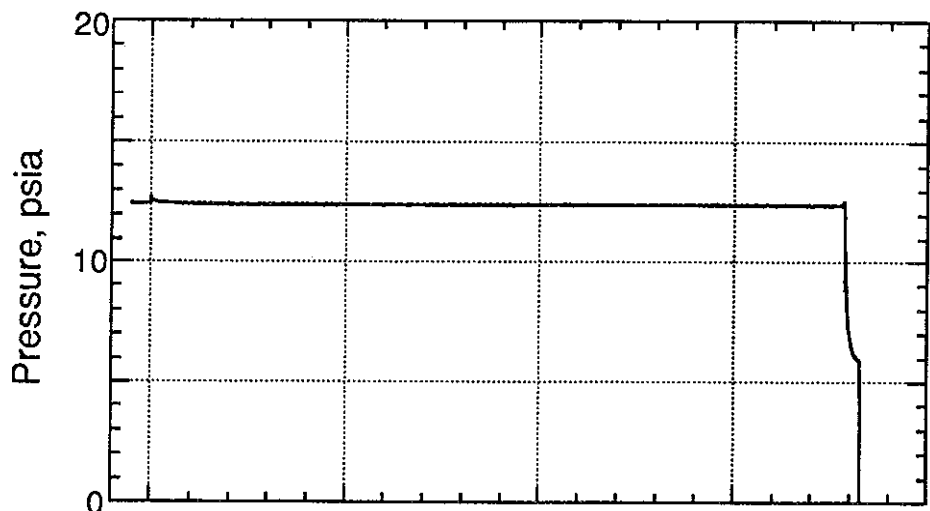
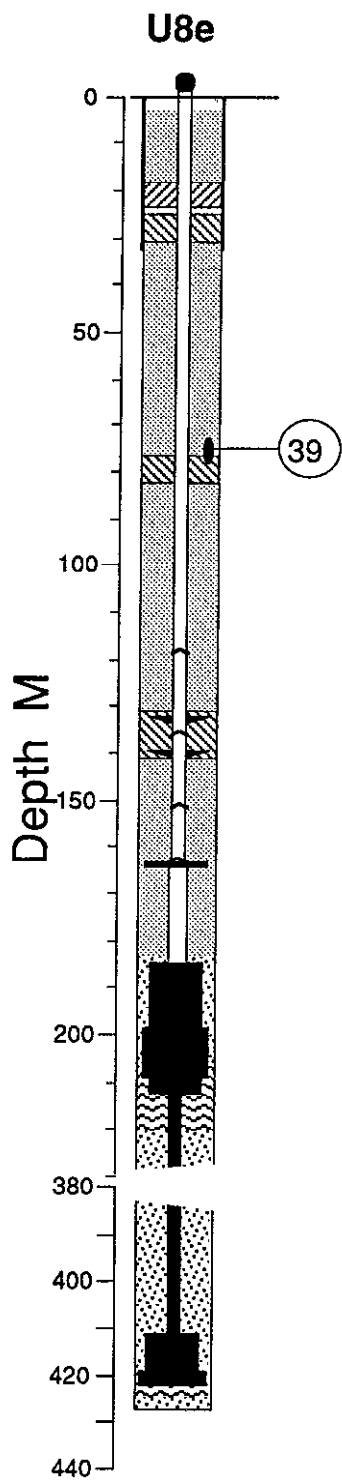


Figure 2.8 Pressure and radiation measured at station 39 (depth 75.0 m), above the stemming platform.

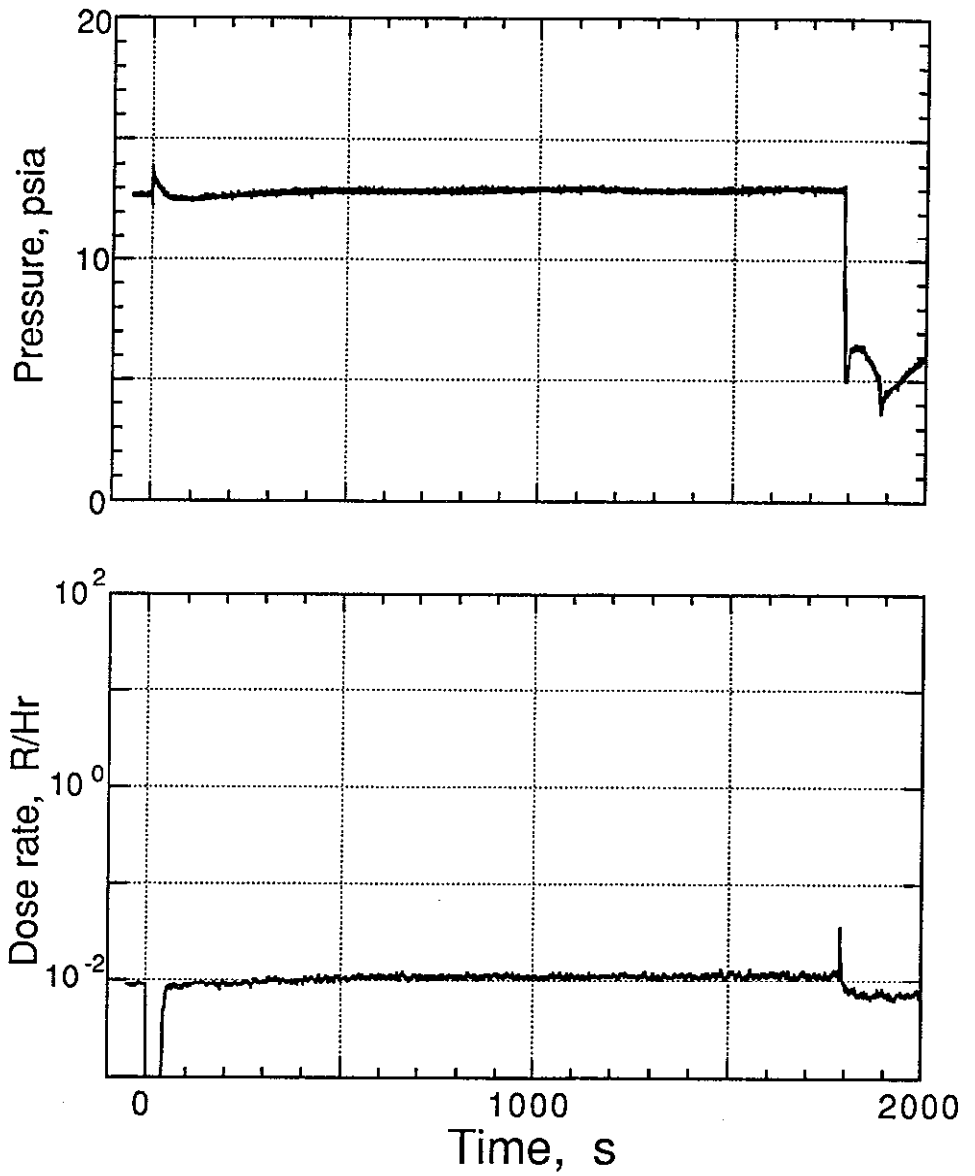
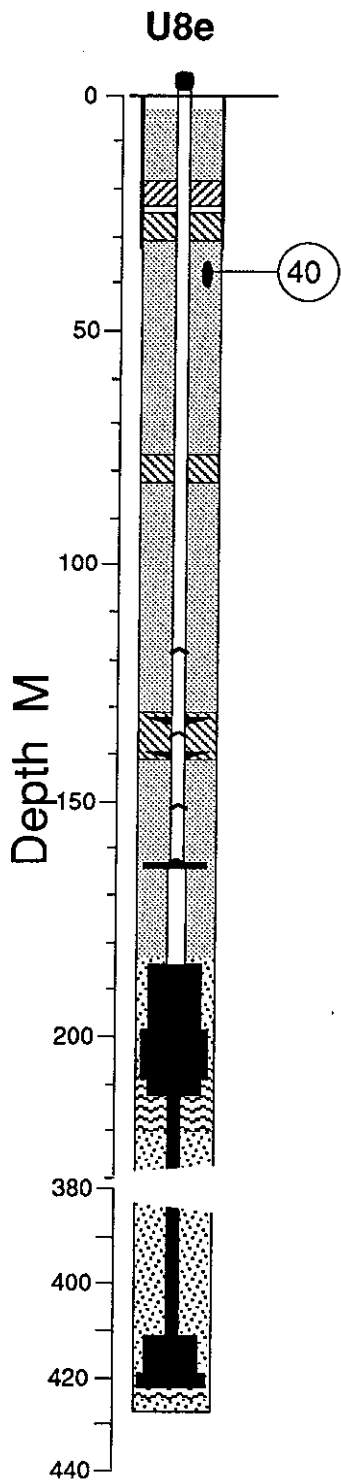


Figure 2.9 Pressure and radiation measured at station 40 (depth 37.8 m) below the top plug.

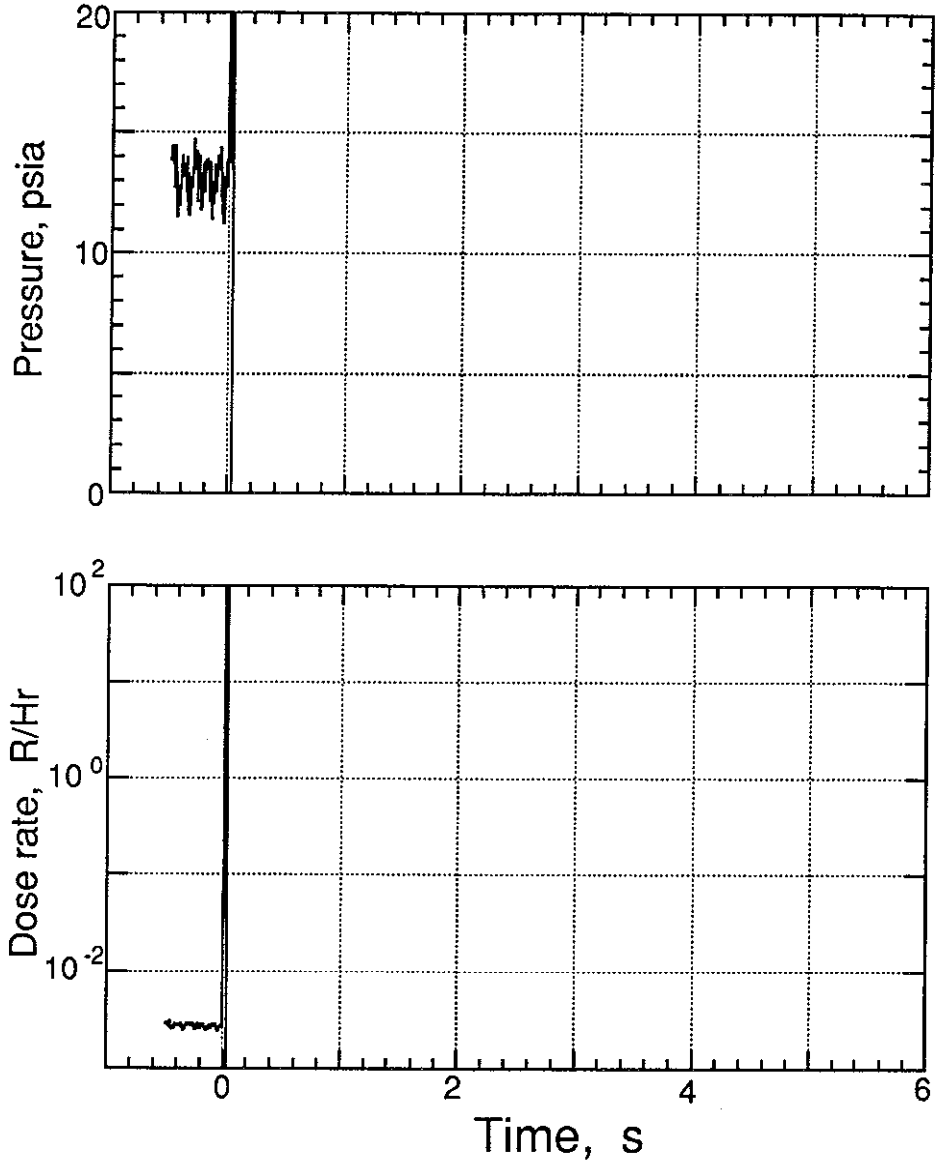
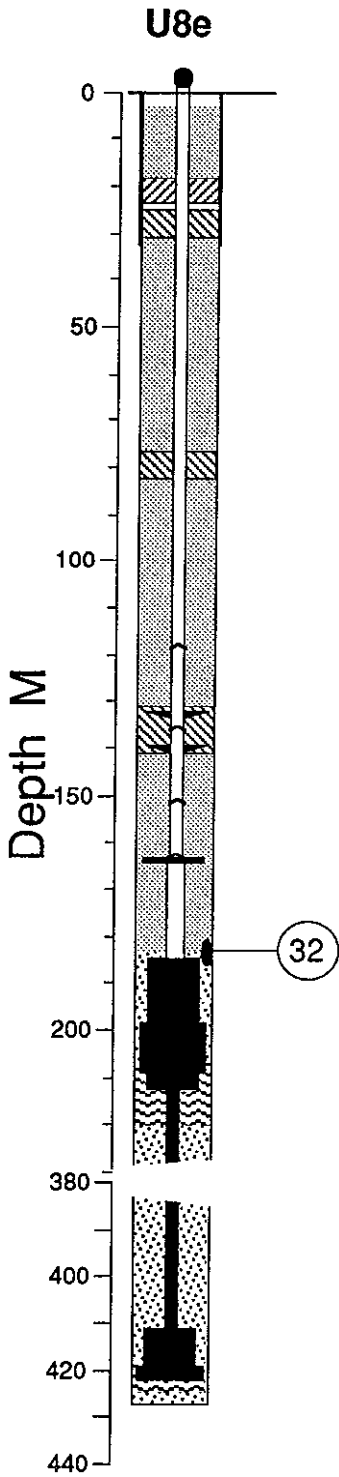


Figure 2.10 The first 6 s of pressure and radiation measured at station 32 (depth 184.7 m). This station was apparently lost close to time zero.

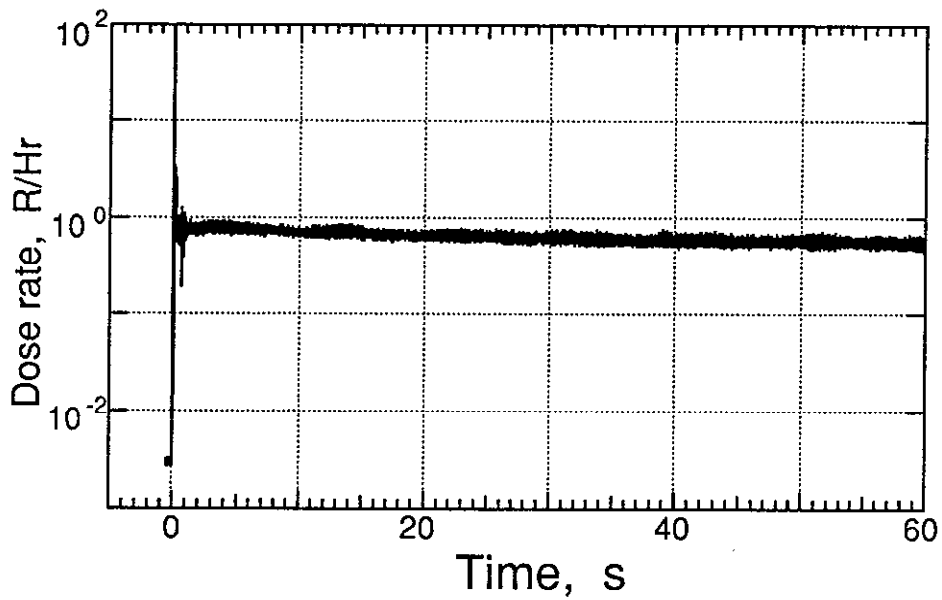
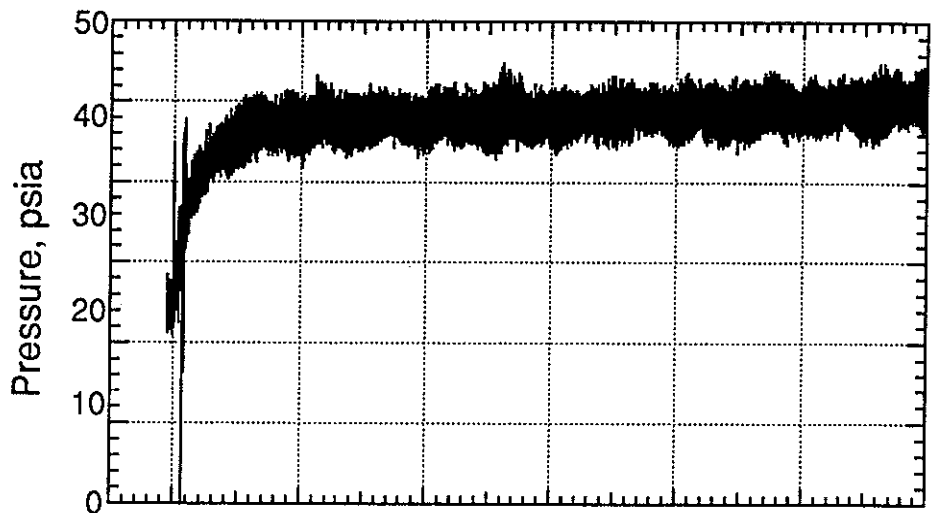
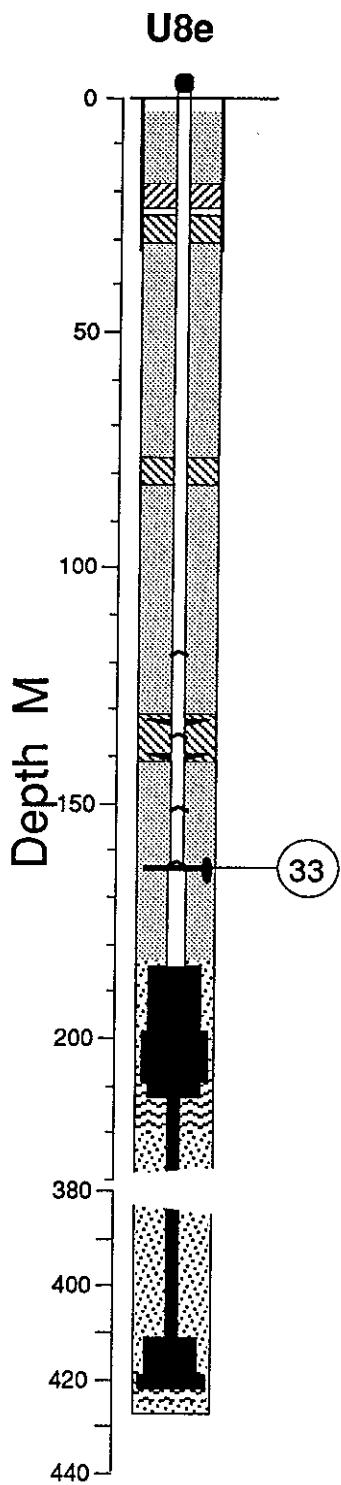


Figure 2.11 The first 60 s of pressure and radiation measured at station 33 (depth 163.6 m), near the first pressure dome, above the tau can.

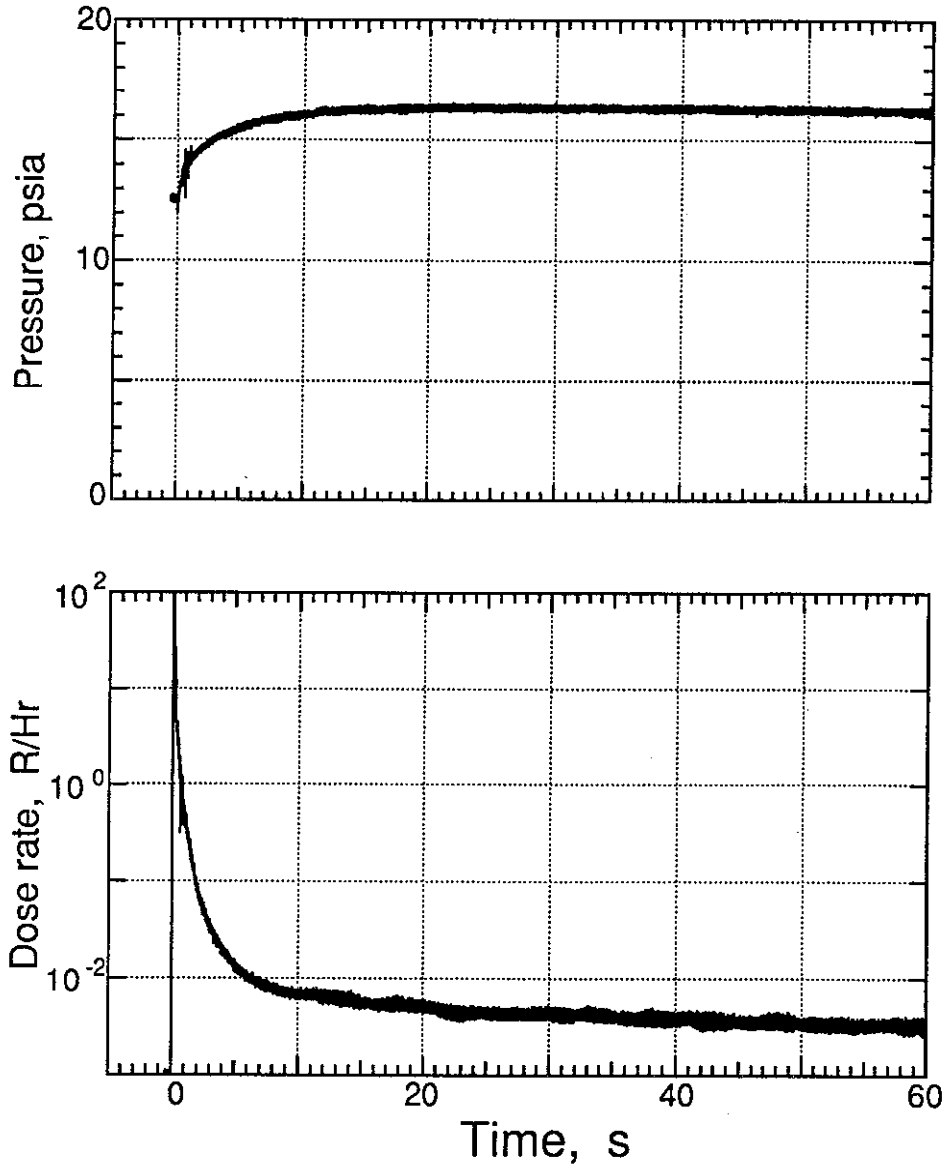
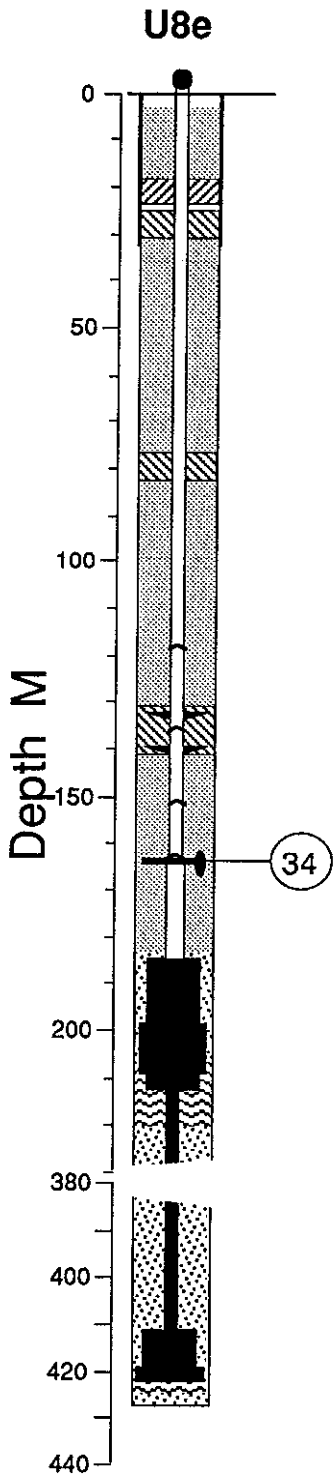


Figure 2.12 The first 60 s of pressure and radiation measured at station 34 (depth 151.5), near the second pressure dome.

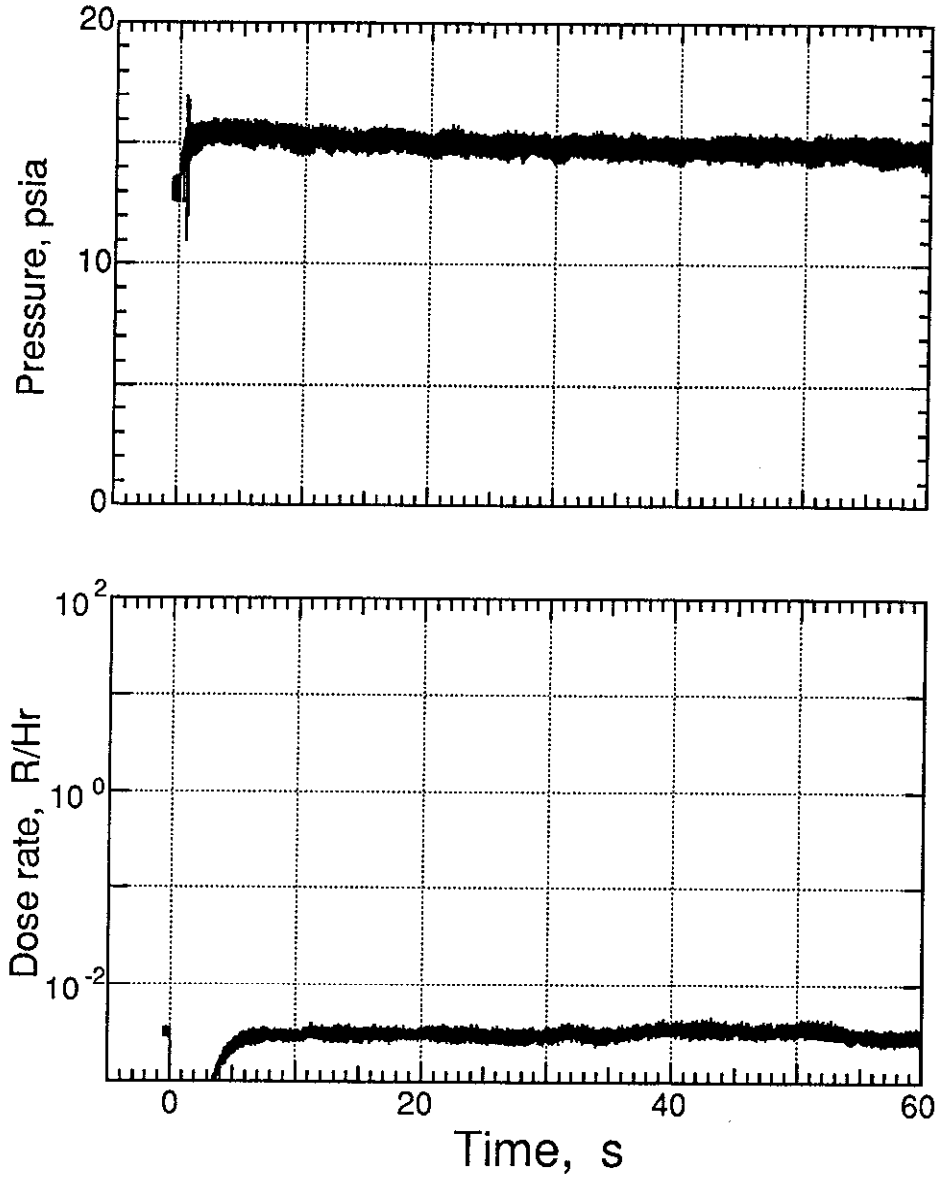
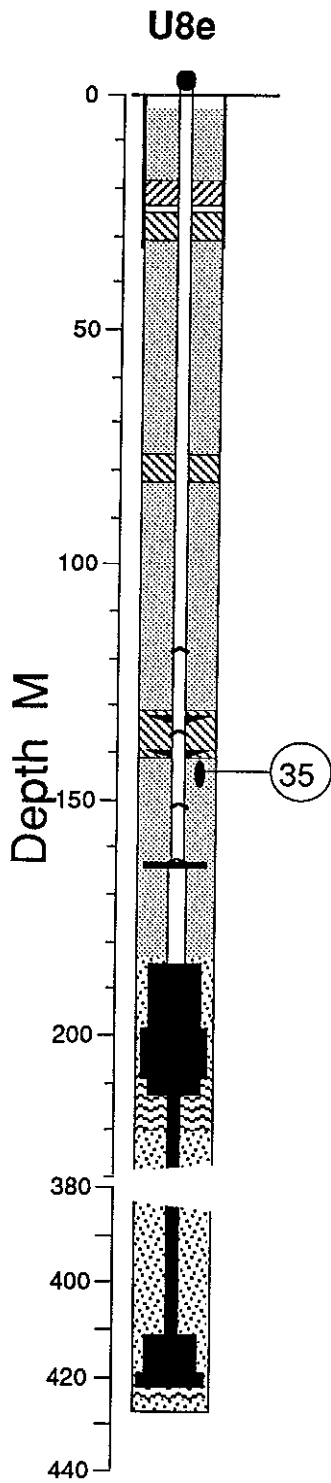


Figure 2.13 The first 60 s of pressure and radiation measured at station 35 (depth 143.9 m), below the formation coupling plug.

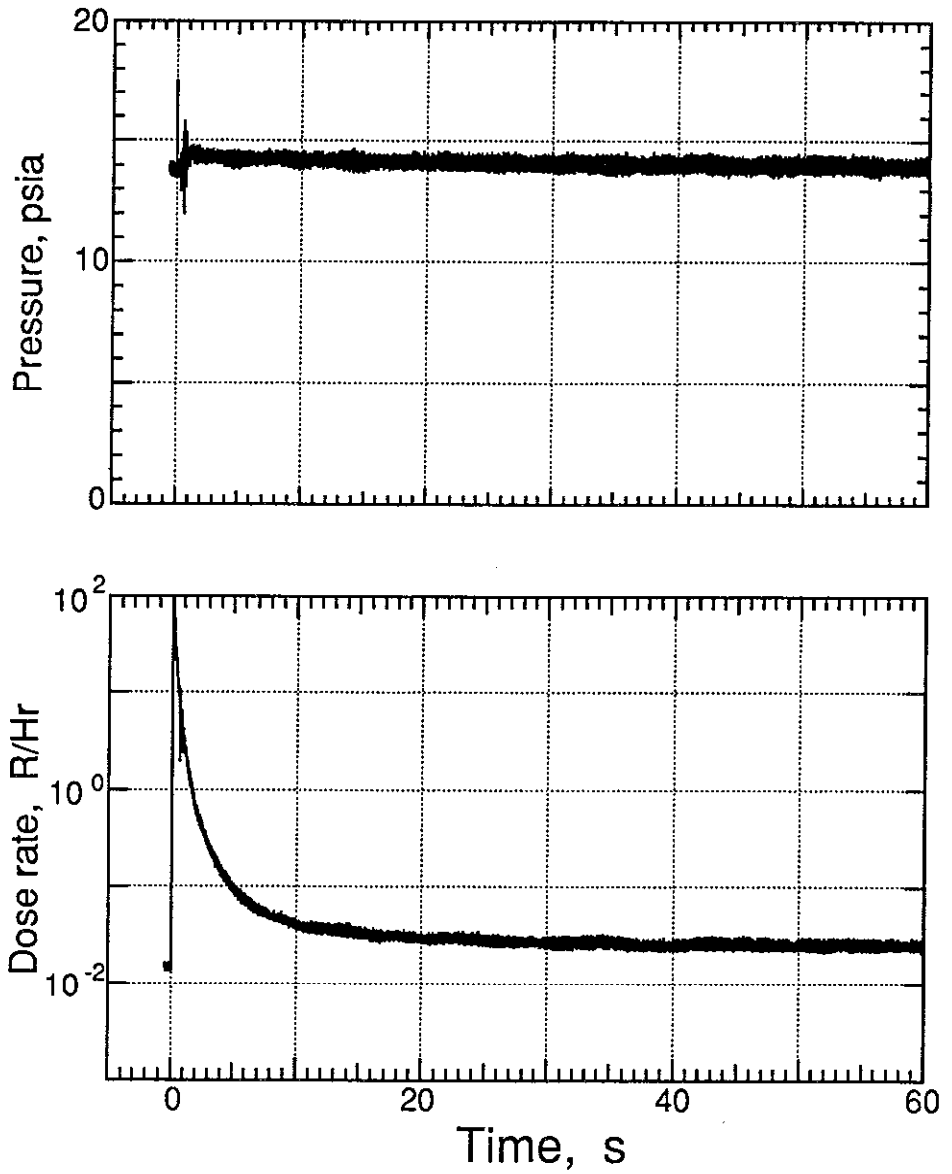
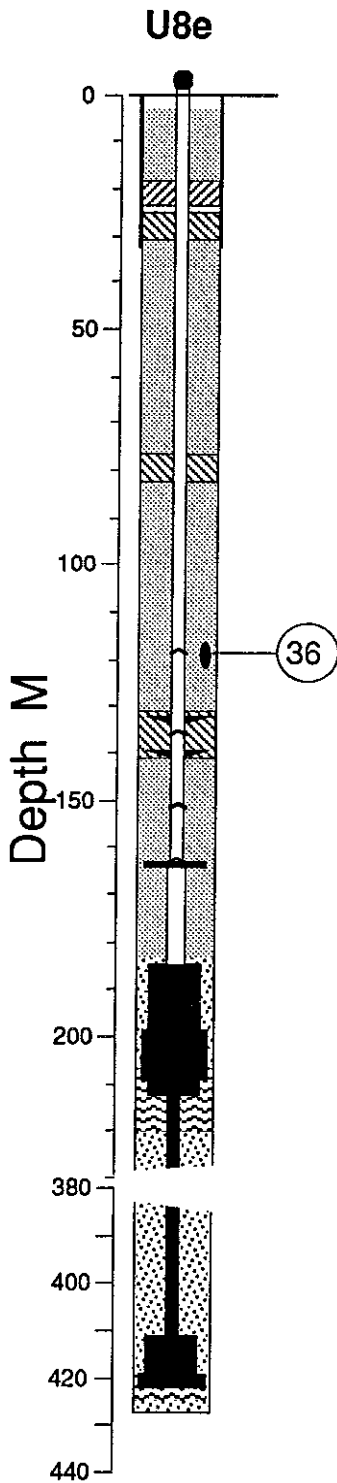


Figure 2.14 The first 60 s of pressure and radiation measured at station 36 (depth 118.4 m), near the detector plate, above the formation coupling plug.

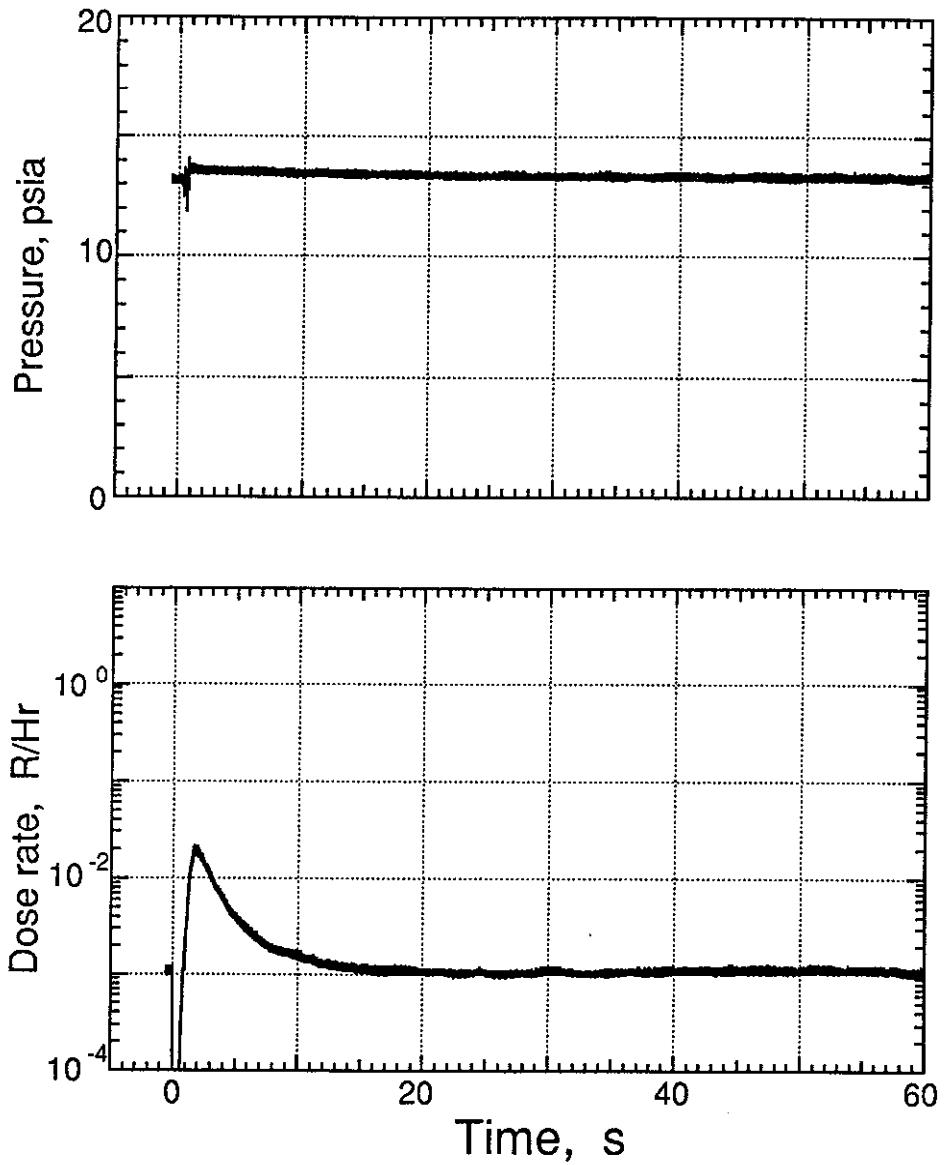
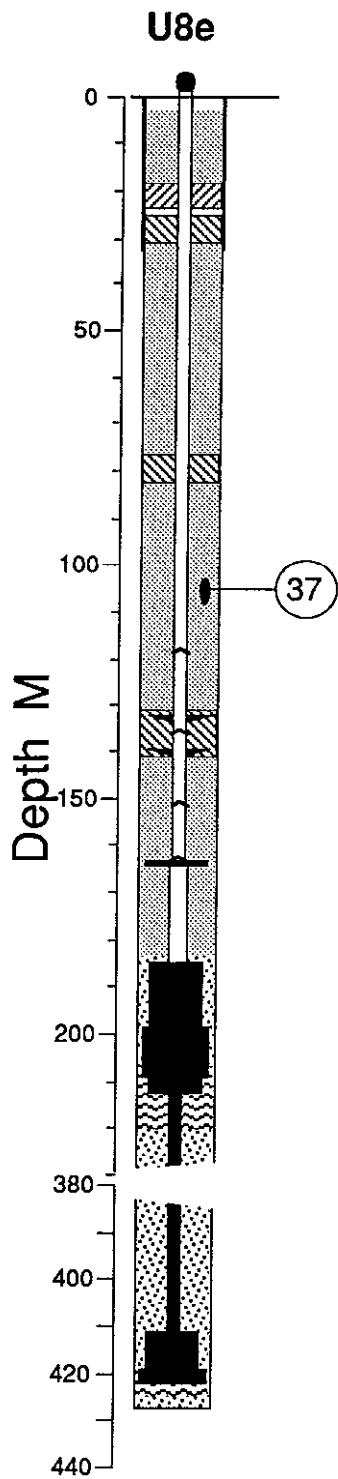


Figure 2.15 The first 60 s of pressure and radiation measured at station 37 (depth 104.7), midway between the formation coupling plug and the stemming platform.

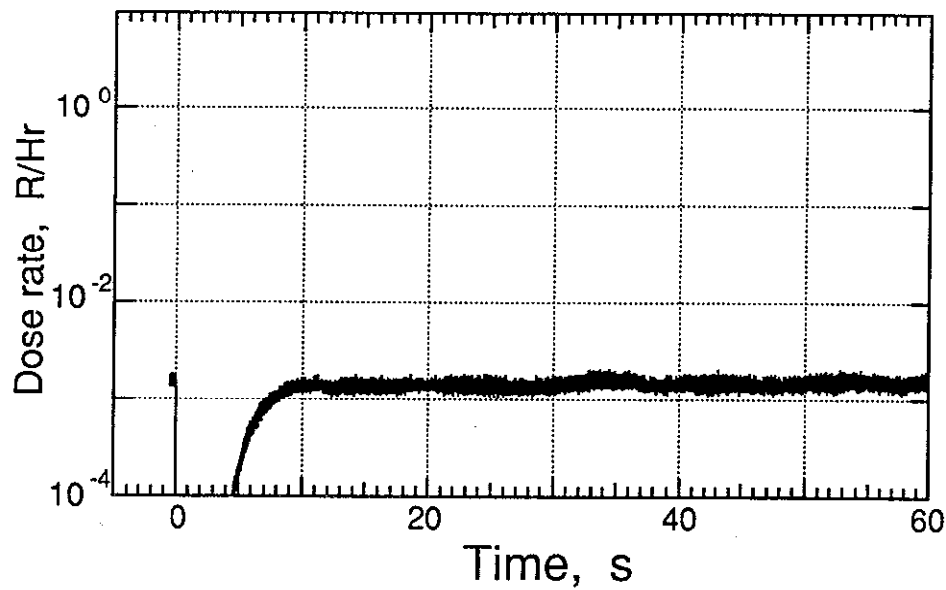
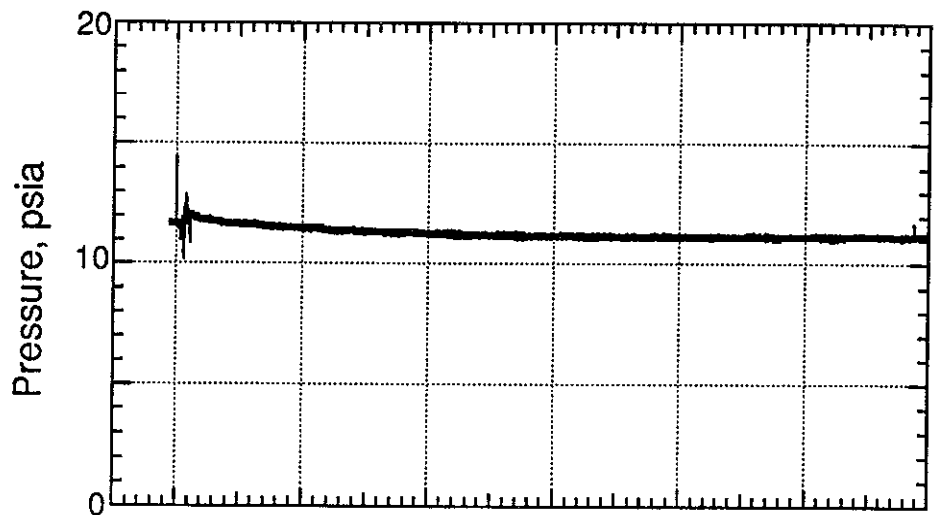
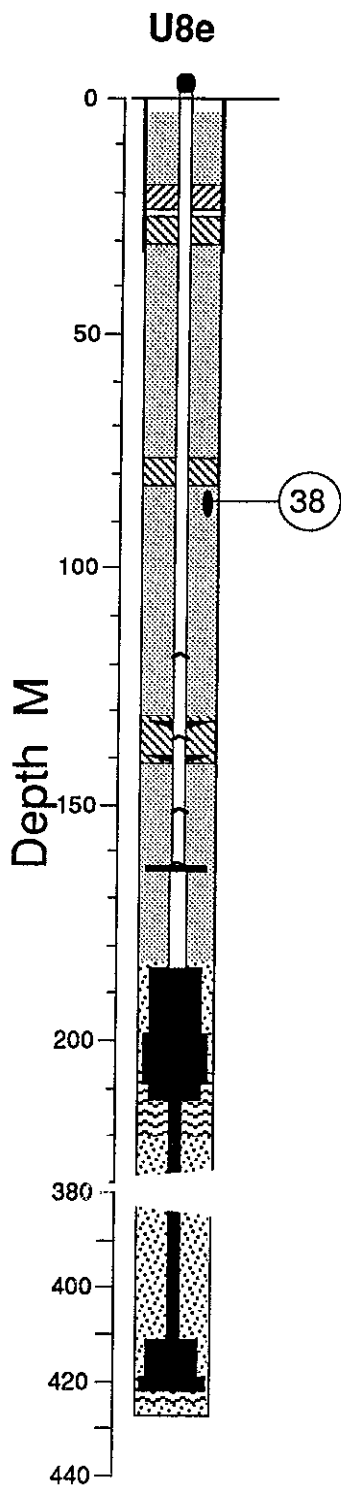


Figure 2.16 The first 60 s of pressure and radiation measured at station 38 (depth 85.7 m), below the stemming platform.

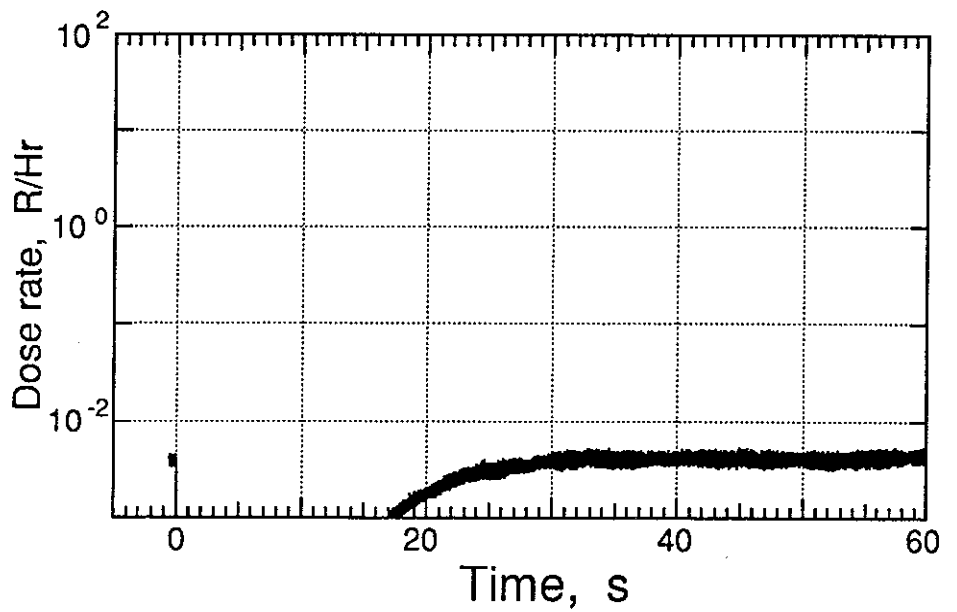
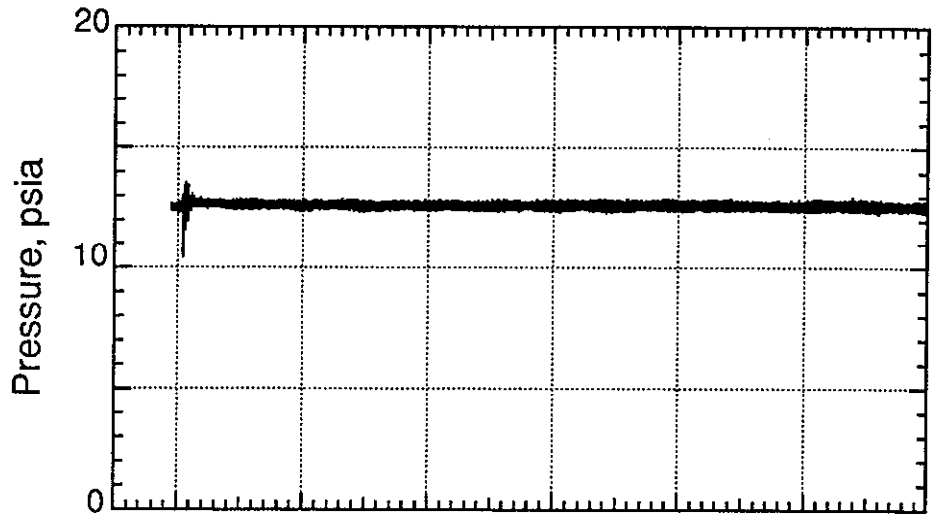
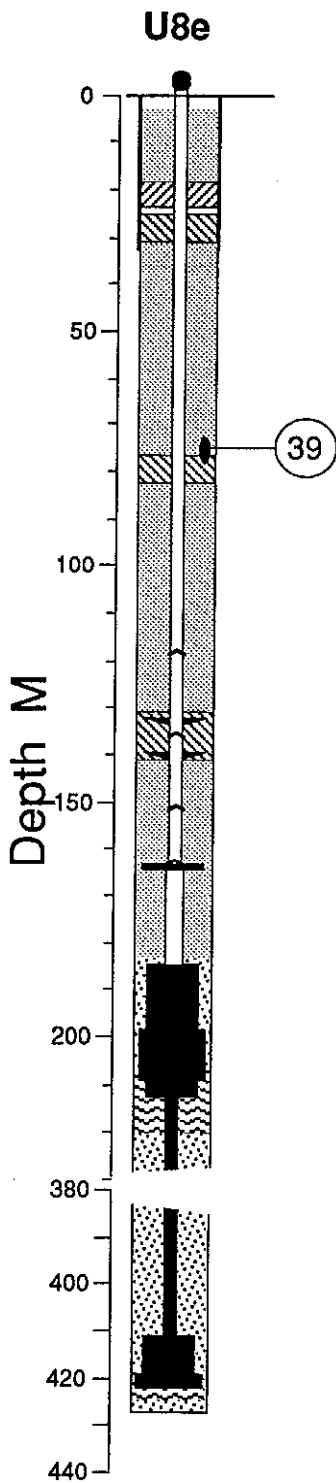


Figure 2.17 The first 60 s of pressure and radiation measured at station 39 (depth 75.0 m), above the stemming platform.

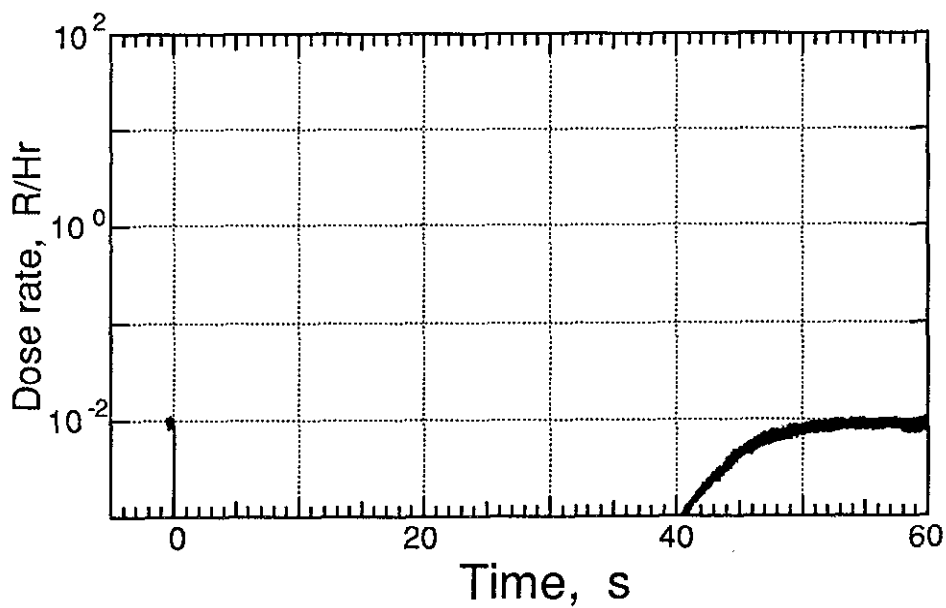
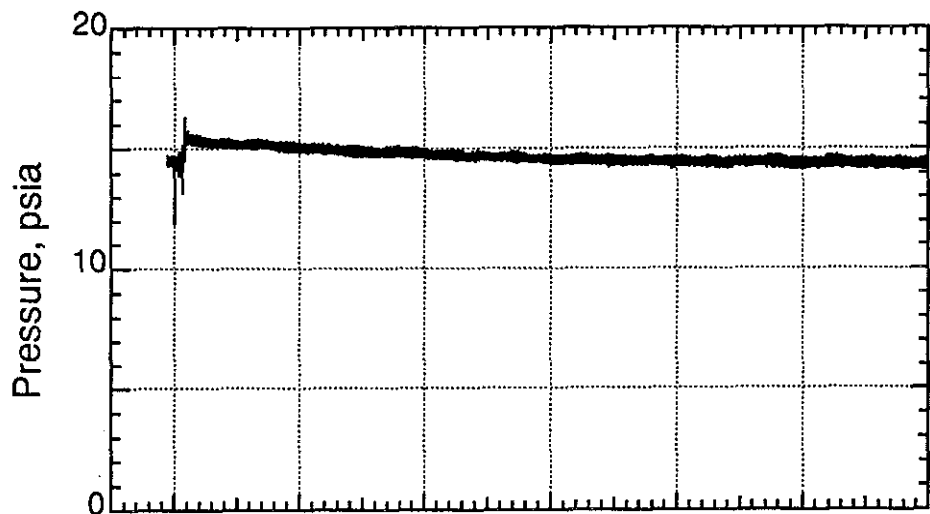
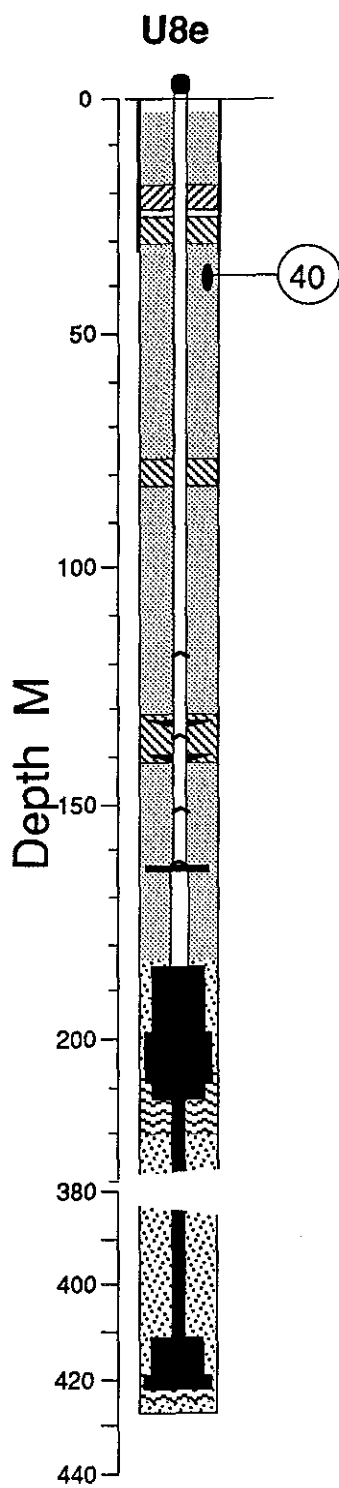


Figure 2.18 The first 60 s of pressure and radiation measured at station 40 (depth 37.8 m) below the top plug.

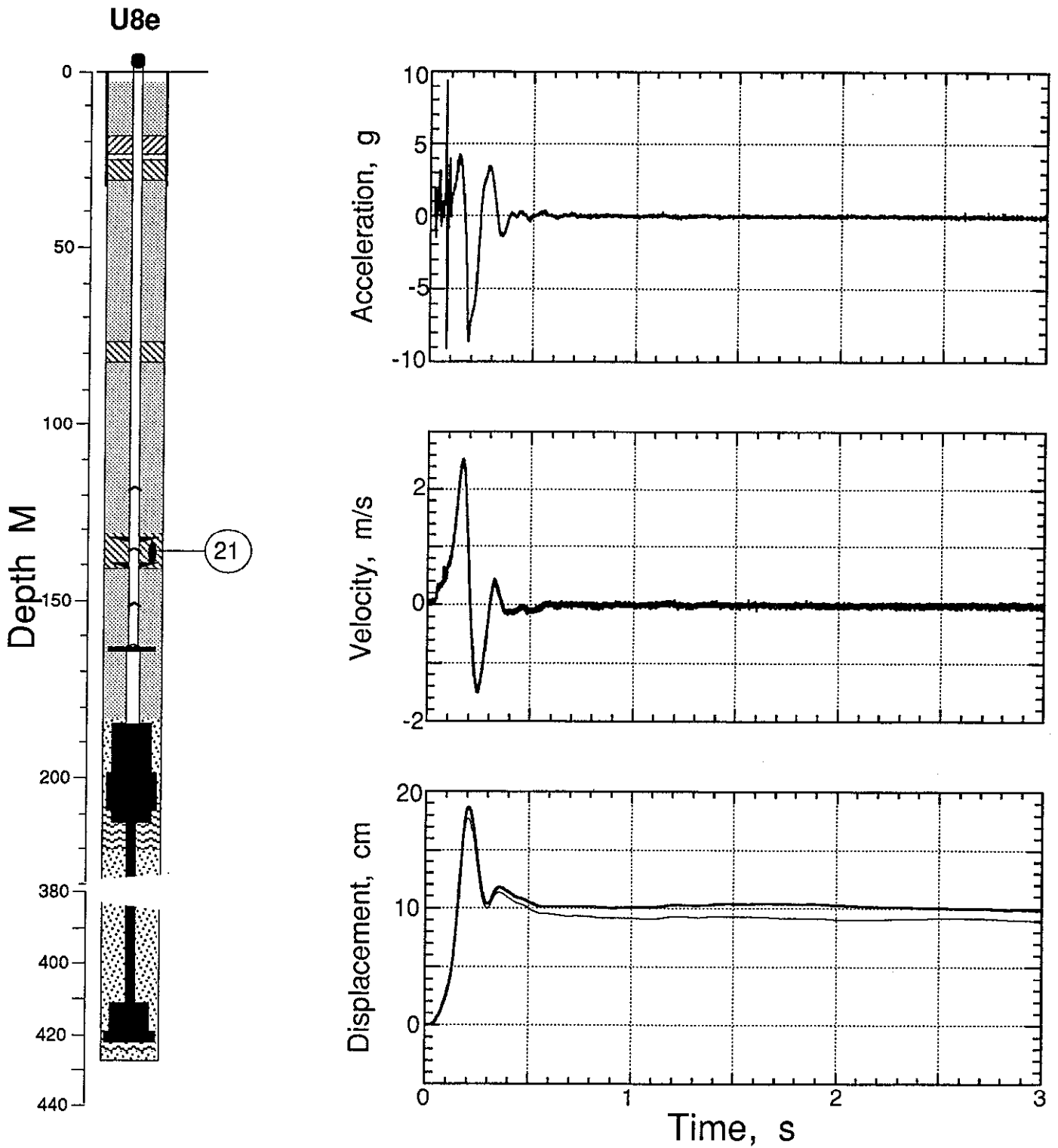


Figure 2.19 Explosion-induced vertical motion at station 21 in the formation coupling plug (depth 136.3 m). When there is more than one trace in a plot, the lighter was derived from the accelerometer.

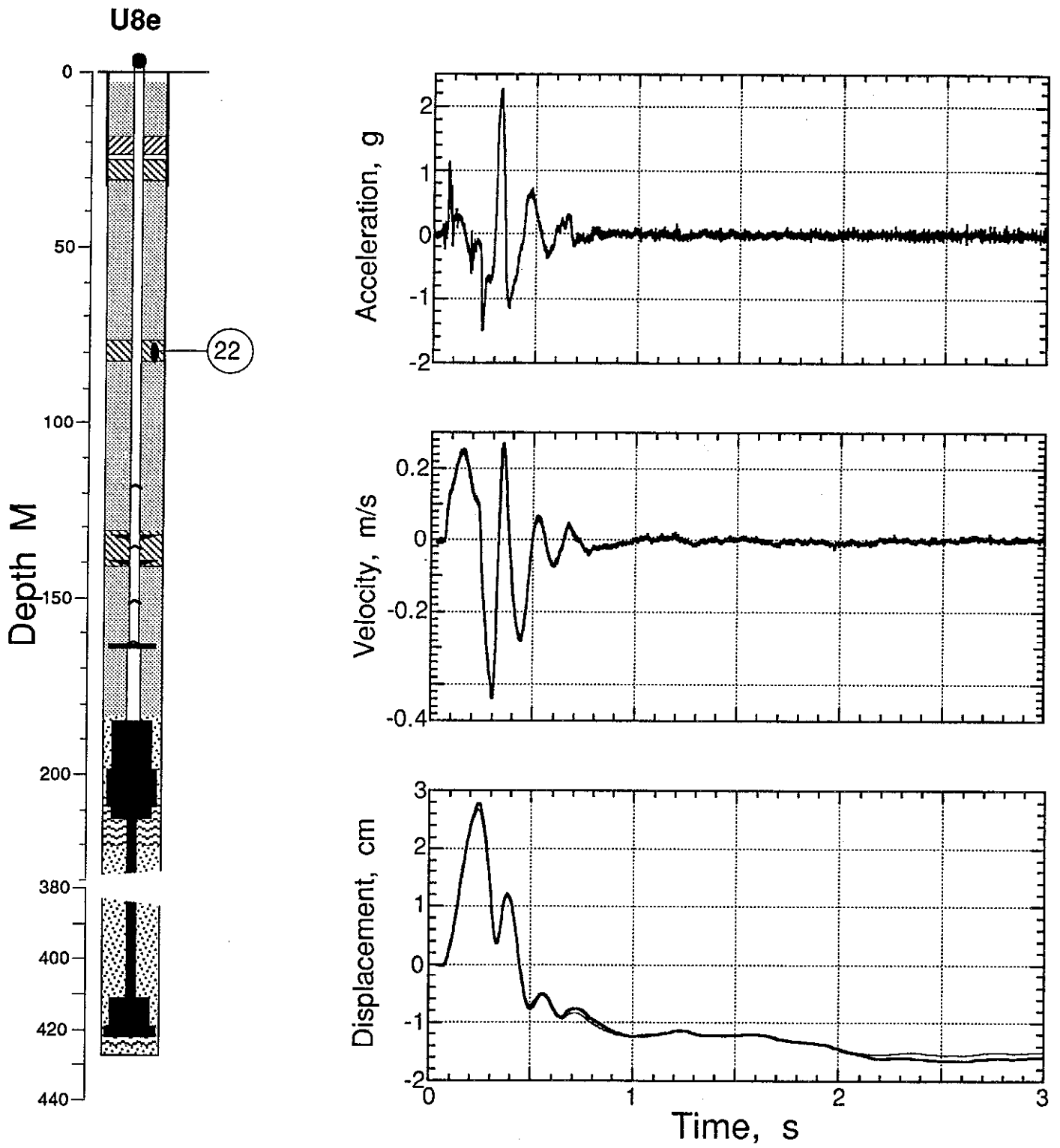


Figure 2.20 Explosion-induced vertical motion at station 22 in the intermediate plug (depth 79.6 m). When there is more than one trace in a plot, the lighter was derived from the accelerometer

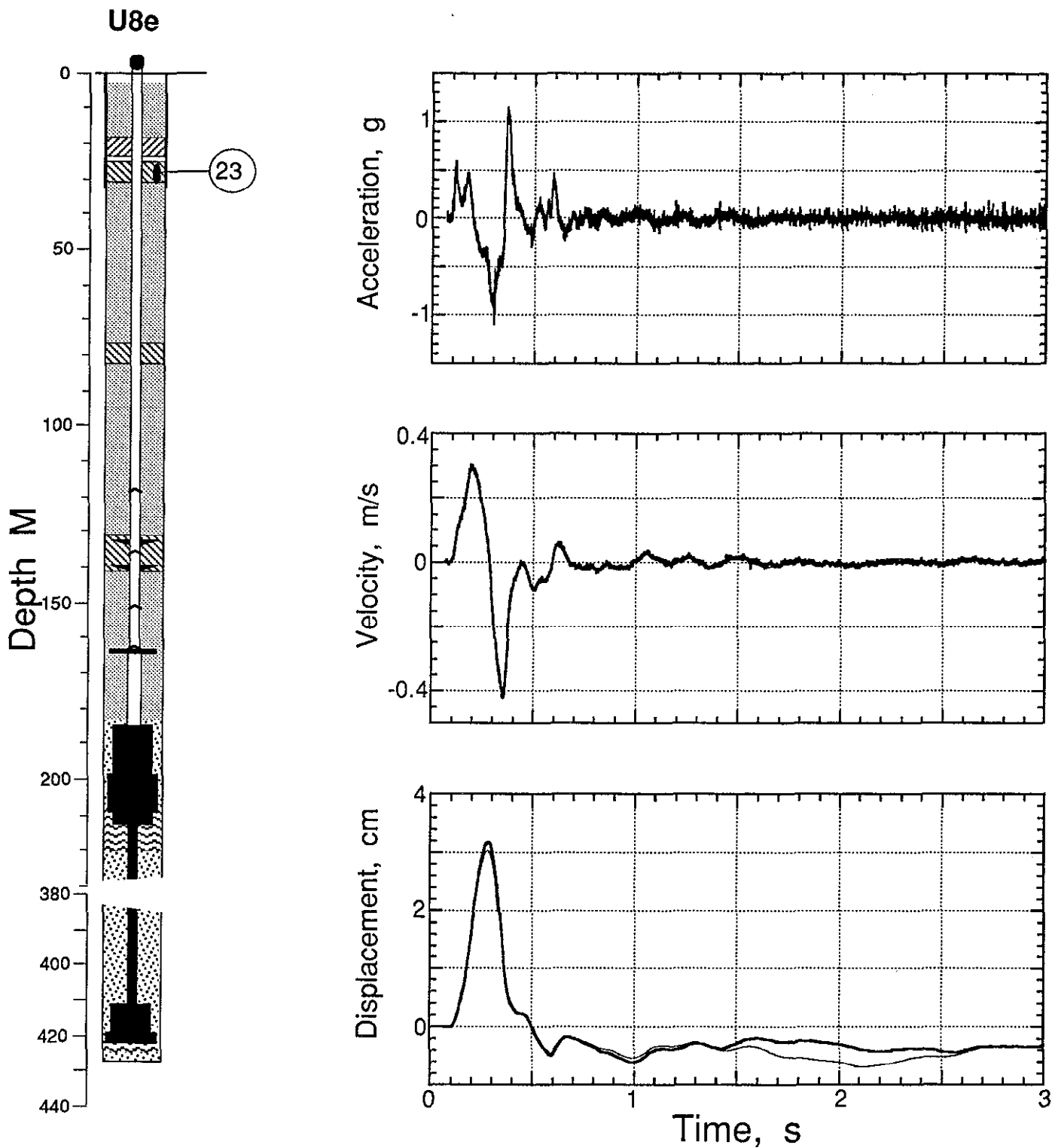


Figure 2.21 Explosion-induced vertical motion at station 23 in top plug (depth 27.7 m). When there is more than one trace in a plot, the lighter was derived from the accelerometer.

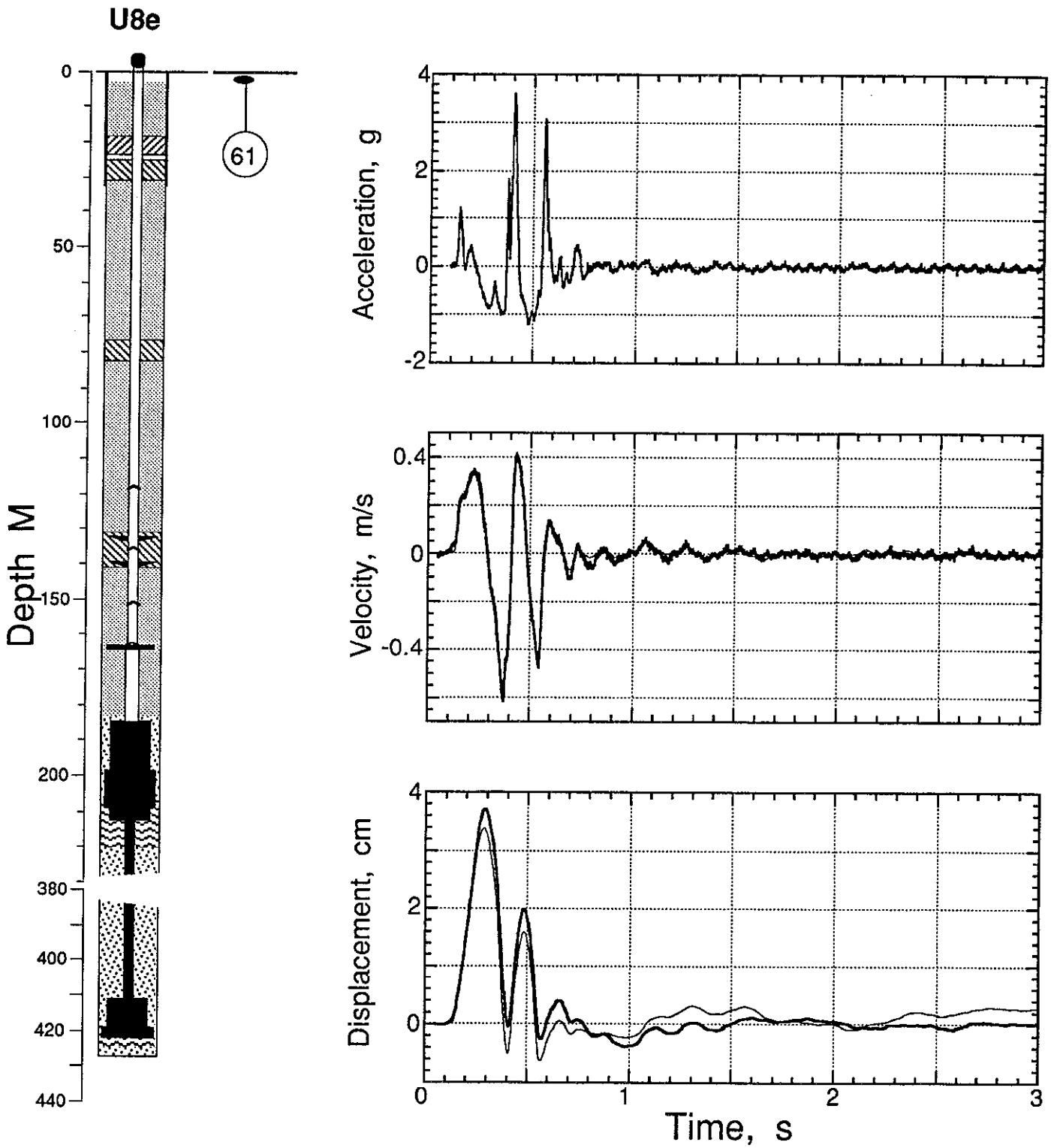


Figure 2.22 Explosion-induced vertical motion at station 61 in the ground surface (horizontal distance of 15.25 m and depth of 1.22 m). When there is more than one trace in a plot, the lighter was derived from the accelerometer.

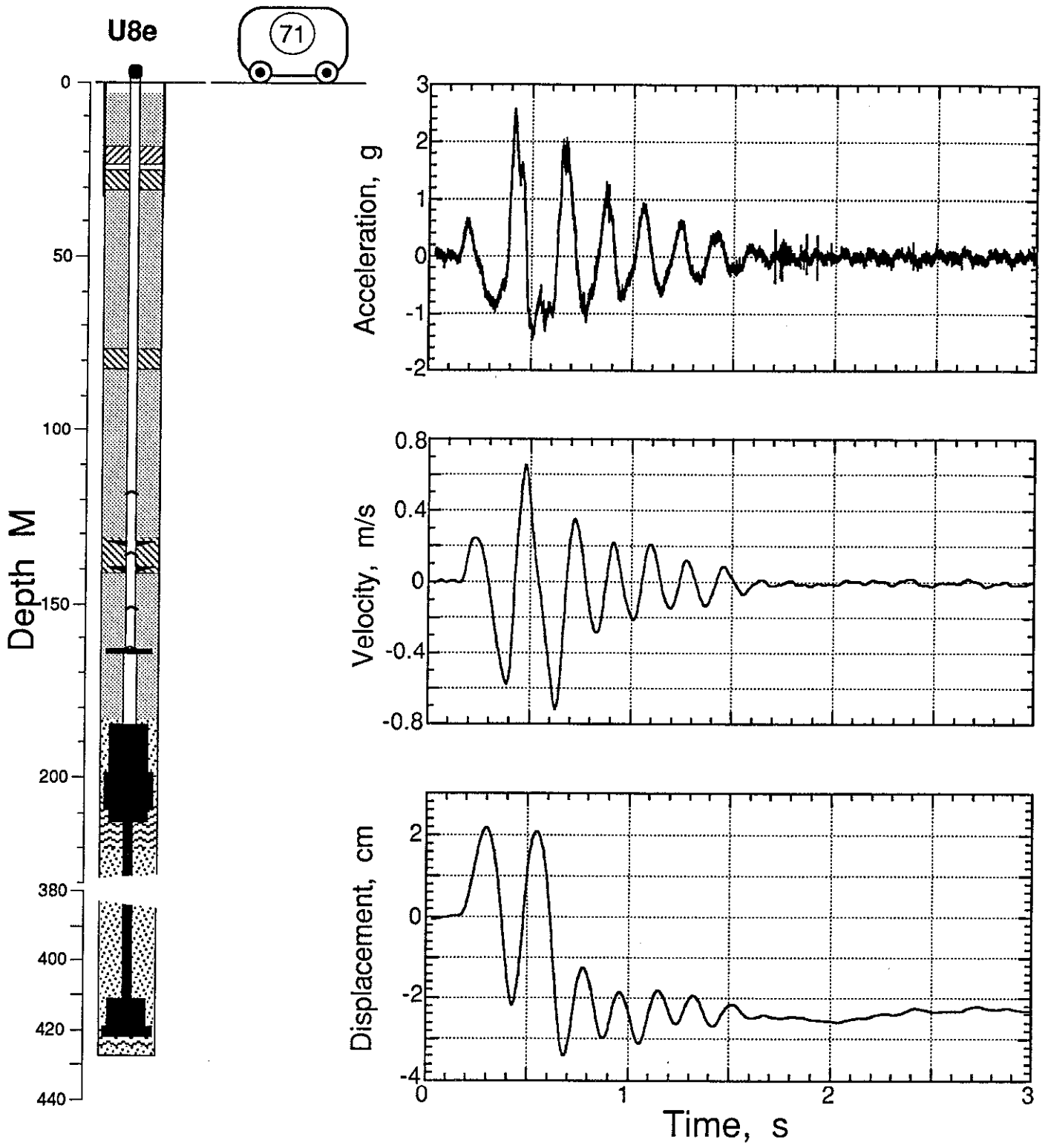


Figure 2.23 Explosion-induced vertical motion of the recording trailer (at a range of about 232 m).

Table 2.1 Summary of Free-Field Motion

| Gauge | Slant Range (m) | Arrival Time (ms) | Acceleration Peak (g) | Velocity Peak (m/s) | Displacement Peak (cm) | Displacement Residual (cm) |
|--------------------|--------------------|--|--------------------------|---------------------|------------------------|----------------------------|
| 4av ^(a) | 42.1 | - | - | - | - | - |
| 4uv ^(a) | | - | - | - | - | - |
| 5av ^(a) | 46.4 | - | - | - | - | - |
| 5uv | | | - | 9.0, 34.0 | 15 | (b) |
| 7av | 58.5 | 12 | 16,95 | 6, 33 | 0.09, 1.05 | (b) |
| 7uv | | | - | 5, 31 | 0.08, (b) | (b) |
| 8av | 66.9 | 15, 70 | 100,690 | 2.7, 9, 3.3 | 32 | (c) |
| 8uv | | | - | 2.7, 14, 3.1 | 37 | 23 |
| 21av | 73.8 | 18 ^(d) , 100 ^(e) | 4.0 | 2.4 | 17.7 | 9 |
| 21uv | | | - | 2.5 | 18.7 | 10 |
| 11av | 91.6 | 22 | 4, 13, 39 | 0.9, 2.3 | 22 | 19 ^(f) |
| 11uv | | | - | 0.7, 2.1 | 16 | 10 |
| 22av | 130.6 | 38 ^(d) , 100 ^(e) | 1.1 ^(e) , 0.3 | 0.24 | 2.7 | -1.5 |
| 22uv | | | - | 0.26 | 2.8 | -1.6 |
| 23av | 182.7 | 96 | 0.52 | 0.285 | 3.0 | -0.3 |
| 23uv | | | - | 0.30 | 3.2 | -0.4 |
| 13av | 210.6 | 65, 100 | 2.6, 5.2 | 0.31 | 2.5 | -6 ^(f) |
| 13uv | | (a) | - | - | - | - |
| 61av | 210.6 | 123 | 1.20 | 0.33 | 3.4 | 0.2 |
| 61uv | | | - | 0.33 | 3.7 | 0 |
| 71av | 235 ^(g) | 152 | 0.6 | 0.25 | 2.2 | -2.5 |

- (a) Channel not responding at zero time.
- (b) Channel lost before this value attained.
- (c) Channel invalid before this value attained.
- (d) Pipe-induced motion.
- (e) Ground motion masked by pipe motion.
- (f) Approximate.
- (g) Station in recording trailer.

Table 2.2 Containment-Related Accelerometer Characteristics

| <u>Gauge</u> | <u>Natural Frequency (Hz)</u> | <u>Damping Ratio</u> | <u>System Range (g's)</u> |
|--------------|-----------------------------------|----------------------|-------------------------------|
| 4av | 1700 | 0.55 | 2000 |
| 5av | 1650 | 0.55 | 2000 |
| 7av | 1900 | 0.65 | 1500 |
| 8av | 1870 | 0.65 | 1500 |
| 21av | 520 | 0.65 | 30 |
| 11av | 1750 | 0.65 | 500 |
| 22av | 350 | 0.55 | 15 |
| 23av | 350 | 0.55 | 15 |
| 13av | 760 | 0.75 | 100 |
| 61av | 400 | 0.65 | 15 |
| 71av | 220 | 0.65 | 10 |

Table 2.3 Containment-Related Velocimeter Characteristics

| Gauge | Natural Frequency (Hz) | Time to 0.5 Amplitude (s) | Calibration Temperature (°F) | Operate Temperature (°F) | Stop-Stop Range (m/s) | System Range (m/s) |
|-------|------------------------|---------------------------|------------------------------|--------------------------|-----------------------|--------------------|
| 4uv | 3.92 | 86 | 75.0 | 72.6 | 515 | 183 |
| 5uv | 3.79 | 65.4 | 74.5 | 72.7 | 380 | 152 |
| 7uv | 4.00 | 29.7 | 74.7 | 73.0 | 227 | 91 |
| 8uv | 4.17 | 33.5 | 74.5 | 76.1 | 274 | 91 |
| 21uv | (a) | (a) | 74.1 | 90.0 | (a) | 12 |
| 11uv | 3.50 | 12.2 | 75.2 | 72.0 | 81 | 30 |
| 22uv | (a) | (a) | 75.1 | 97.0 | (a) | 9 |
| 23uv | (a) | (a) | 74.6 | 102.0 | (a) | 9 |
| 13uv | 3.49 | 8.8 | 75.2 | 75.2 | 58 | 15 |
| 61uv | 3.61 | 8.3 | 74.8 | 71.0 | 52 | 12 |

(a) Values not available.

3. Emplacement Pipe Measurements

The deepest four sections of the emplacement pipe above the diagnostics canister were pressure sealed with either pressure domes or pressure plates. The deepest section was about 35 m long and contained the pin hole of the PINEX experiment near its top. The fourth sealed section was terminated with a pressure plate on top of which was the detector. The emplacement pipe between the detector plate (which was extracted to a receptacle above the ball valve closure on the top of the pipe) and the receptacle was evacuated. Shortly after the detonation the detector plate was recovered, the ball valve closed, and this receptacle was detached from the pipe and pulled to a location beyond the expected extent of the resulting collapse crater.

3.1 Pressure, Temperature, and Radiation

Each of the four sealed sections was monitored just below its sealing elevation for pressure and temperature. Additionally the bottom section was similarly monitored on both sides of the pipe near the diagnostics canister and at one point midway between the diagnostics canister and the first pressure dome. Pressure and radiation were monitored in the emplacement pipe near its top. The data received from these seven stations are shown in figures 3.1 -3.7. Unfortunately, the sample rate was too low to give a good representation of the data for stations 2 - 6. Appendix A contains the plots (figures A1 - A4) of the data from stations 2, 3, and 4 as digitized in 1978 and reported by C. W. Olsen. These are the only existing data sampled at a rate sufficient for analysis.

The data of figure 3.1 are suggestive of a temperature pulse of around 20 °C at about 60 ms and the pressure data suggest an early increase to nearly 130 bar before the gauge was lost. Only the low-ranged pressure transducer gave an acceptable reading at station 3 midway up the first sealed section of the emplacement pipe and the temperature probe yielded what appears to be useful information suggestive of gas flow in the section (figure 3.2). In figure 3.3 the pressure and temperature data at the end of the first sealed section indicate gas stagnation before the station was lost. Temperature and pressure at the upper end of the second sealed section of the emplacement pipe were monitored by station 6 (figure 3.4). It appears that this station measured no data until it was lost at about 110 ms.

Above the formation coupling plug, stations 9 and 10, monitoring the last two sealed sections of the emplacement pipe, disclosed that there was no increase in temperature and only a slight pressure increase in the section extending below that plug (figures 3.5 and 3.6). This suggests that there may have been a slow leak introduced in the second pressure dome and that the first and second pressure plates remained uncompromised. Failure of the second pressure dome is consistent with the suggestion of pipe failure in the region of station 34 (figure 2.3) at the elevation of the second pressure dome.

Radiation and pressure within the top portion of the emplacement pipe was monitored at station 12 (figure 3.7). No radiation was seen in the emplacement pipe above the detector plate before collapse, when the station was lost. The pressure remained constant and low until about 5.5 minutes when the PINEX detector recovery operations occurred, possibly resulting in a slow leak in the ball valve.

3.2 Motion

Vertical motion of the emplacement pipe was measured at six locations; at both of the pressure domes, at the detector plate, and near the top of the pipe below the ball valve. Additionally, positions just below the formation coupling plug and about 2.2 m below the tau can were monitored. Wave forms of motion from these locations are shown in figures 3.8 - 3.13. Transducer and wave form characteristics are given in Tables 2.1 -2.3.

Station 4 (figure 3.8) below the tau can does not appear to have yielded useful information, it is reported for completeness, as is the record recovered from the accelerometer at station 5 on the first pressure dome, above the tau can (figure 3.9). The wave form of the velocity at station 5 agrees quite well with that of station 7 at the elevation of the second pressure dome (figure 3.10). This wave form appears to travel up the pipe at a speed of about 4.5 Km/s, near the shear speed of the emplacement pipe (time of travel about 2.7 ms). See figure 3.14. The cause of signal loss can not be unambiguously determined from these data whether the cables or the pipe failed, however, the data beyond 120 ms are highly suspect. Above station 7, there are surviving motion data until collapse suggesting that the pipe remained intact at higher elevations.

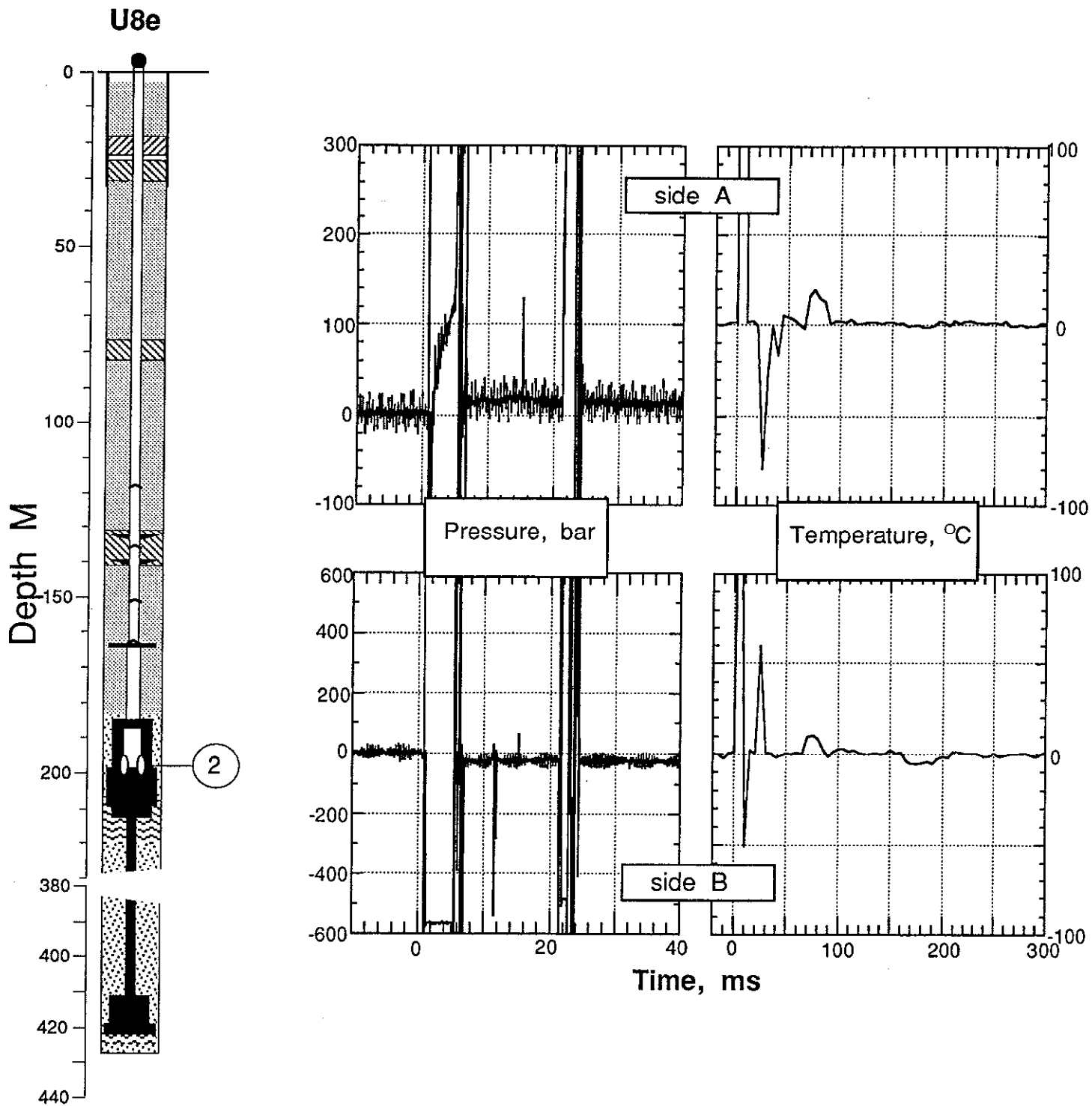


Figure 3.1 Pressure and temperature measured on opposite sides of the PINEX line-of-sight pipe near the diagnostics canister (station 2 at a depth of 197.66m). Detail and amplitude information was lost by inadequate data sample rate. Figures A1 and A2 show much of the same data at greater time resolution.

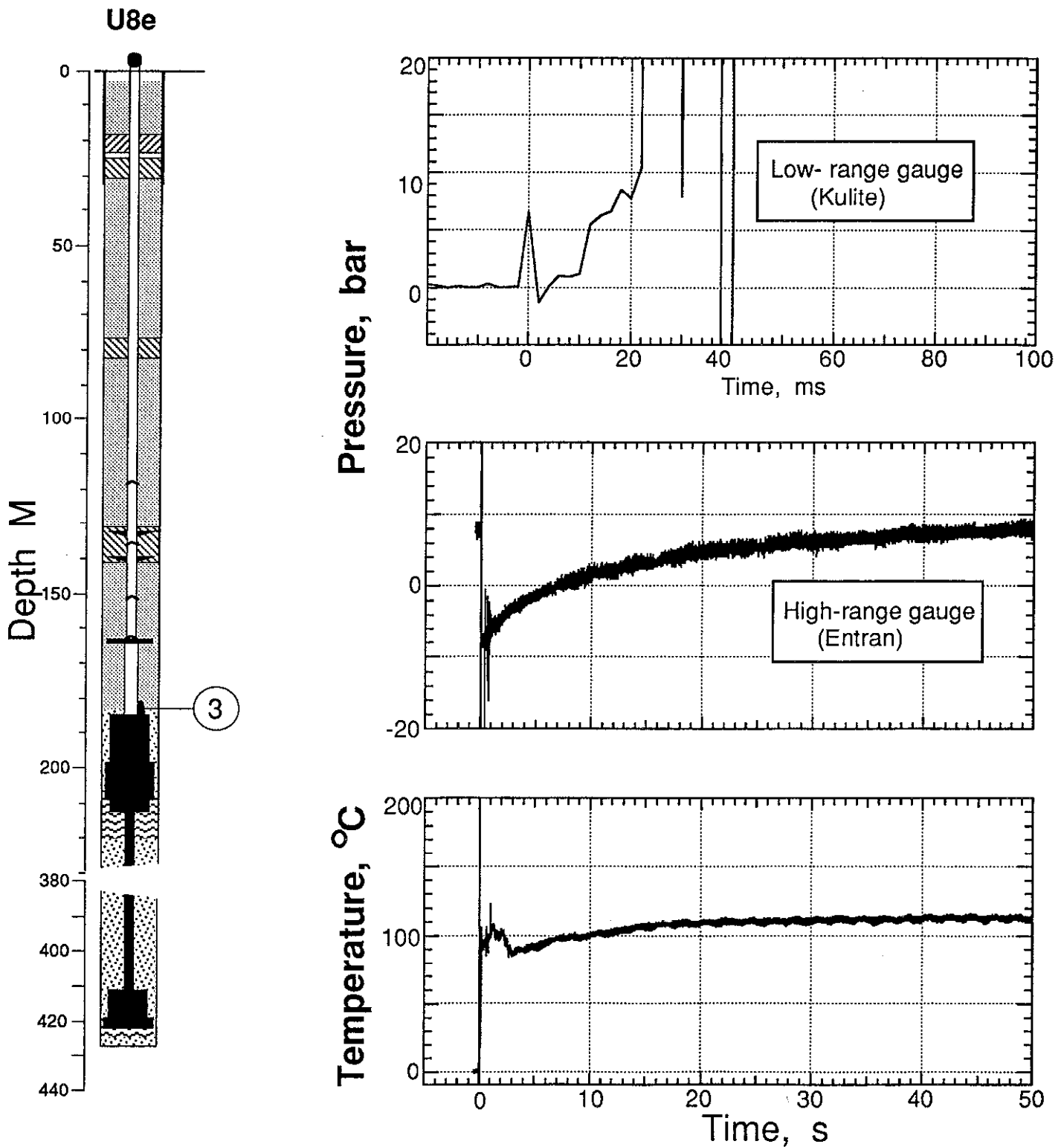


Figure 3.2 Pressure and temperature measured half way up the first sealed section of the emplacement pipe (station 3 at a depth of 183.12 m). Detail and amplitude information on the low-range pressure channel was lost by inadequate data sample rate. Figure A3 shows much of the same data at greater time resolution.

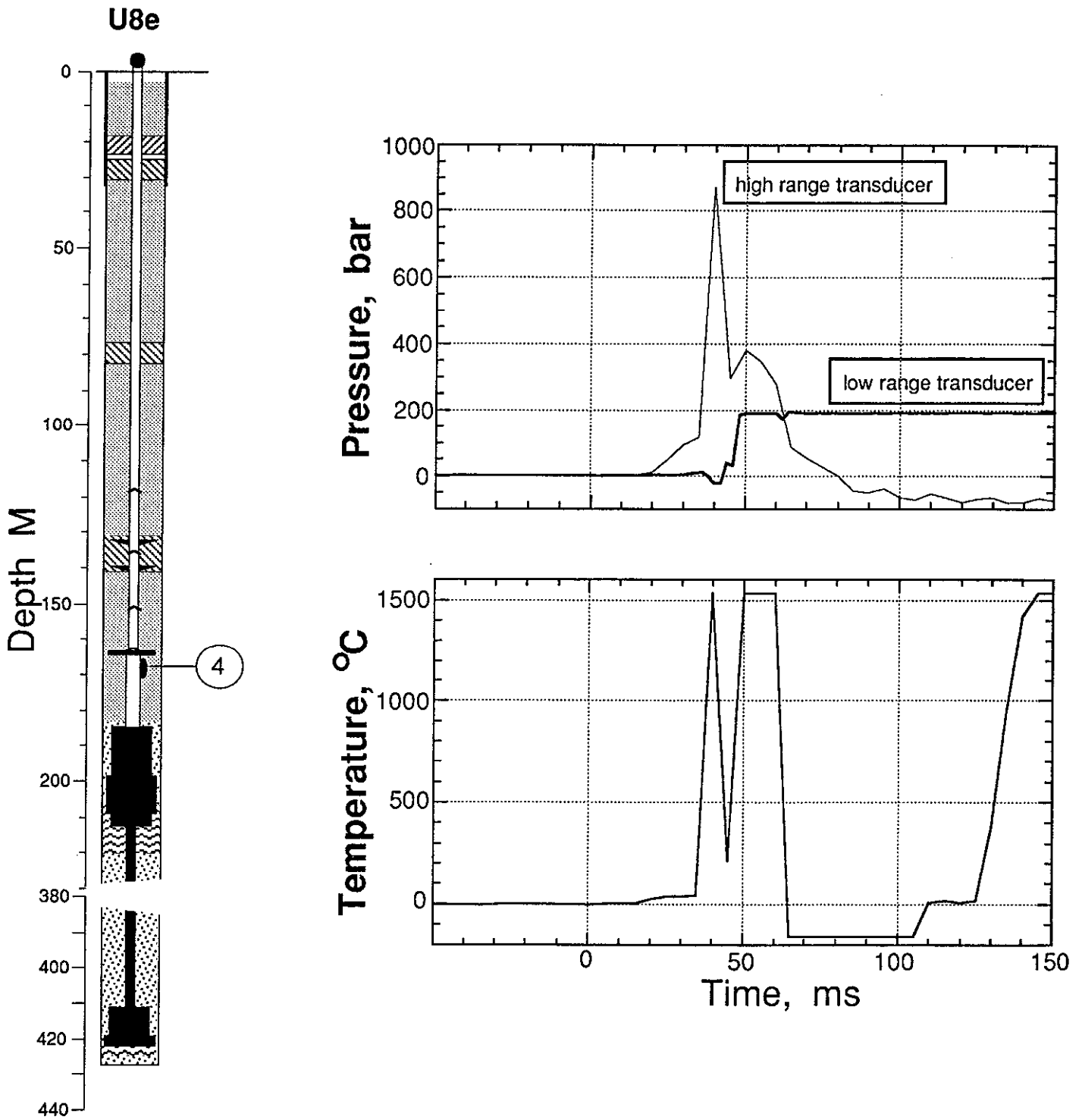


Figure 3.3 Pressure and temperature measured 4.41 m below the first pressure dome and 2.16 m below the bottom of the tau can (station 4 at a depth of 176.88m). Detail and amplitude information was lost by inadequate data sample rate. Figure A4 shows some of the same data at greater time resolution.

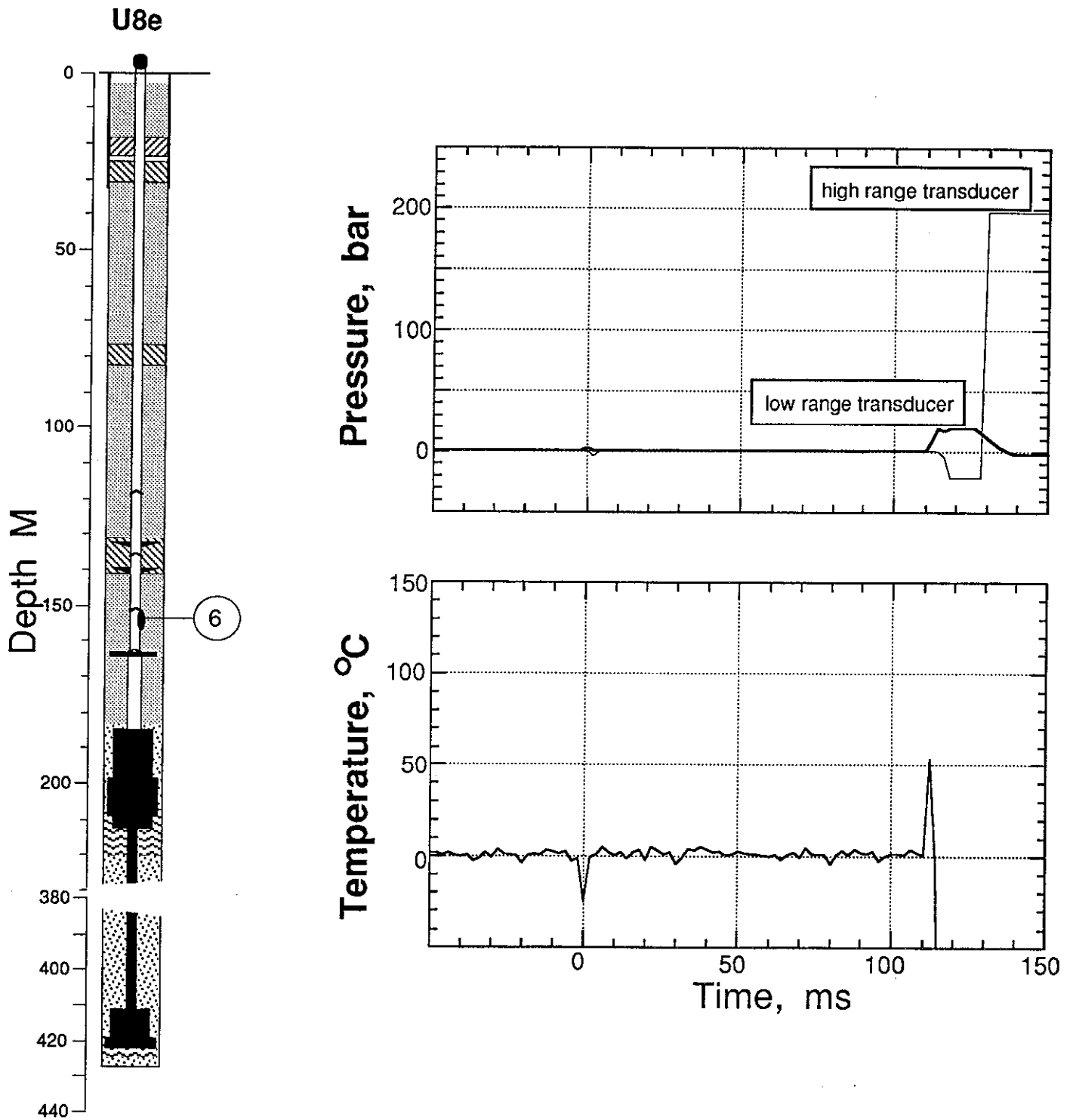


Figure 3.4 Pressure and temperature measured 0.15 m below the second pressure dome (station 6 at a depth of 163.62m). Detail and amplitude information was lost by inadequate data sample rate.

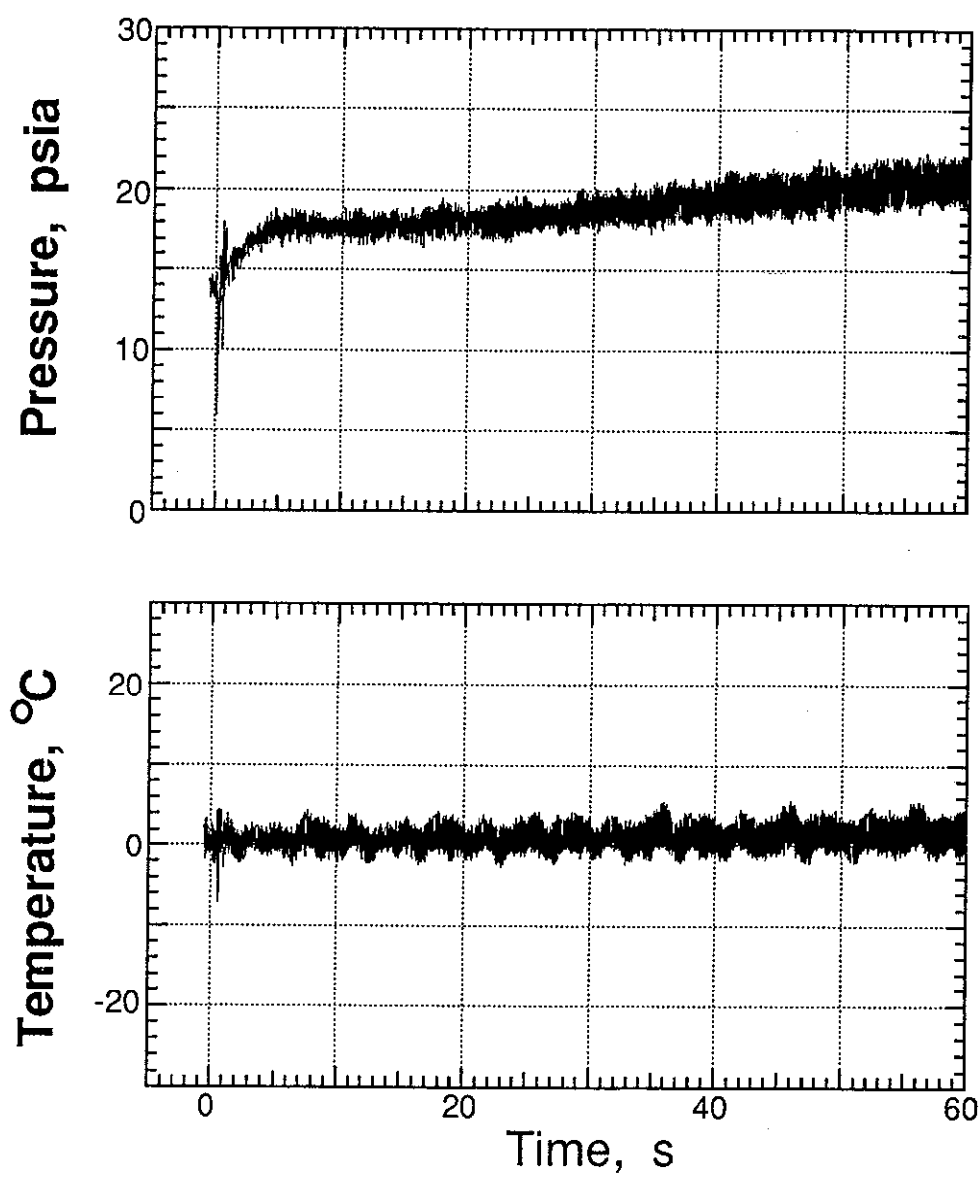
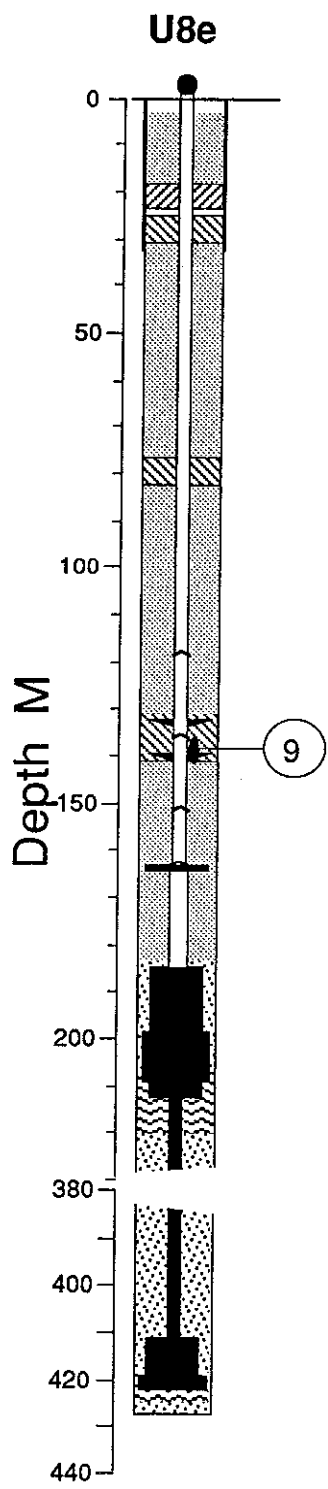


Figure 3.5 Pressure and temperature measured 1.83 m below the first pressure plate (station 9 at a depth of 138.07 m).

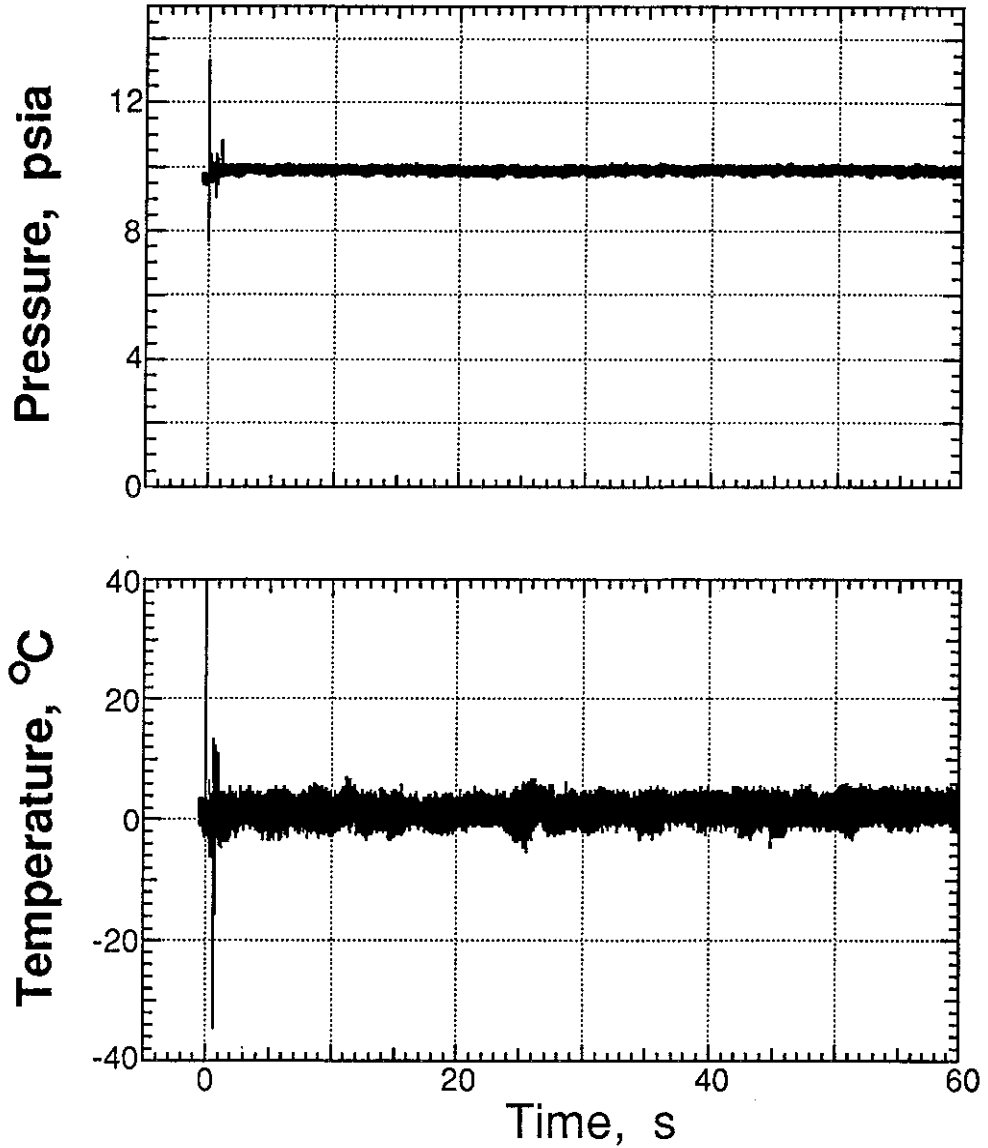
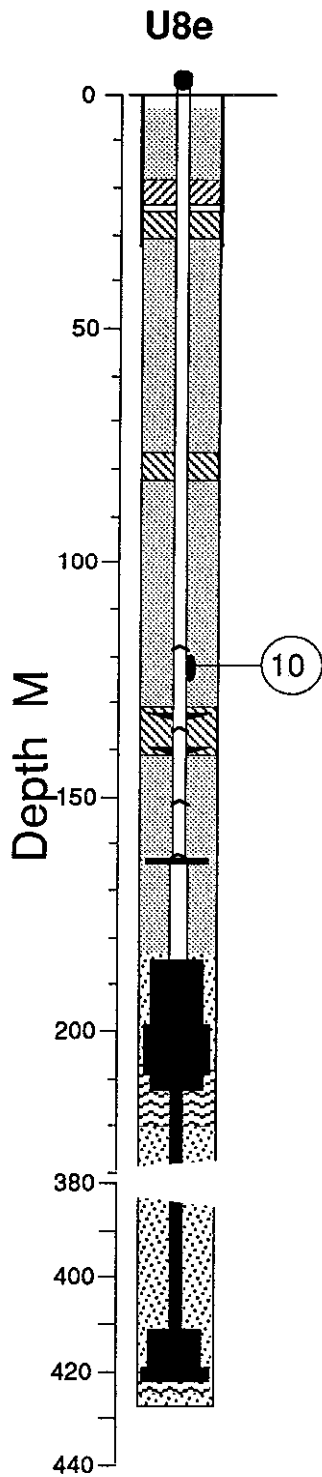


Figure 3.6 Pressure and temperature measured 3.88 below the second pressure plate (station 10 at a depth of 121.92 m).

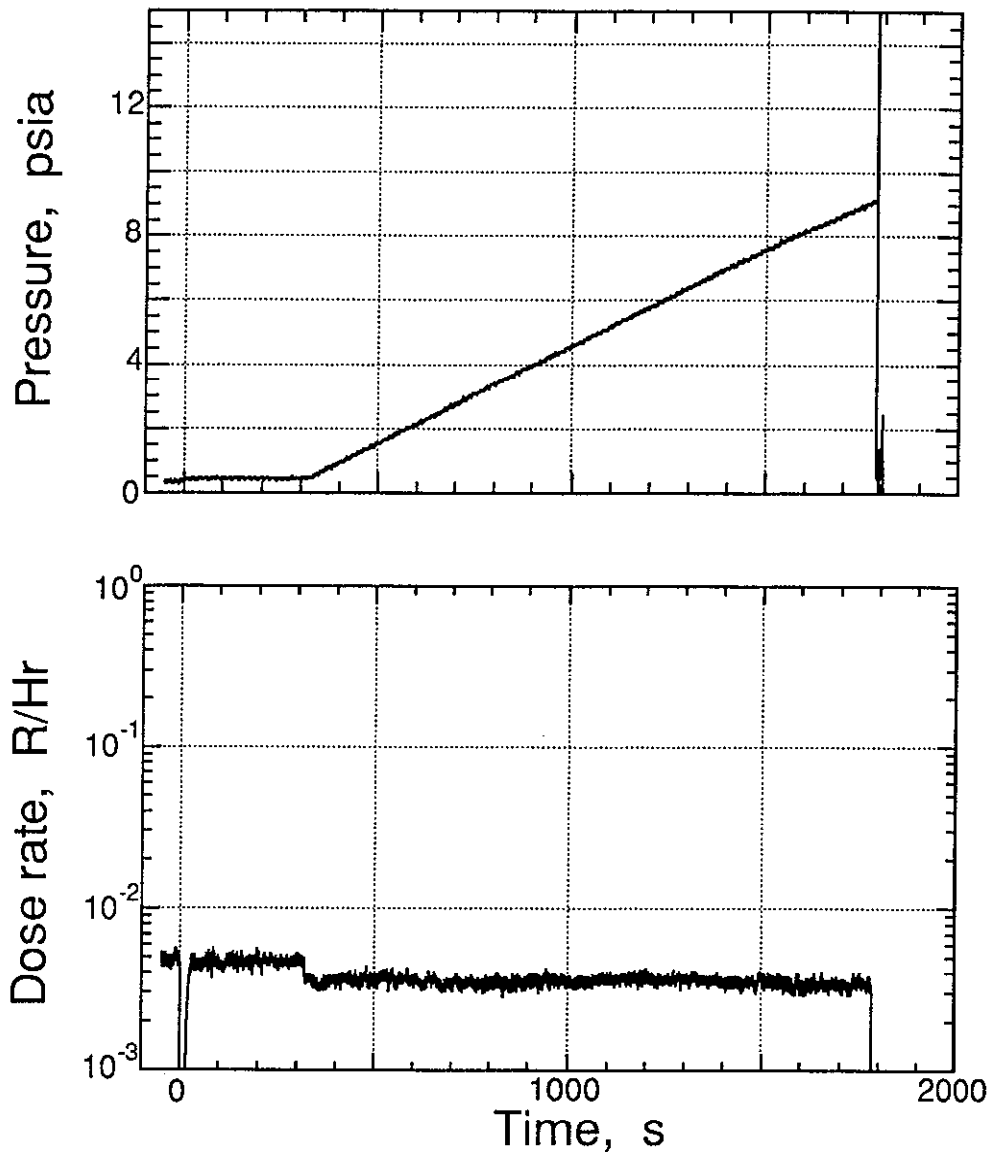
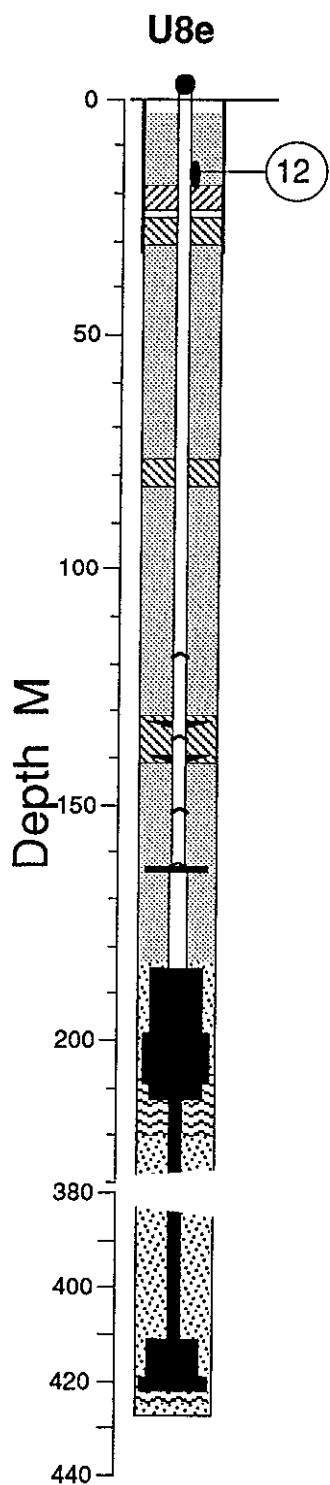


Figure 3.7 Pressure and radiation measured in the emplacement pipe near its top (station 12 at a depth of 15.54 m).

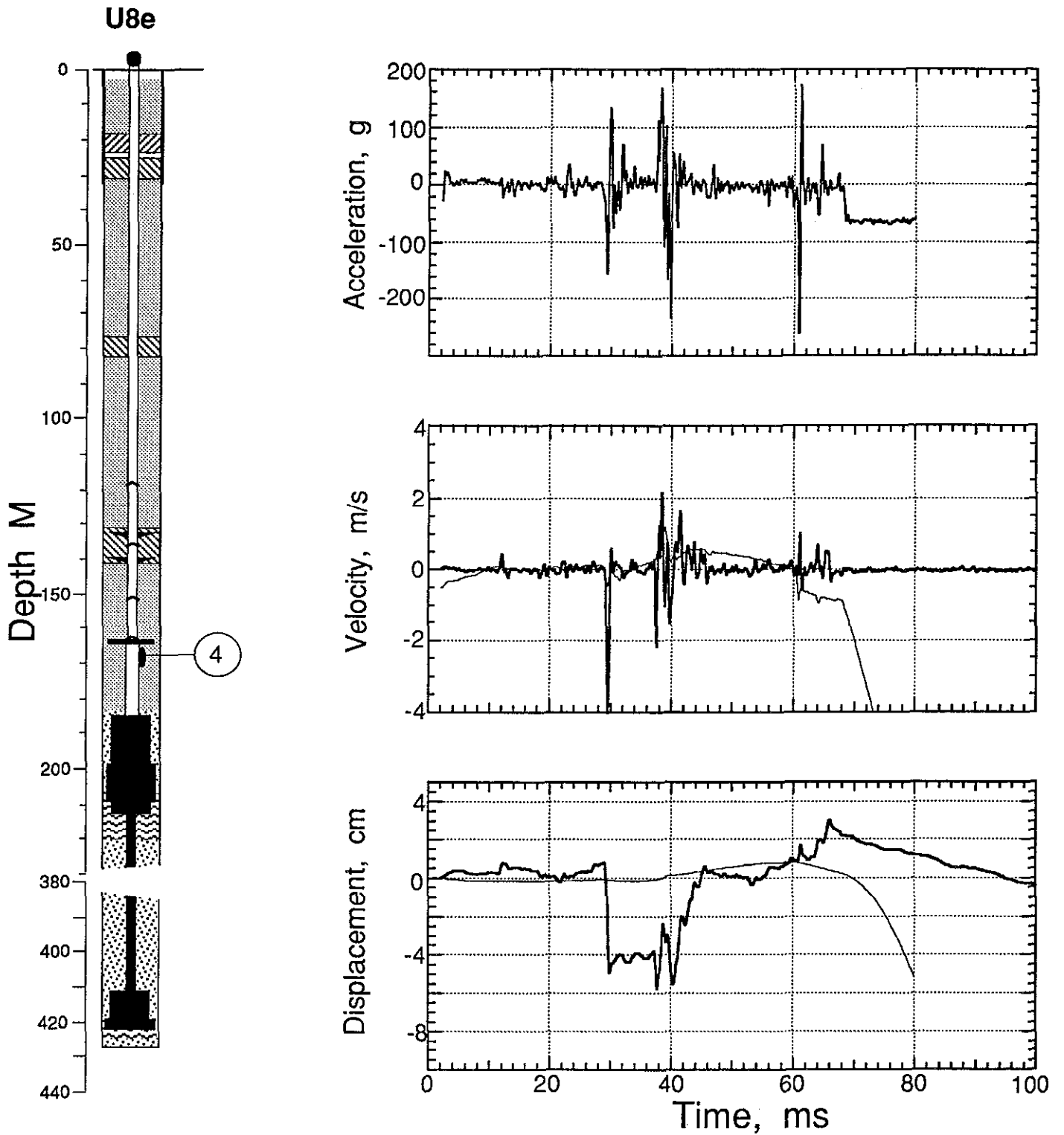


Figure 3.8 Vertical motion of the emplacement pipe 4.41 m below the first pressure dome and 2.16 m below the bottom of the tau can (station 4 at a depth of 176.88m). When there is more than one trace on a plot, the heavier is derived from the velocimeter.

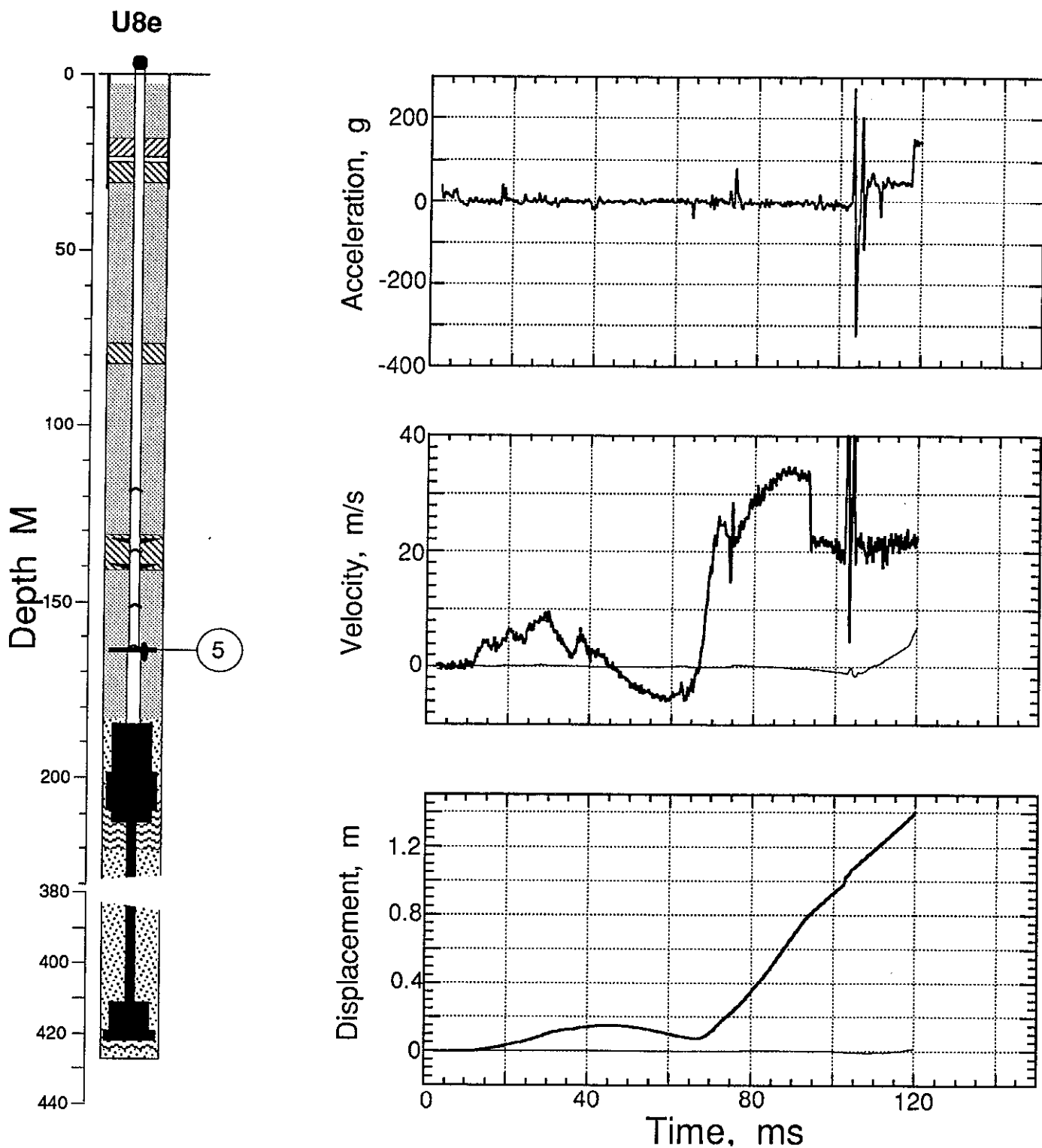


Figure 3.9 Vertical motion of the emplacement pipe 0.18 m below the first pressure dome (station 5 at depth of 163.62 m). When there is more than one trace on a plot, the heavier is derived from the velocimeter.

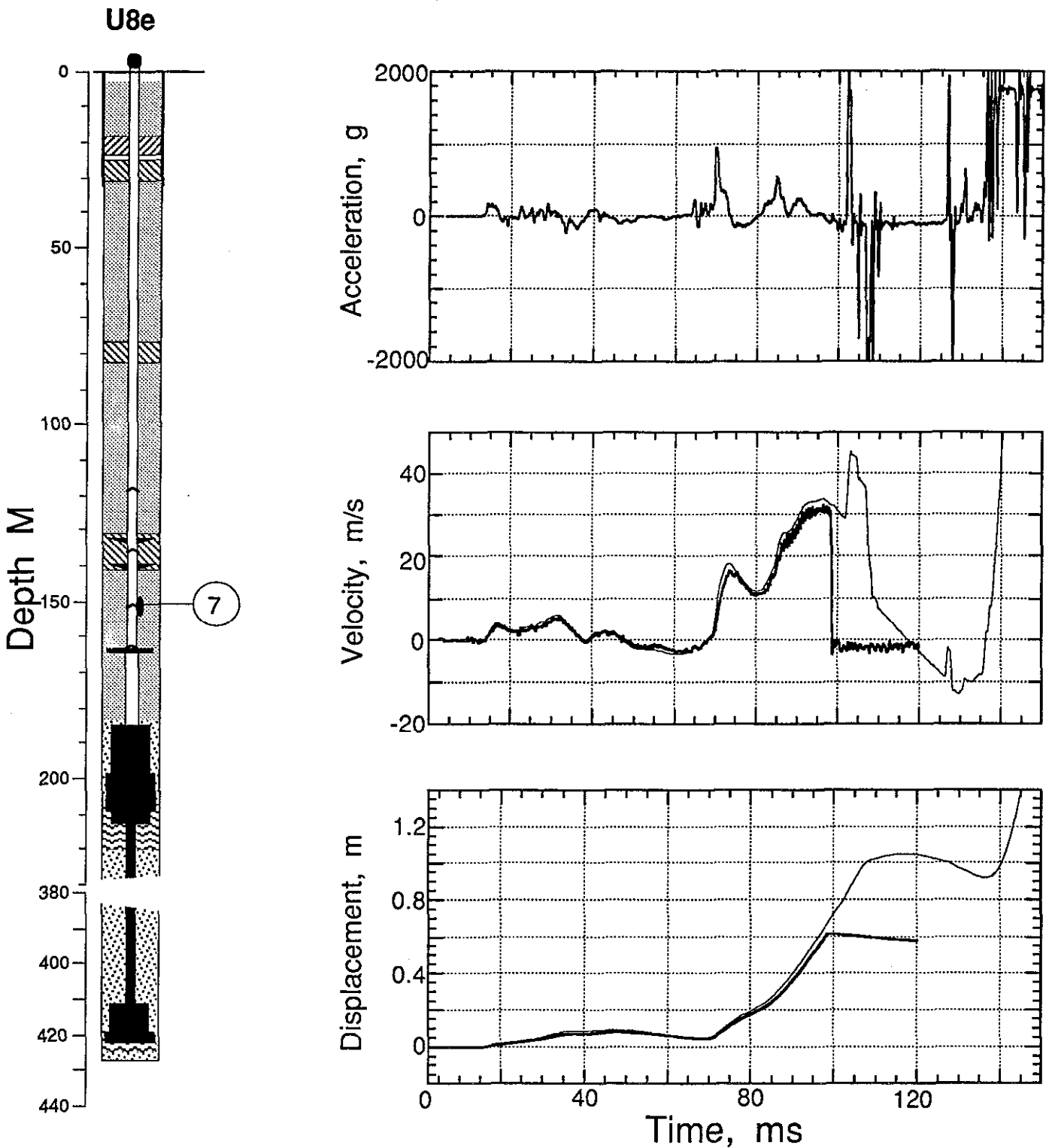


Figure 3.10 Vertical motion of the emplacement pipe measured 0.18 m below the second pressure dome (station 7 at a depth of 151.59 m). When there is more than one trace on a plot, the heavier is derived from the velocimeter.

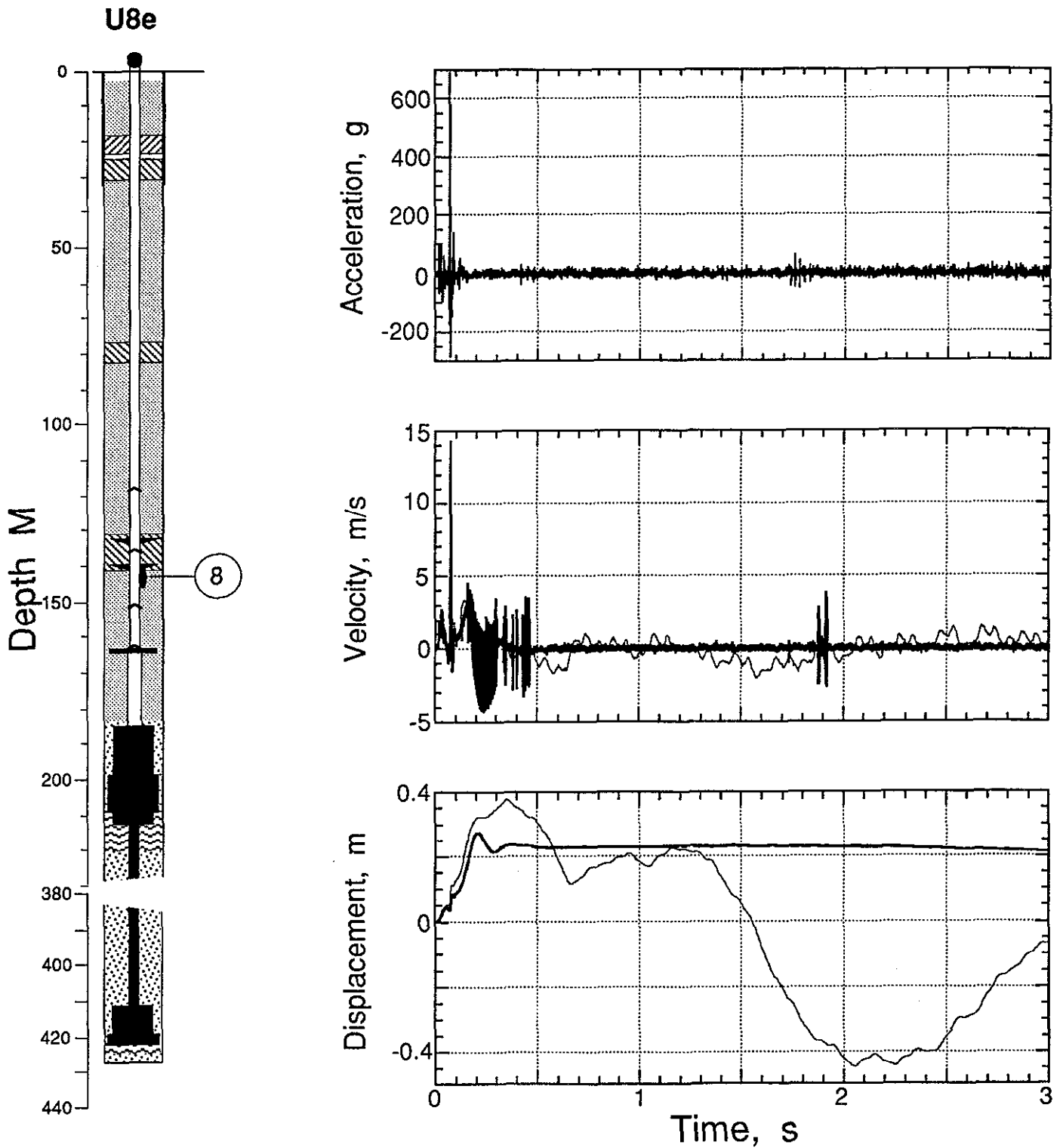


Figure 3.11 Vertical motion of the emplacement pipe measured 1.98 m below the bottom of the formation coupling plug (station 8 at a depth of 142.1 m). When there is more than one trace on a plot, the heavier is derived from the velocimeter.

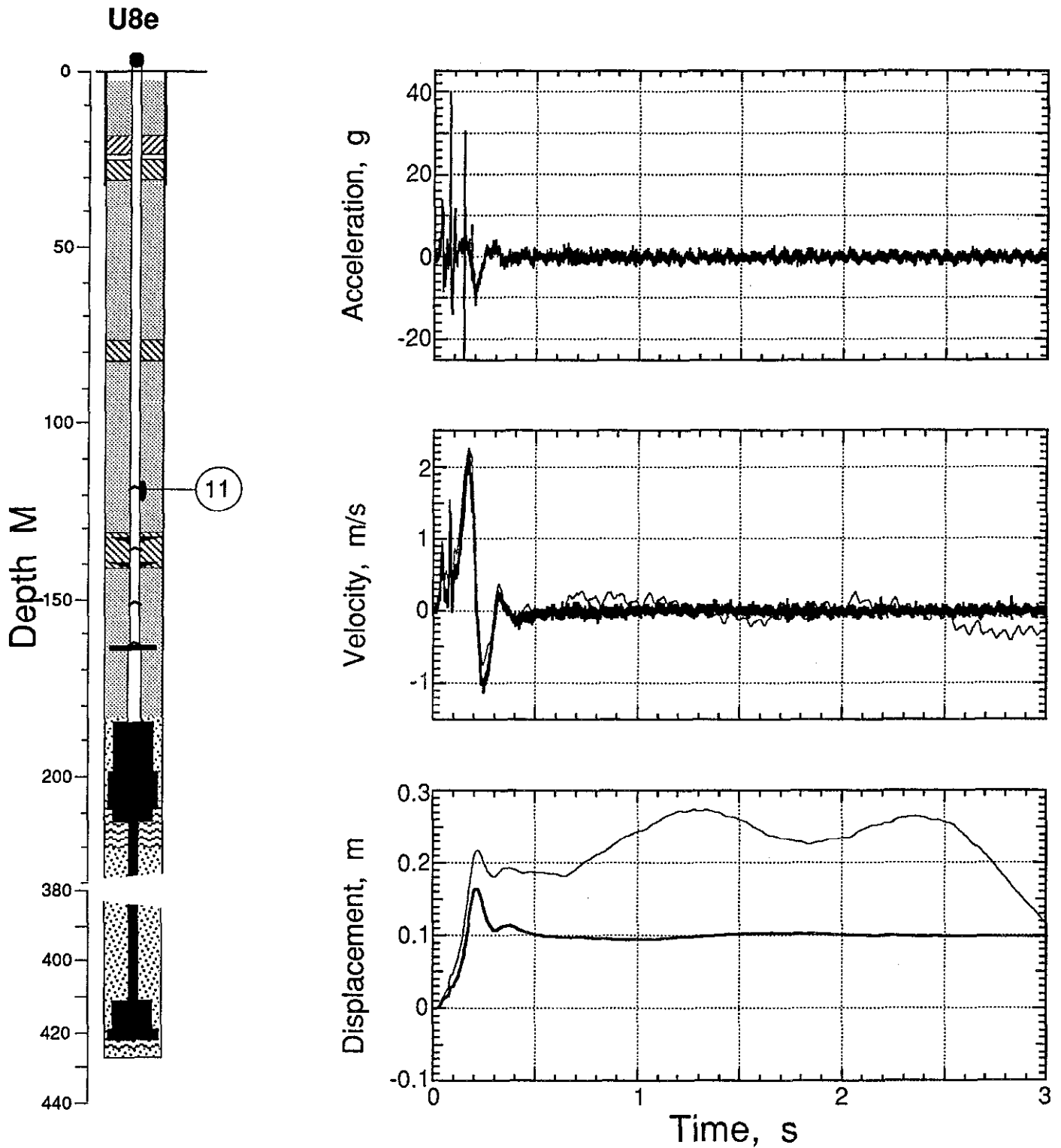


Figure 3.12 Vertical motion of the emplacement pipe measured 0.15 m below the second pressure plate (station 11 at a depth of 118.41 m). When there is more than one trace on a plot, the heavier is derived from the velocimeter.

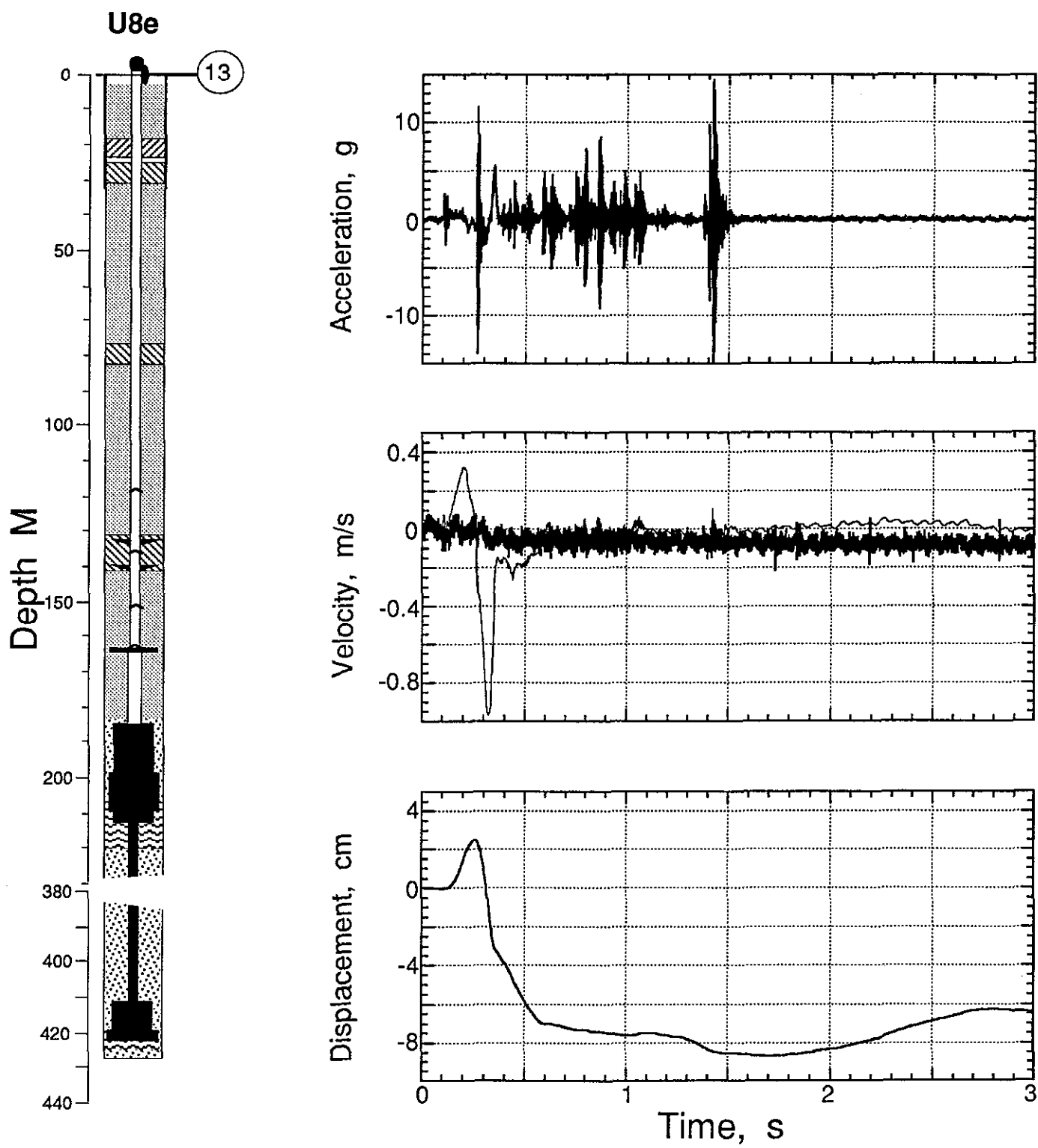


Figure 3.13 Vertical motion of the top of the emplacement pipe measured 0.61 above the ground surface and below the ball valve (station 13). When there is more than one trace on a plot, the heavier is derived from the velocimeter. Note that the velocimeter data are not represented in the displacement plot.

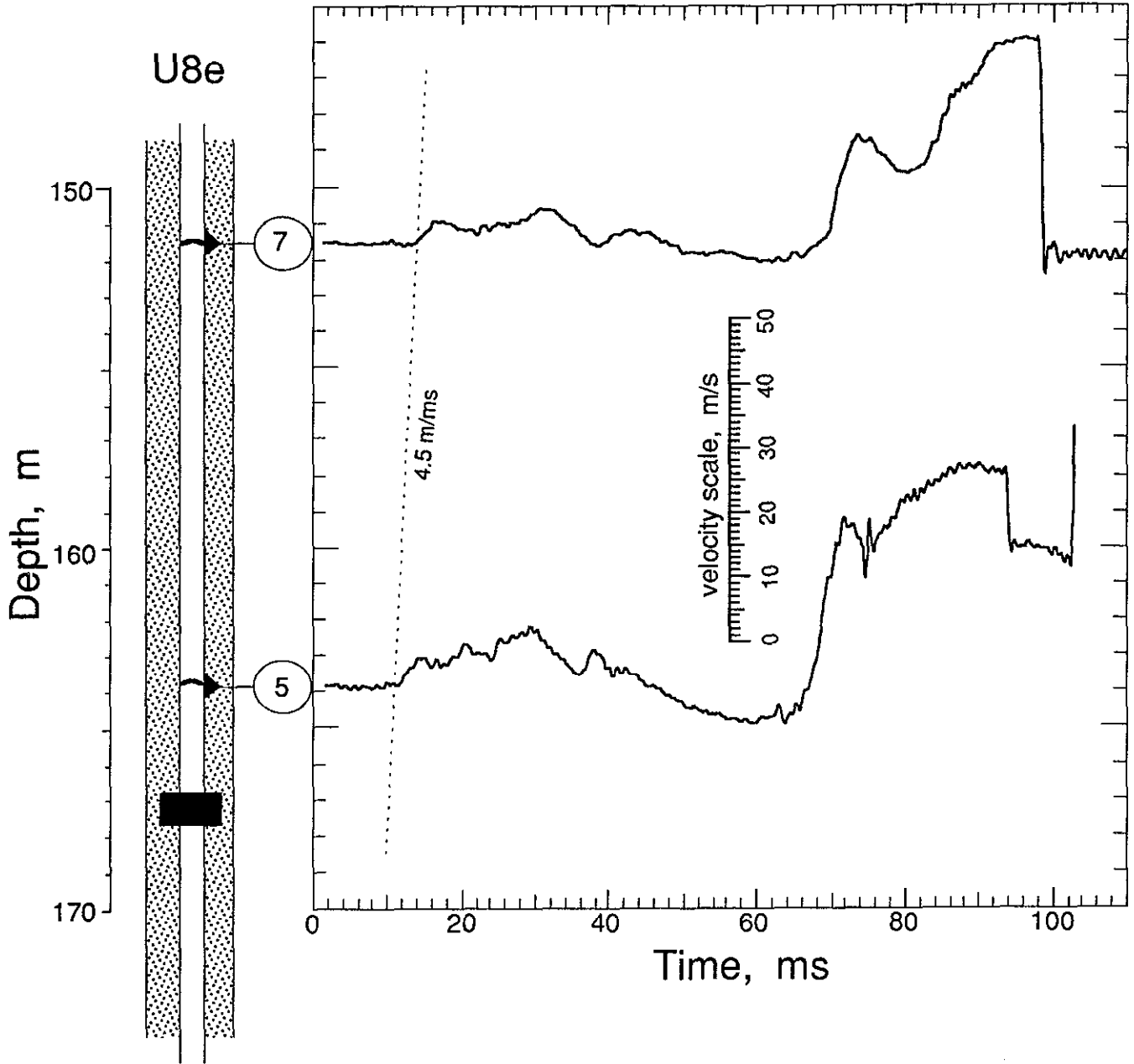


Figure 3.14 Comparison of velocity wave forms obtained from the emplacement pipe at the two pressure domes. The nearly identical wave forms are separated by 12 m and 2.7 ms.

4. Measurements During Collapse

4.1 Motion

Figures 4.1 - 4.7 contain the wave forms of the motion captured during the collapse phase measured in the rigid plugs of the emplacement hole and on the emplacement pipe. The accelerometer channels of stations 8 and 11 were not recorded at collapse and are thus not represented in figures 4.1 and 4.3. The velocimeter of station 13 was defective for the detonation (figure 3.12), but the velocimeter data are shown in figure 4.6 for completeness. Data from the top plug (station 23) and the ground surface (station 61) are also presented in figures 4.4 and 4.7 for completeness but should probably be disregarded.

The first few seconds of collapse (from about 1781 s to 1784 s) yield nearly the same motion for all stations fastened to the emplacement pipe (figures 4.1, 4.2, 4.3, and 4.6). Stations 8 and 11 were lost after about a 1 m drop and station 21, in the formation plug, fell almost 3 m before its cables were parted. Stations 21, 22, and 23 were emplaced with 6-pair stretch cable which is rated at 30% strain before failure. These data strongly suggest that the emplacement pipe was an integral unit between stations 8 (at a depth of 143 m) and the top. The data from station 13 at the top of the pipe (initially about 1 m above the ground surface) shows a drop of nearly 10 m before being lost. (By inference, the formation coupling plug also dropped by at least this much.) This motion would place station 13 about 6 m below the top surface of the stemming in the hole. Erosion of the cables during the drop through the stemming could account for that station's loss. This could also account for the loss of pressure and radiation signals at station 12 (figure 4.8).

The emplacement pipe was "greased" with hydroseal at the elevation of the stemming platform allowing smooth motion of the pipe through it. Station 22 was fielded in this plug (the stemming platform) and the collapse motion at this location (figure 4.4) does not show the motion of the emplacement pipe. However, the velocity of station 13 (figure 4.6) shows an offset at about 1786 s, the time of collapse of station 22. Close observation of the raw data shows that the signals from station 22 were lost at about 1817.4 s with the acceleration and velocity channel losses being separated by about 0.1 s.

4.2 Pressure and Radiation

Pressure and radiation histories obtained during the collapse period are displayed in figures 4.8 - 4.16. Data from station 32 are omitted since it was determined that signals from that station were lost shortly after detonation.

All of the pressure histories show the usual pressure drop resulting from stemming fall. The pressure channel of station 33 (figure 4.9) survived the collapse for about 17 s and then was lost at 1796.8 s. See figure 2.2. At the same station, the radiation channel indicates a decrease in dose rate possibly due to an increase in stemming shielding of the radiation upon collapse until 1829 s at which time the radiation abruptly jumps to almost 3000 R/Hr and last for about 1 s and is then lost.

The radiation channel of station 37 (figure 4.13) appears to survive collapse, however the constant level for an extended time tends to negate its validity. Slight radiation changes immediately upon collapse at all stations above the formation coupling plug (figures 4.12 - 4.16) may have been, at least partly, due to collapse-induced motion of the source chips relative to the detectors in each of the stations.

Station 38 (figure 4.14, below the stemming platform) survived collapse until 1831.8 s while the station just above the platform (station 39, figure 4.15) was lost at about 1827 s. Such a long survival in view of the 2 m drop of the stemming platform at 1786 s and that the pressure and radiation stations were not fielded with stretch cable is surprising.

Again, there is a stemming drop-induced pressure decrease at station 40 just below the top plug (figure 4.16) accompanied by a slight, abrupt change in radiation level resulting in a lower level than that produced by the reference chip before the experiment. This strongly suggests that the chip moved relative to the detector due to collapse motion. Since this station survived indefinitely, the data are presented for a period of about 33 hours after detonation in figure 4.17. This plot required the "patching" together of the records from at least 10 analog tapes. The discontinuous nature of the traces was occasioned by the lack of tape speed compensation, individual calibrations on each tape, and the switching of tapes during the run. What is apparent is the arrival of radiation at the bottom of the top plug at about 4300 s (1.19 hours). At about 11.6 hours there appears to be an additional stemming fall onto the station that briefly increases pressure without changing the radiation level.

Figure 4.18 is a composite plot of all the pressure records during the collapse phase as functions of both time and initial depth. Also displayed are the wave forms of the displacement of the two bottom rigid plugs; no motion was registered during this time period in either the top plug nor the ground surface. Breakage positions of the two CLIPER cables in the emplacement hole are also shown; station 93 on the emplacement pipe and station 94 on the instrumentation pendant in the stemming.

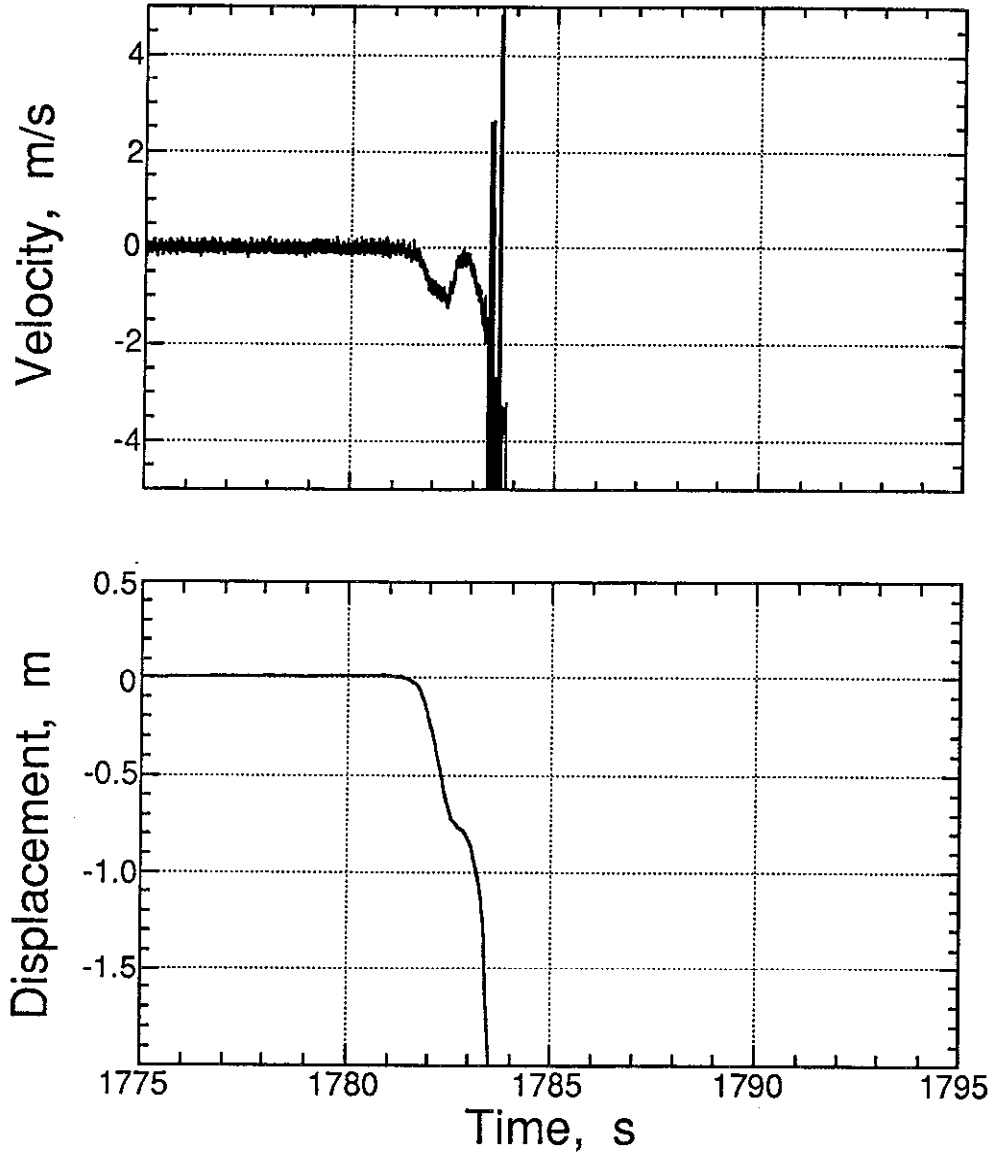
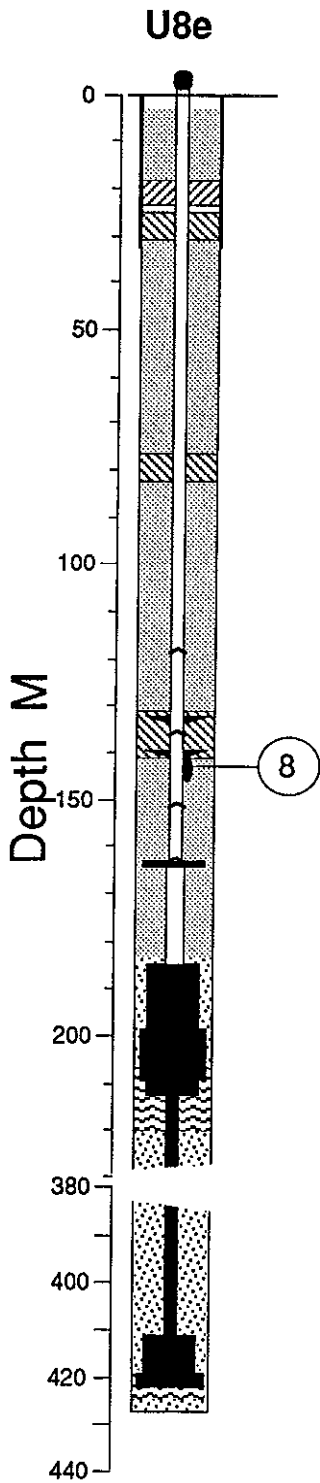


Figure 4.1 Vertical motion of the emplacement pipe just below the formation coupling plug (station 8 at a depth of 143.1 m) during collapse.

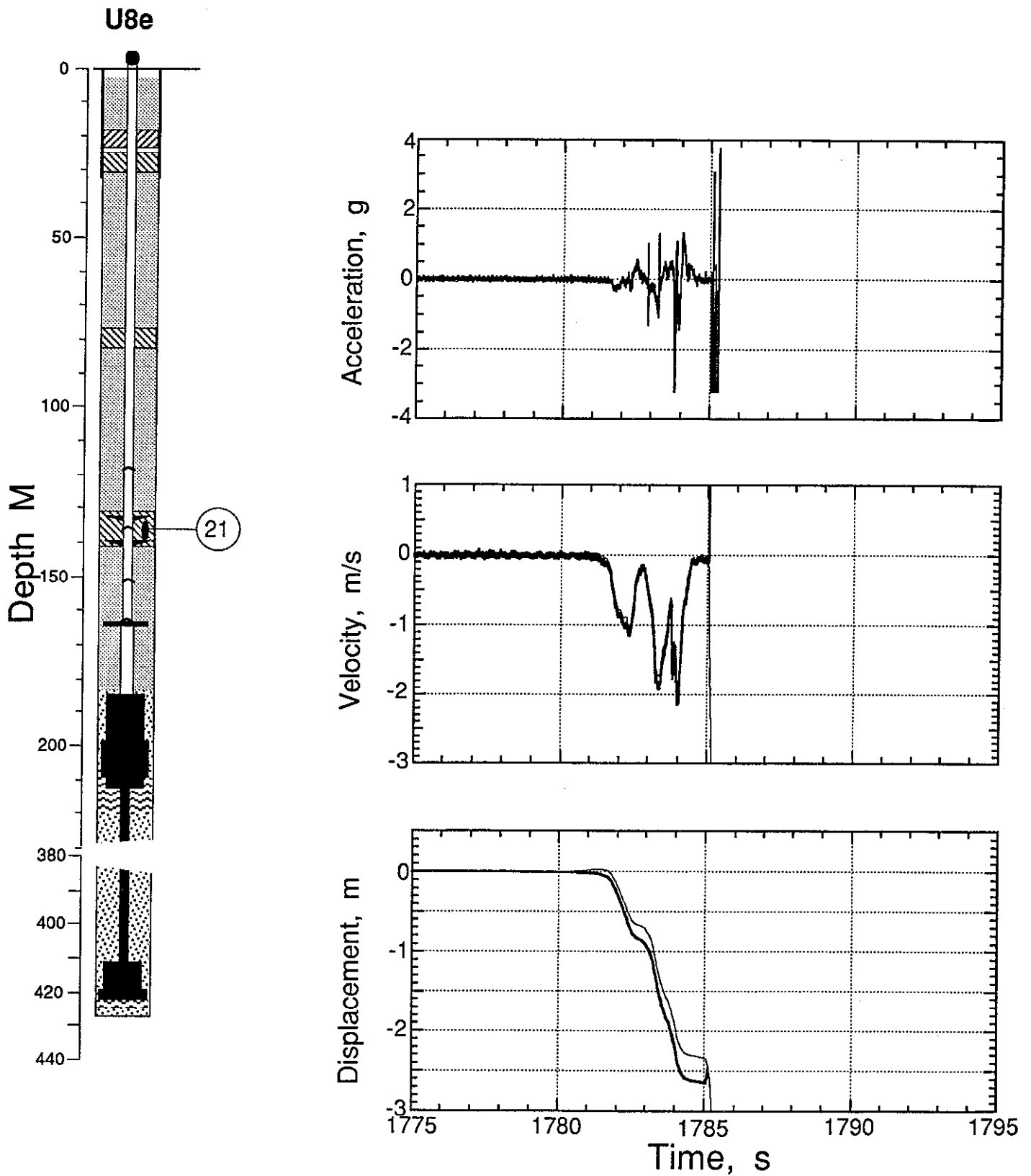


Figure 4.2 Vertical motion of the formation coupling plug (station 21 at a depth of 136.3 m) during collapse. When there is more than one trace on a plot, the heavier is derived from the velocimeter.

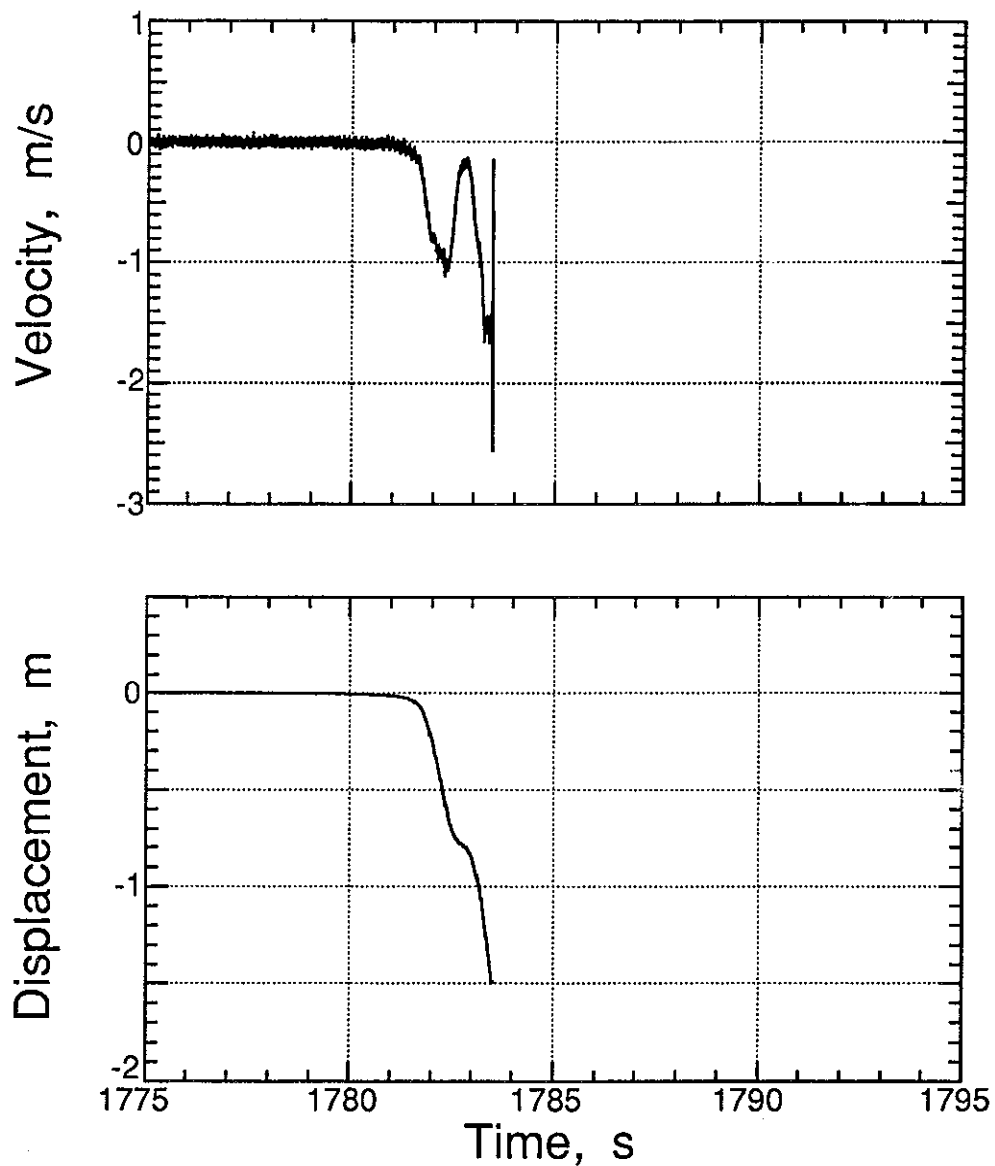
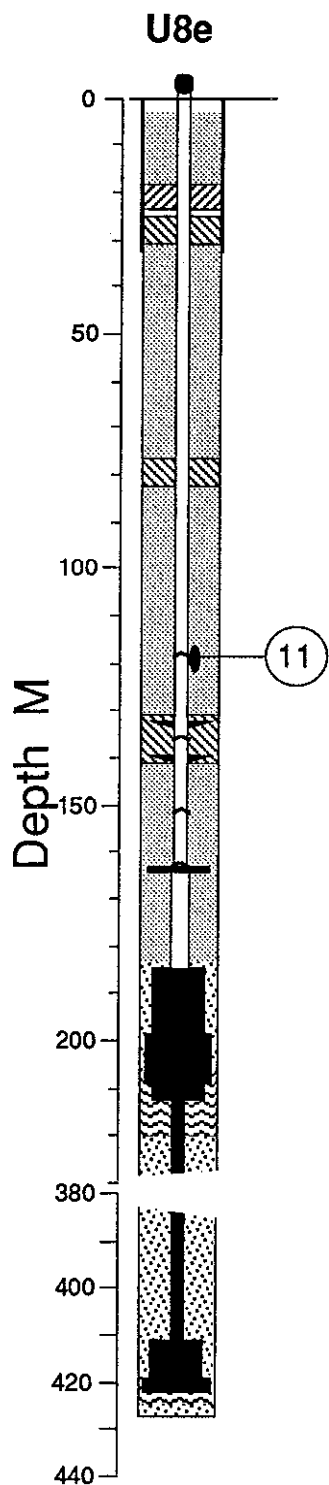


Figure 4.3 Vertical motion of the emplacement pipe above the formation coupling plug at the top pressure plate (station 11 at a depth of 118.4 m) during collapse.

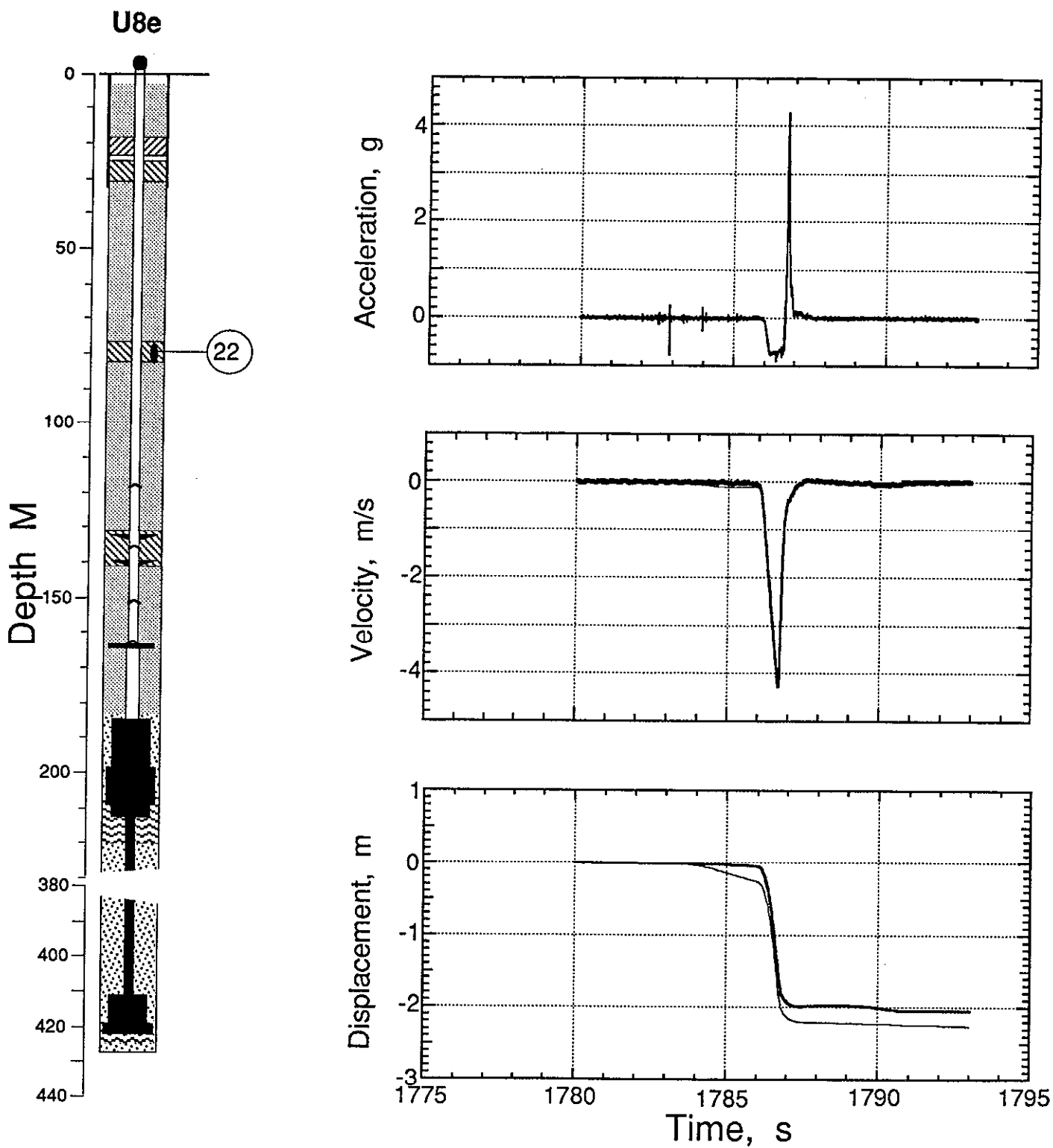


Figure 4.4 Vertical motion of the stemming platform (station 22 at a depth of 79.6 m) during collapse. When there is more than one trace on a plot, the heavier is derived from the velocimeter.

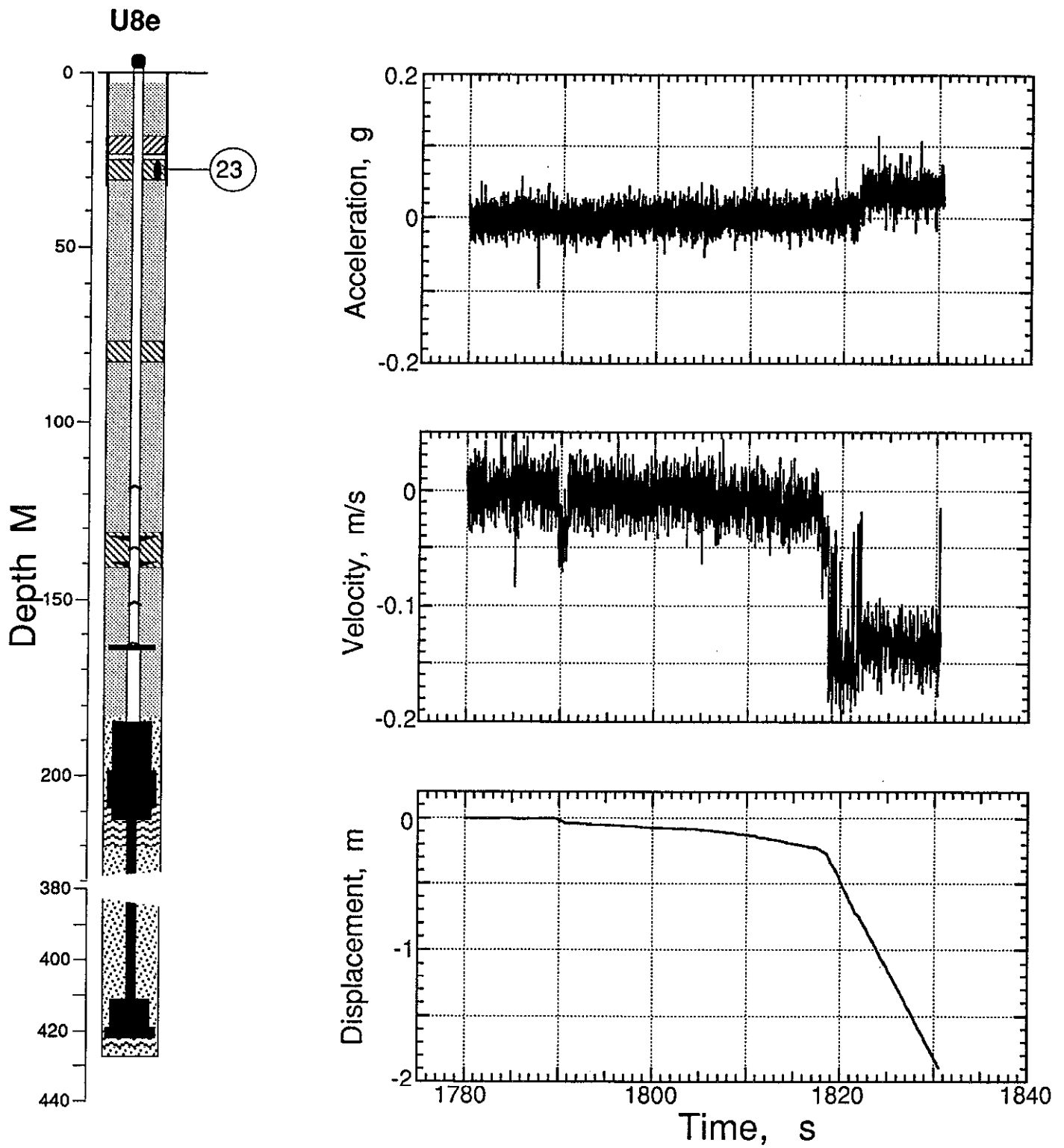


Figure 4.5 Vertical motion registered in the top plug (station 23 at a depth of 27.7 m) during collapse.

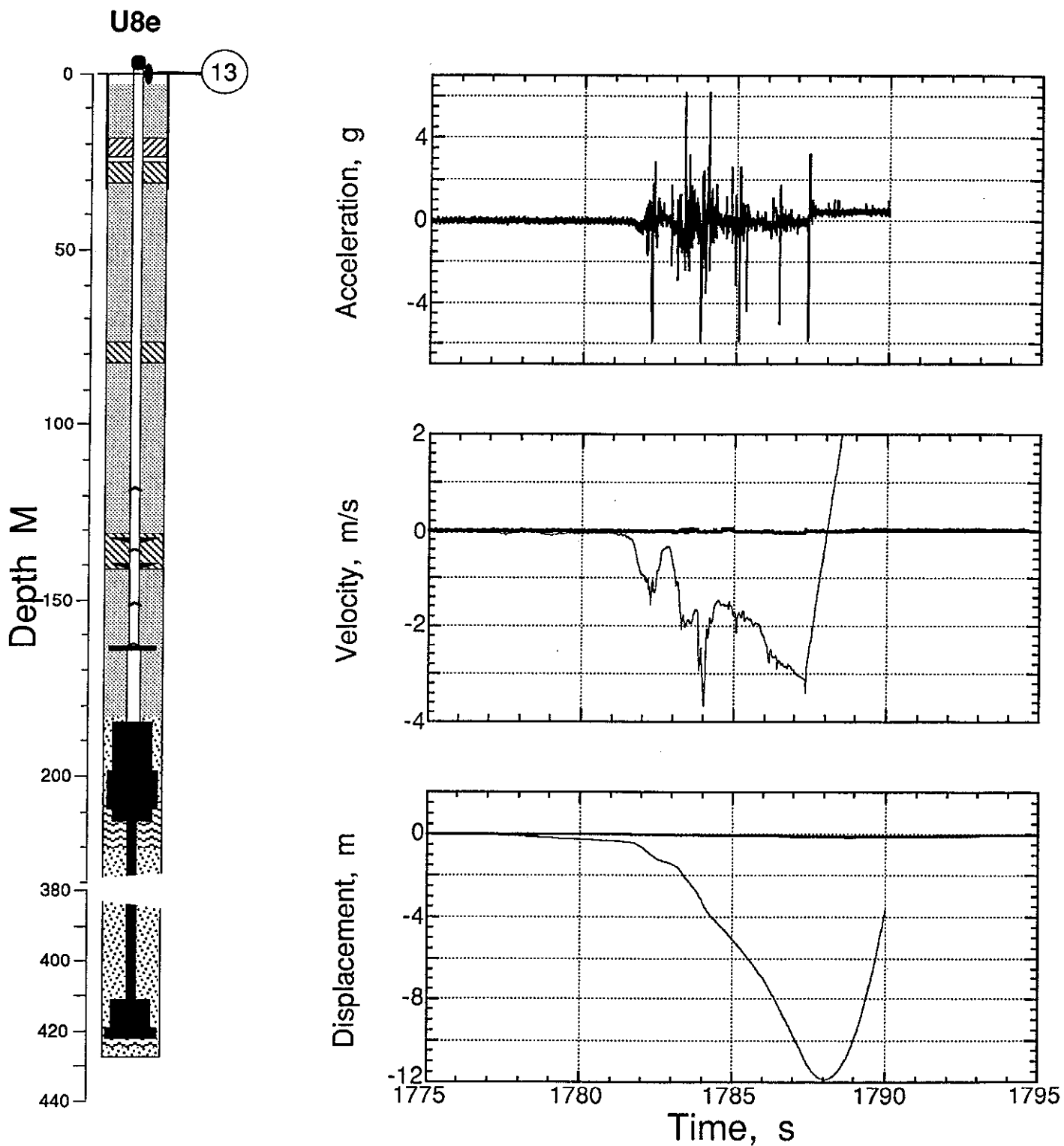


Figure 4.6 Vertical motion of the top of the emplacement pipe just below the ball valve (station 13 at an elevation of 0.8 m above ground surface) during collapse. When there is more than one trace on a plot, the heavier is derived from the velocimeter.

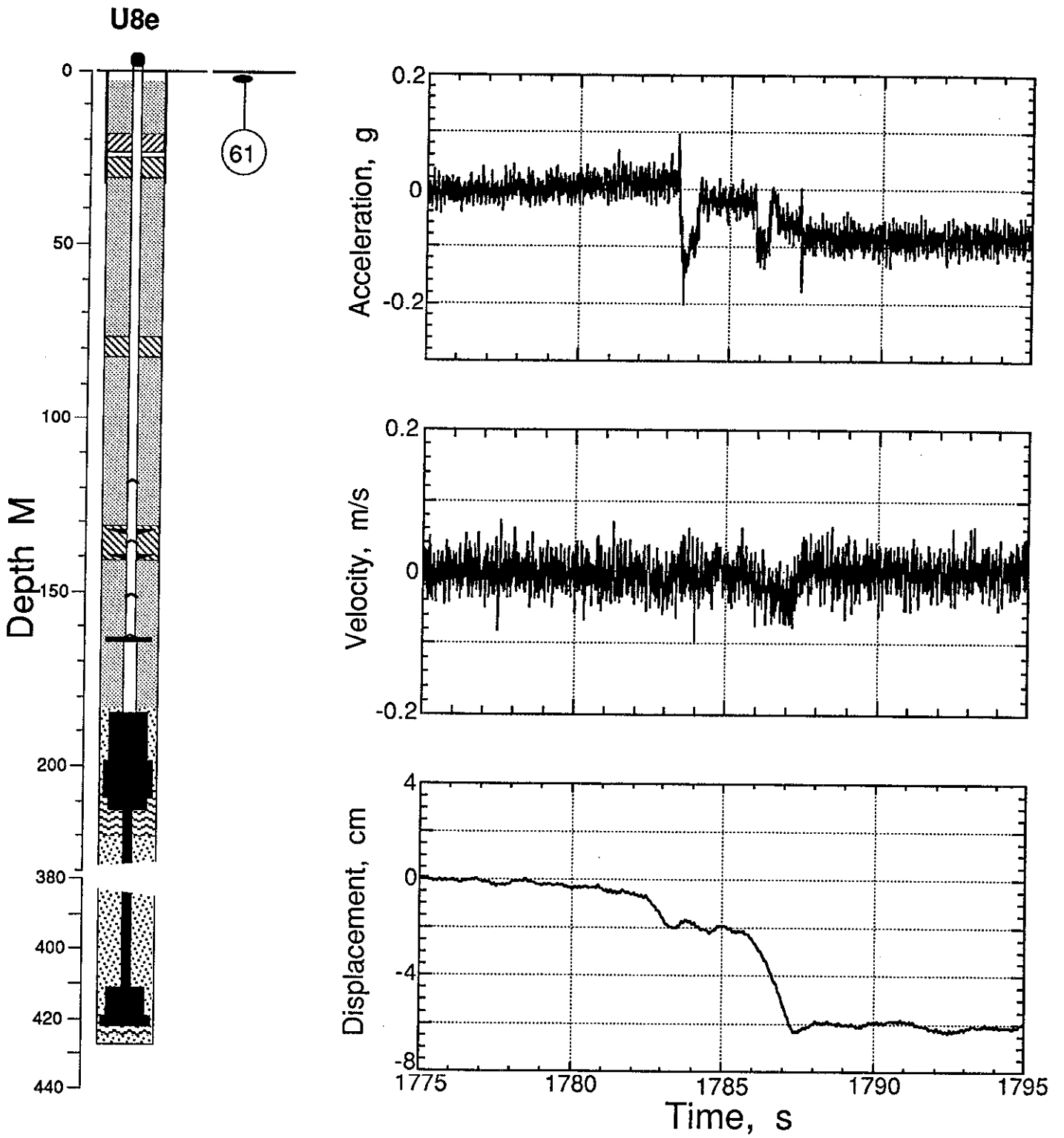


Figure 4.7 Vertical motion of the ground surface (station 61 at depth of 1.2m and horizontal range of 15.2 m) during collapse.

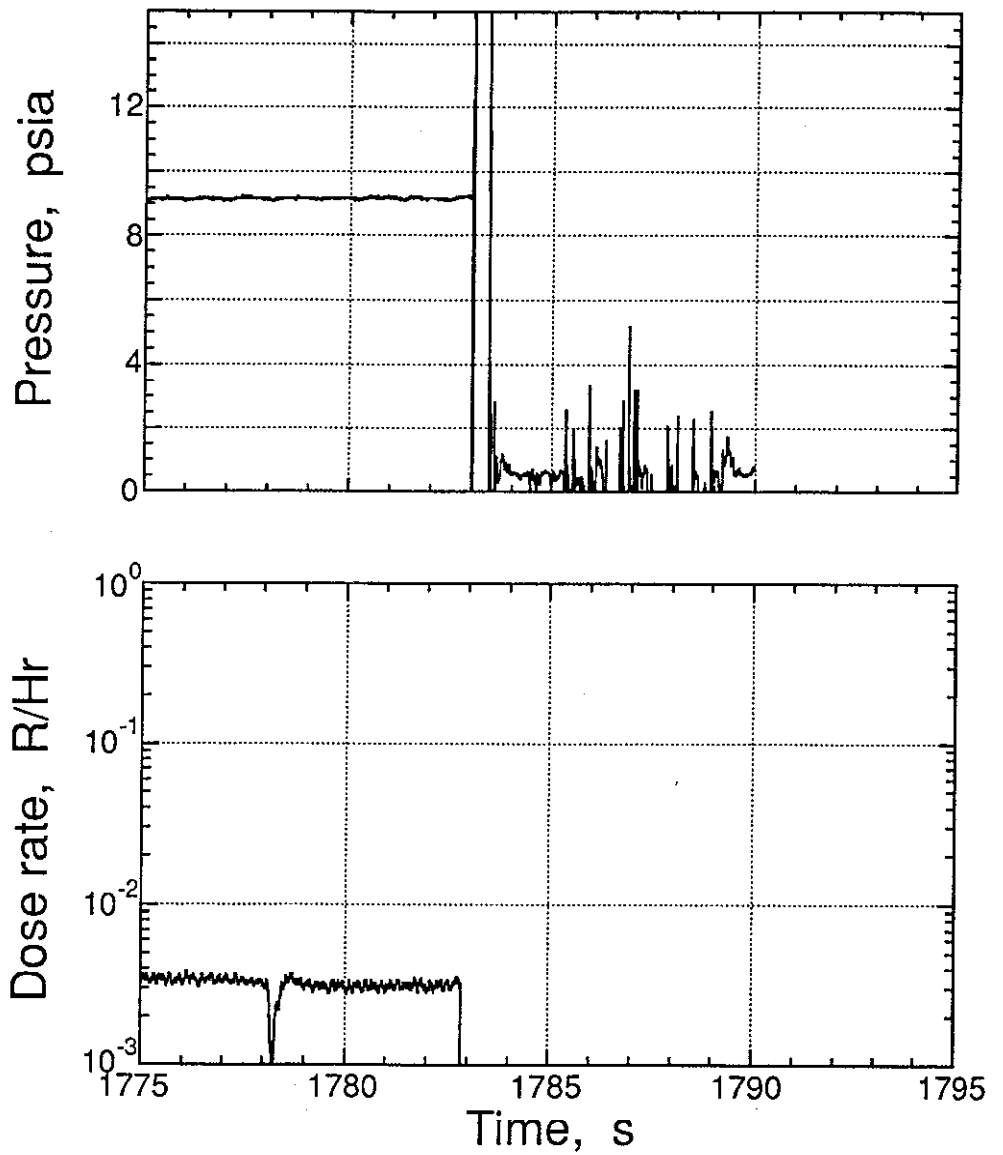
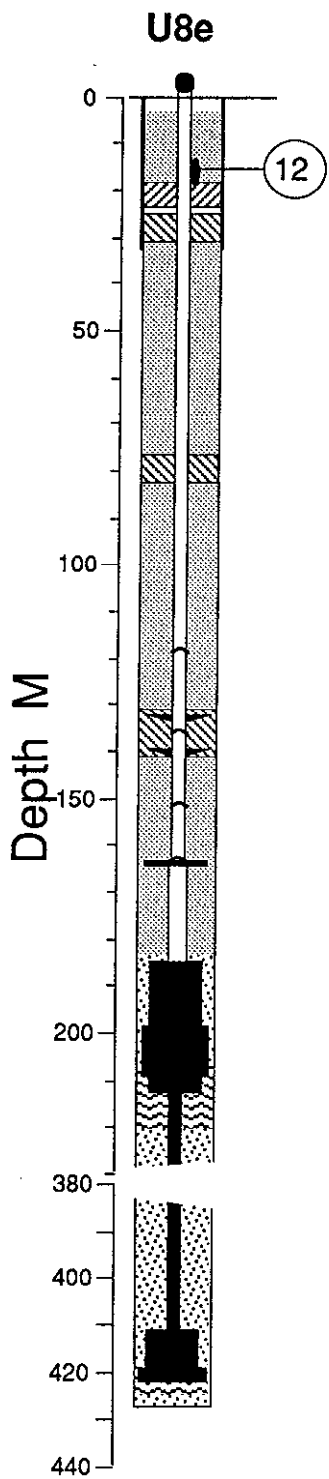


Figure 4.8 Pressure and radiation measured in the emplacement pipe during collapse (station 12 at a depth of 15.5 m).

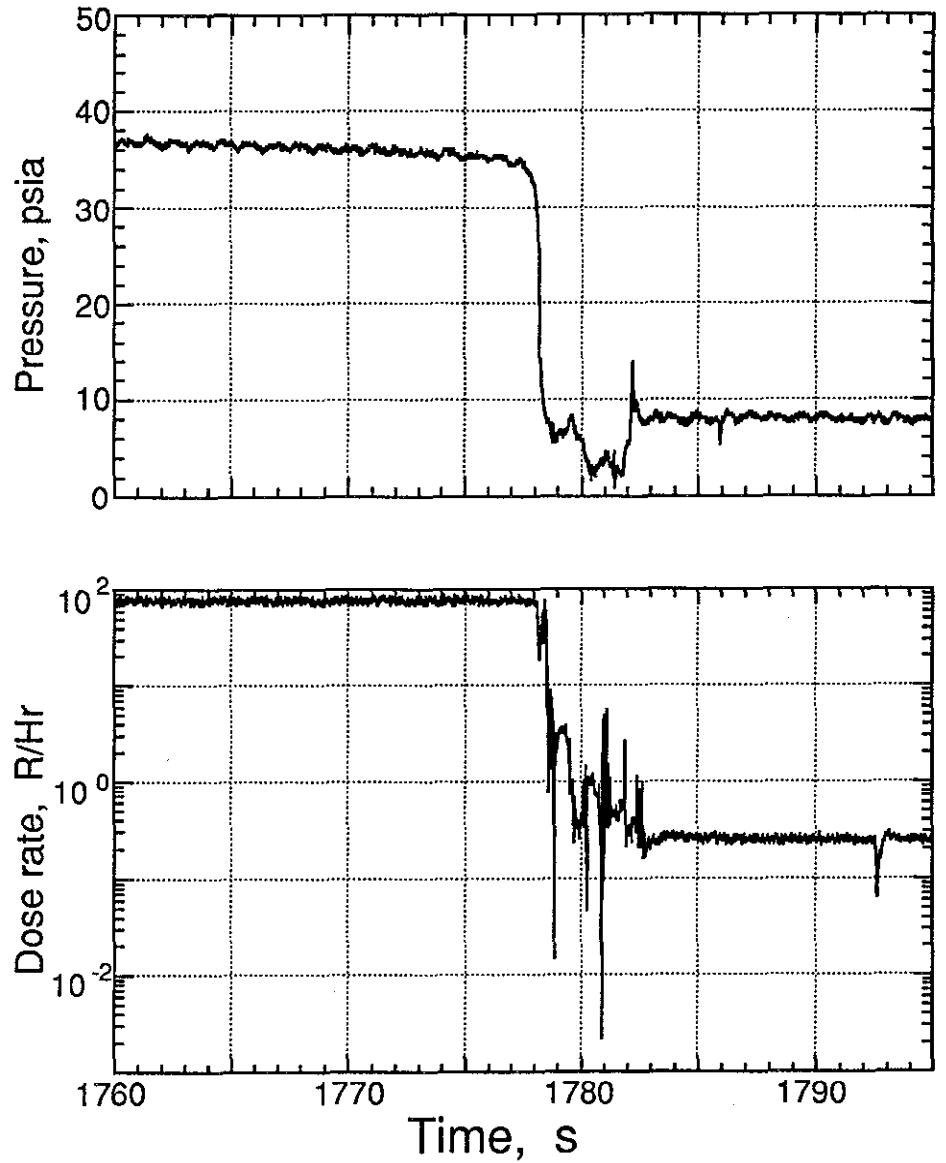
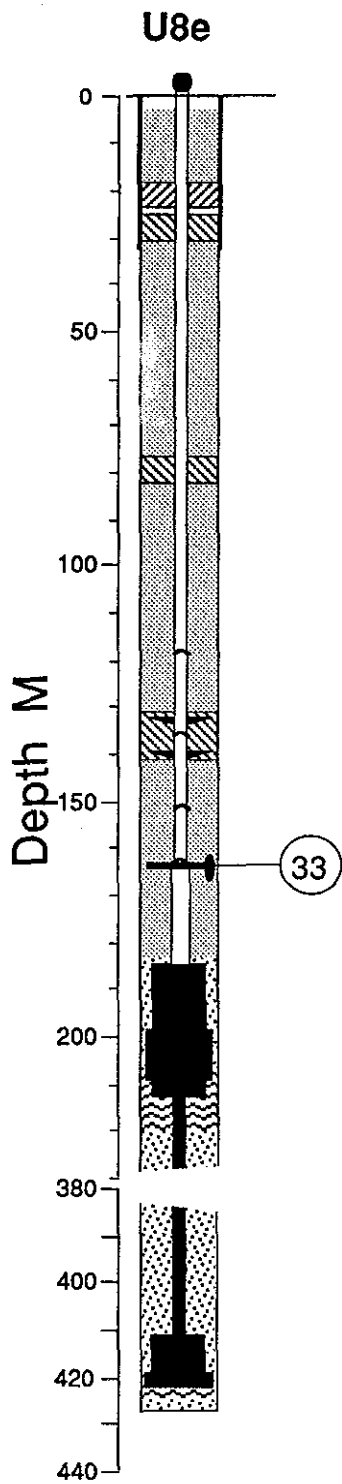


Figure 4.9 Collapse epoch pressure and radiation measured at station 33 (depth 163.6 m), near the first pressure dome, above the tau can.

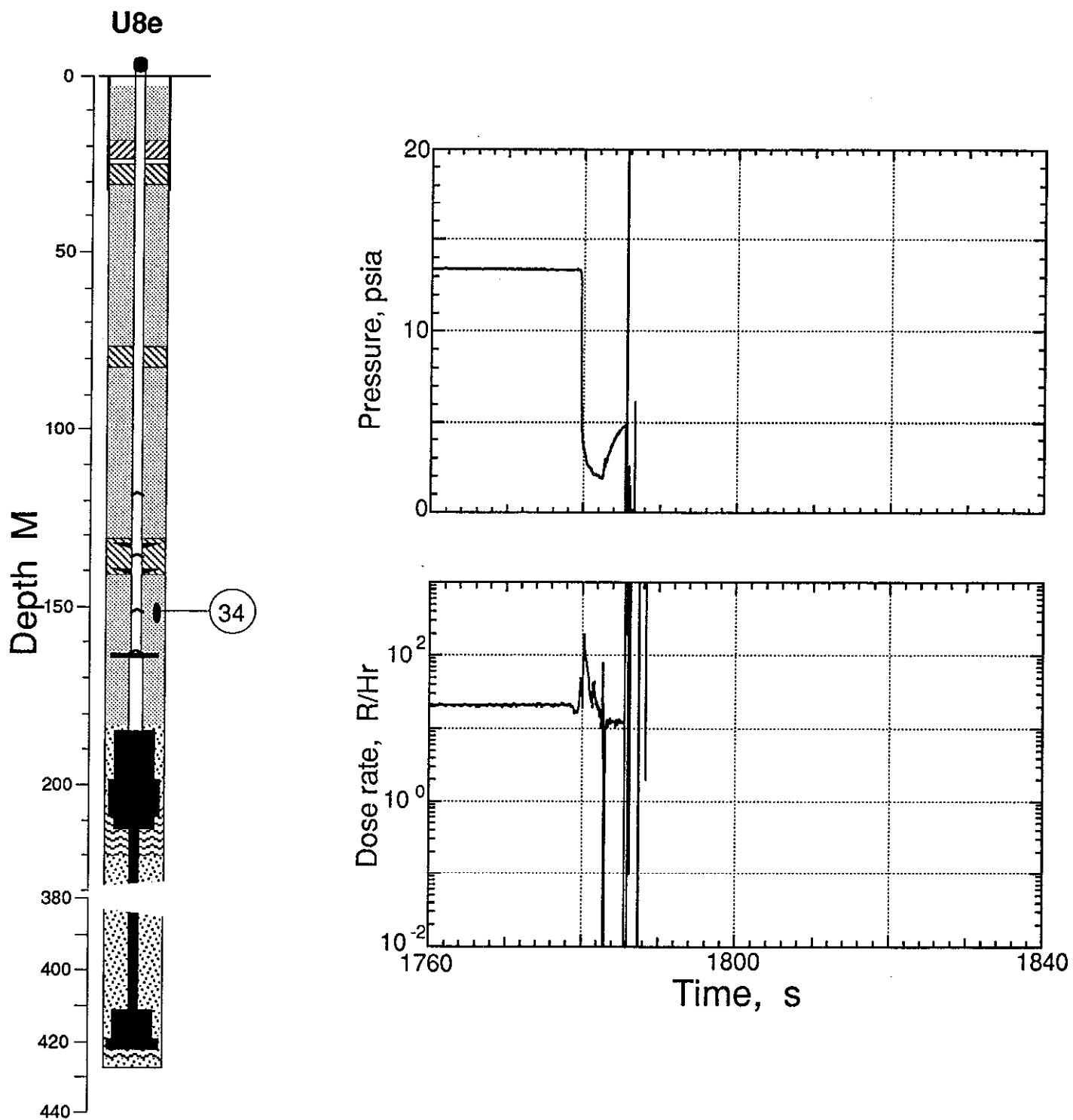


Figure 4.10 Collapse epoch pressure and radiation measured at station 34 (depth 151.5), near the second pressure dome.

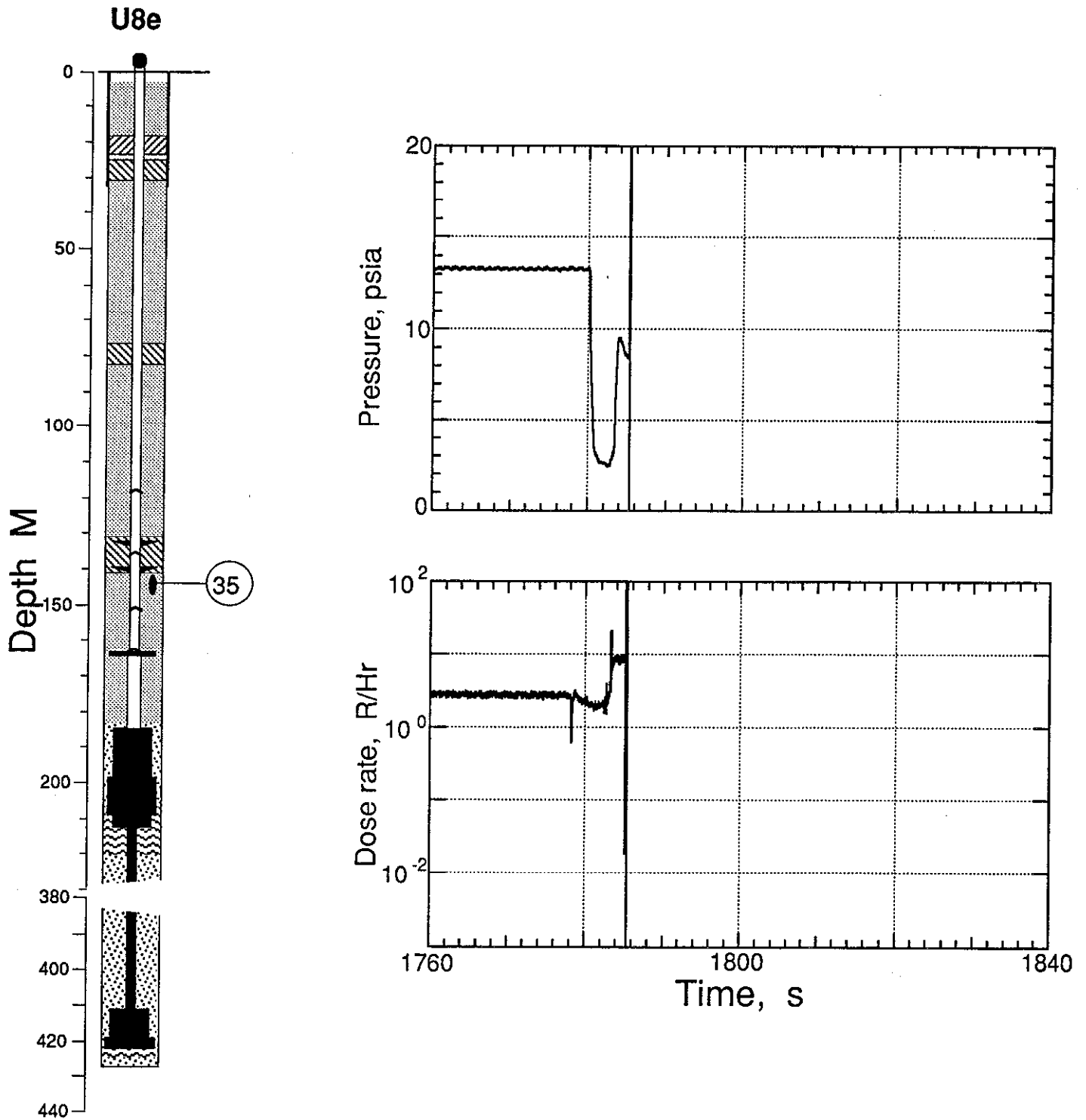


Figure 4.11 Collapse epoch pressure and radiation measured at station 35 (depth 143.9 m), below the formation coupling plug.

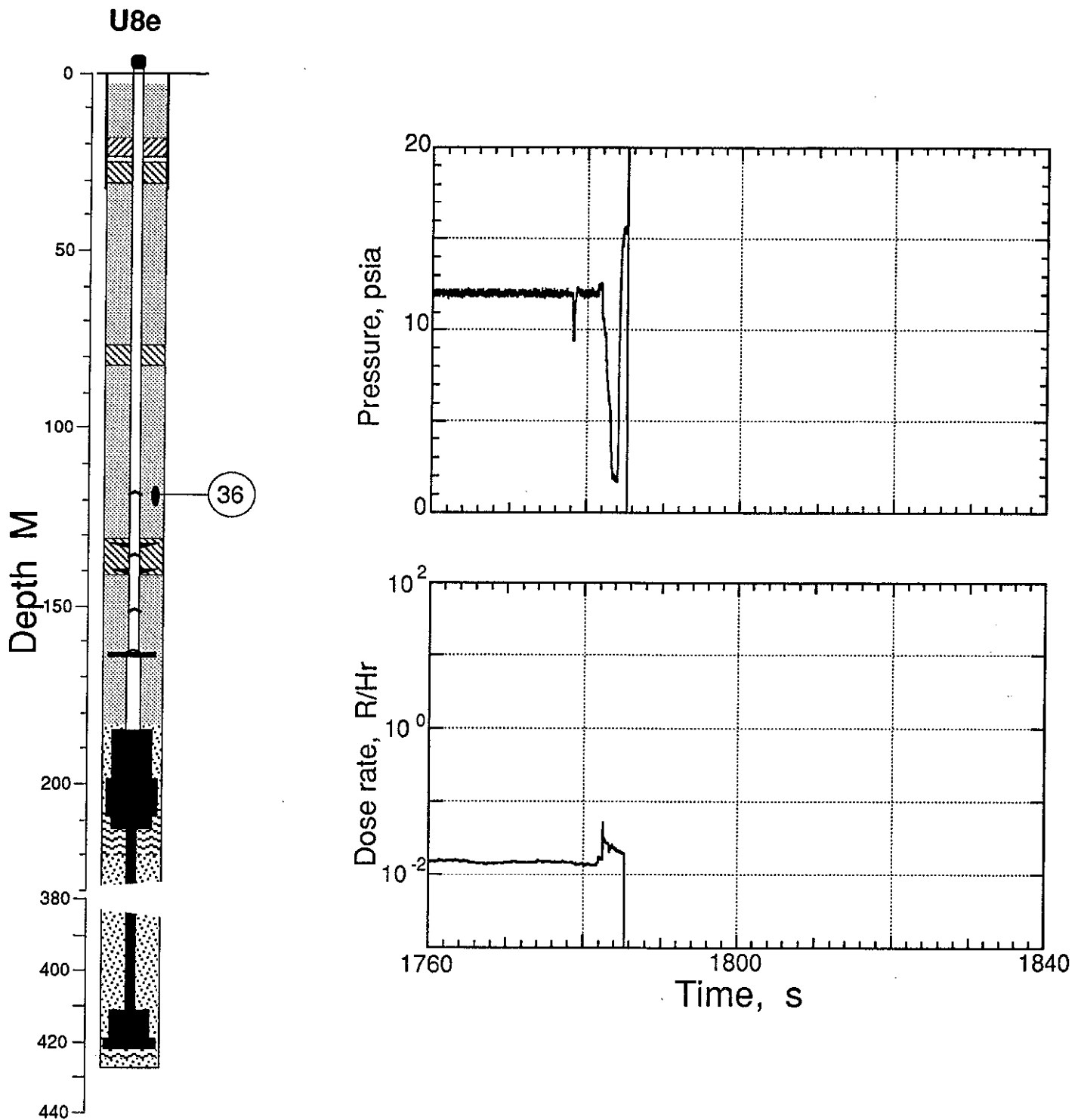


Figure 4.12 Collapse epoch pressure and radiation measured at station 36 (depth 118.4 m), near the detector plate, above the formation coupling plug.

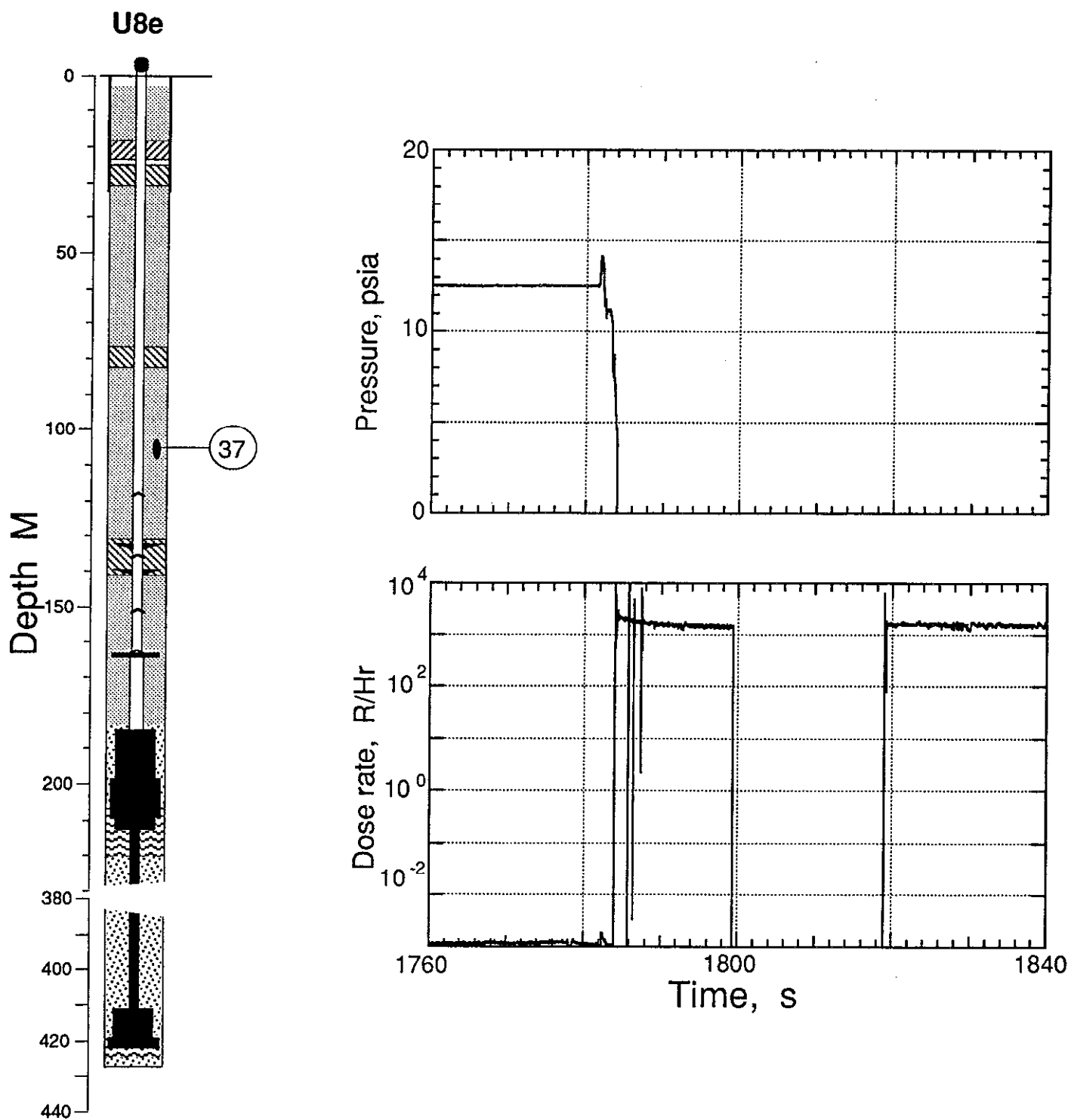


Figure 4.13 Collapse epoch pressure and radiation measured at station 37 (depth 104.7), midway between the formation coupling plug and the stemming platform.

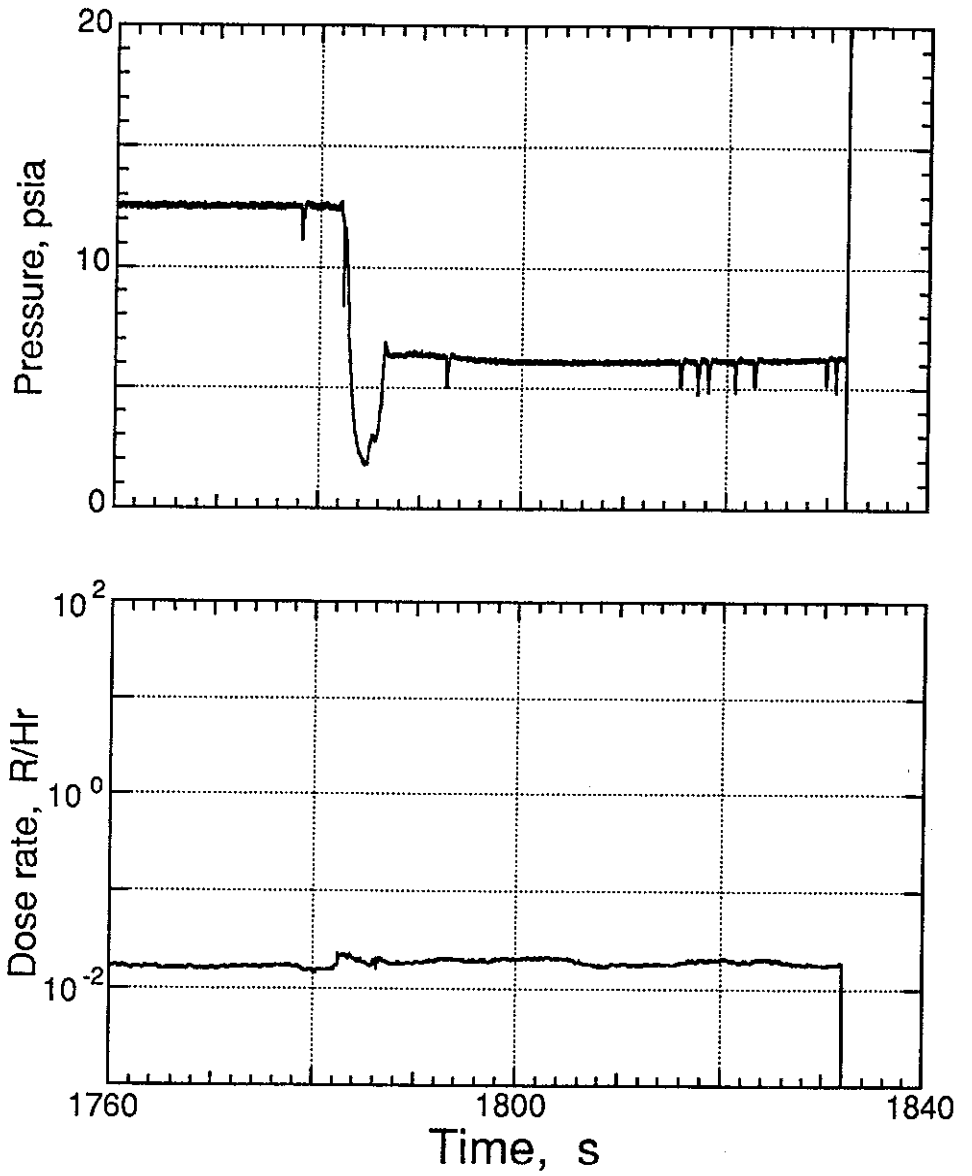
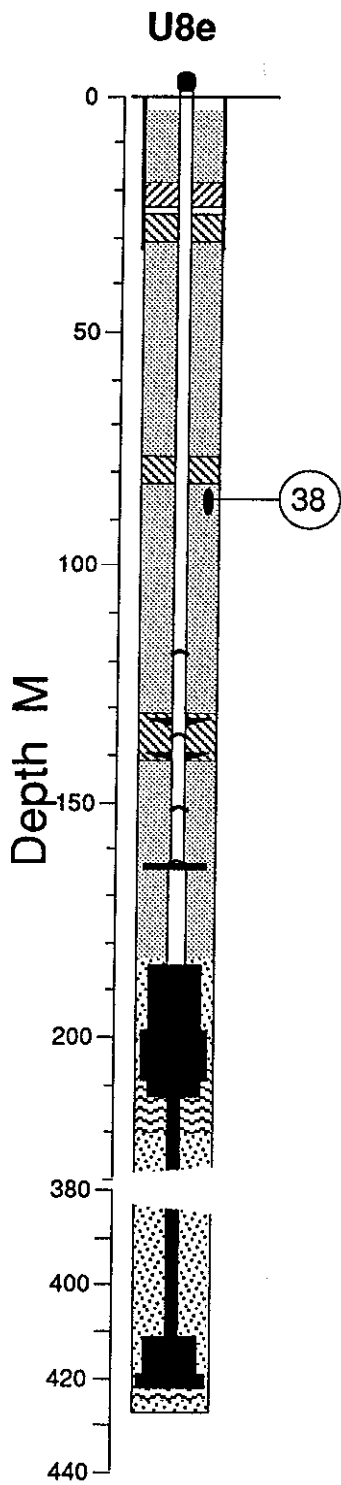


Figure 4.14 Collapse epoch pressure and radiation measured at station 38 (depth 85.7 m), below the stemming platform.

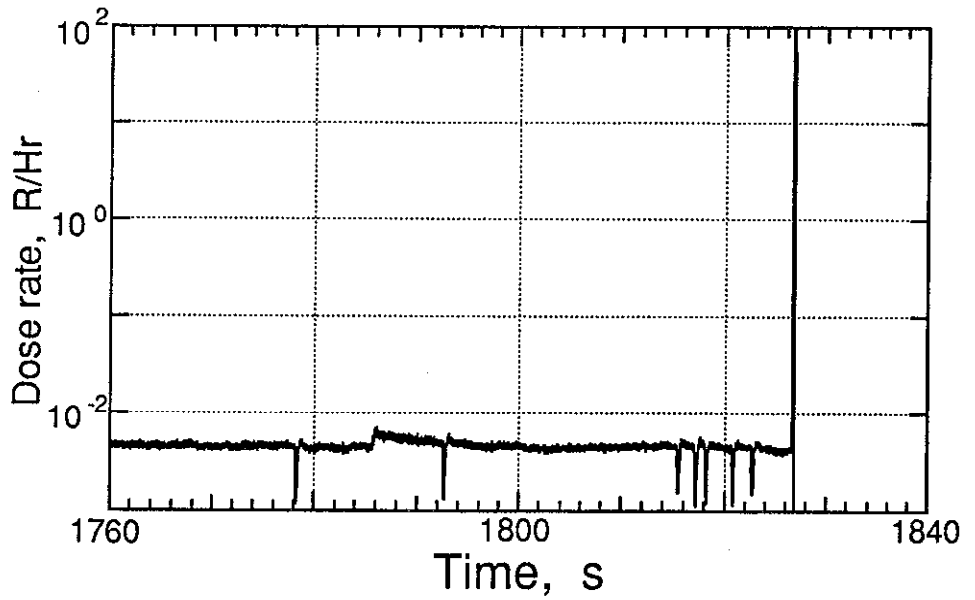
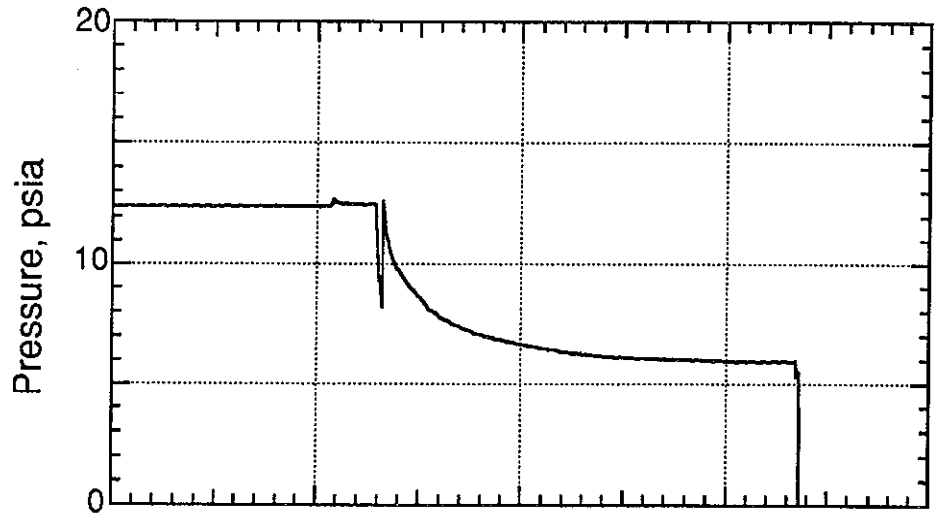
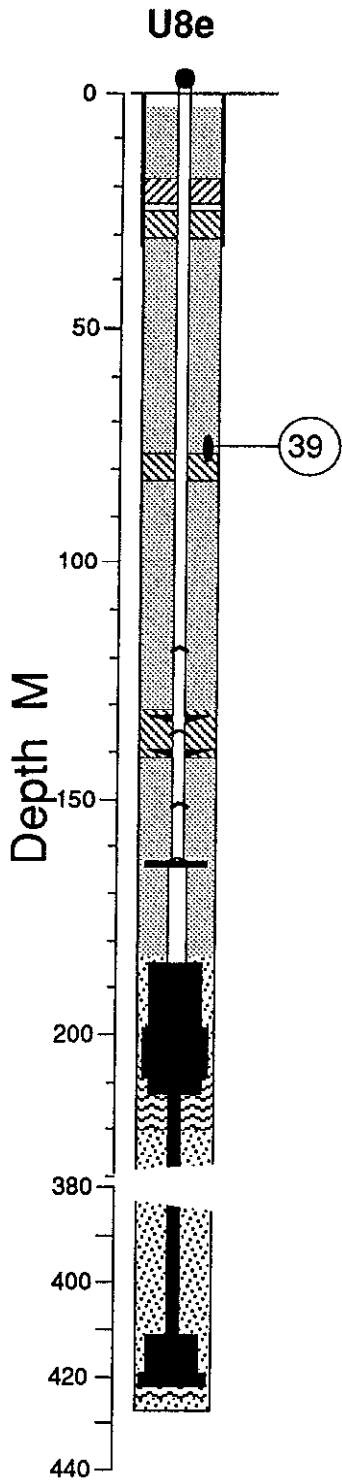


Figure 4.15 Collapse epoch pressure and radiation measured at station 39 (depth 75.0 m), above the stemming platform.

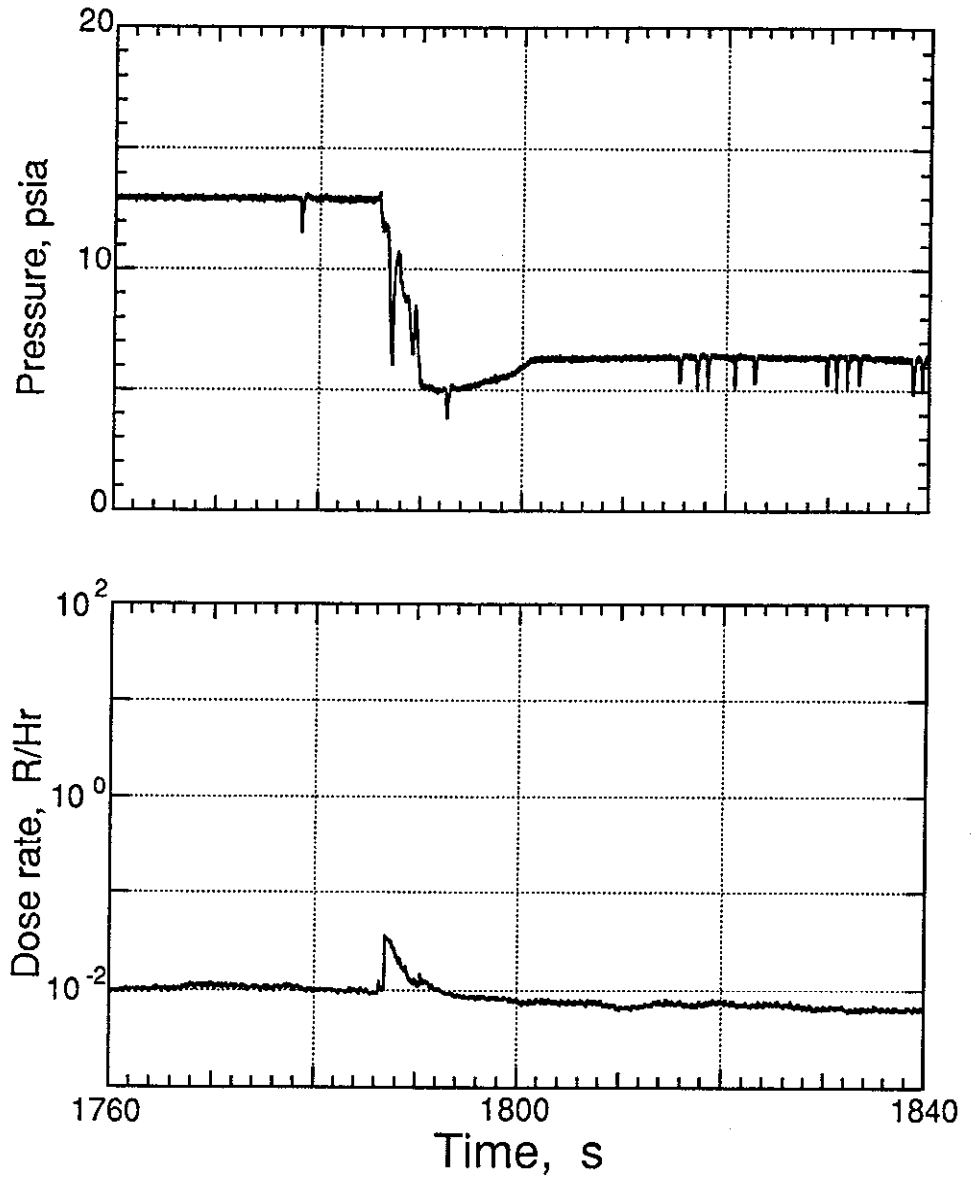
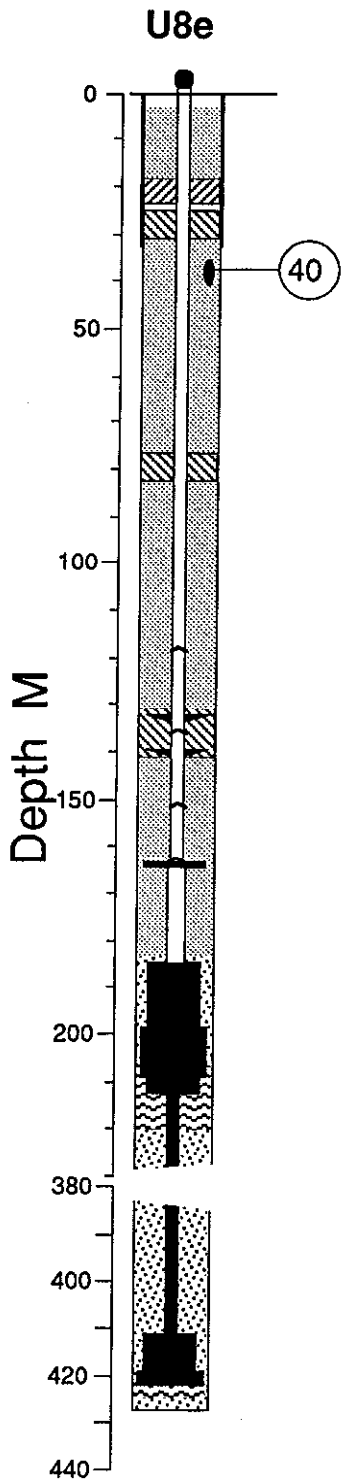


Figure 4.16 Collapse epoch pressure and radiation measured at station 40 (depth 37.8 m) below the top plug.

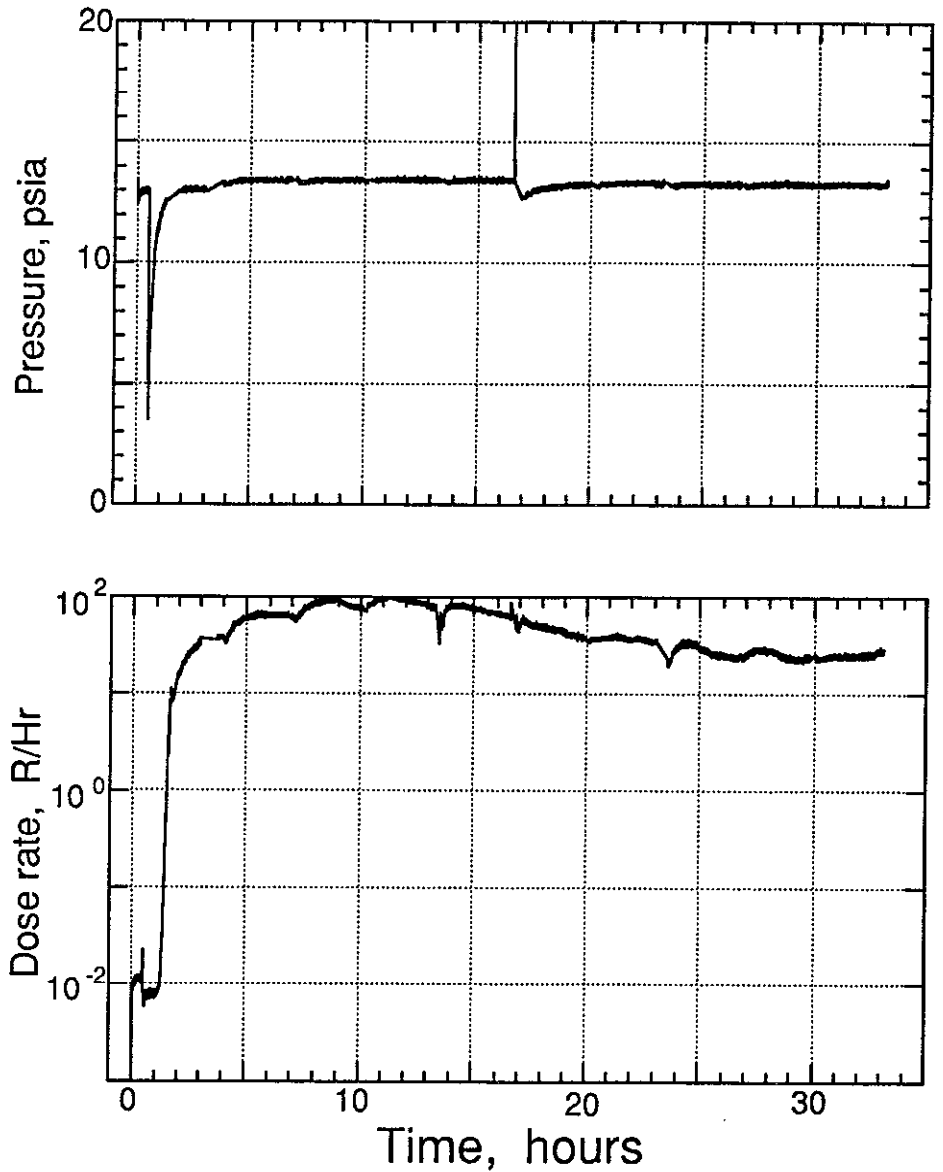
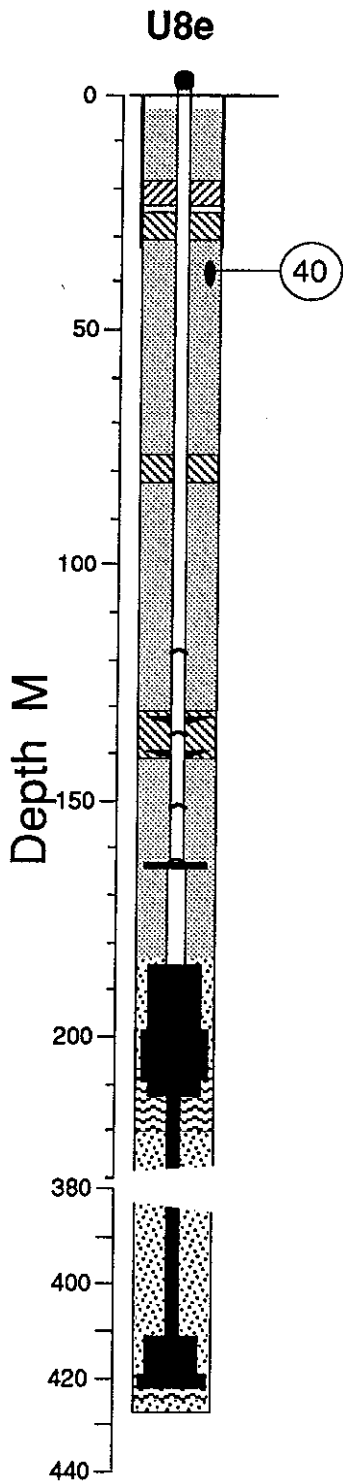


Figure 4.17 Pressure and radiation measured at station 40 (depth 37.8 m) below the top plug. The data cover a period of about 33 hours after detonation. The discontinuities in the wave forms are due to the requirement of joining the records from ten separate analog tapes.

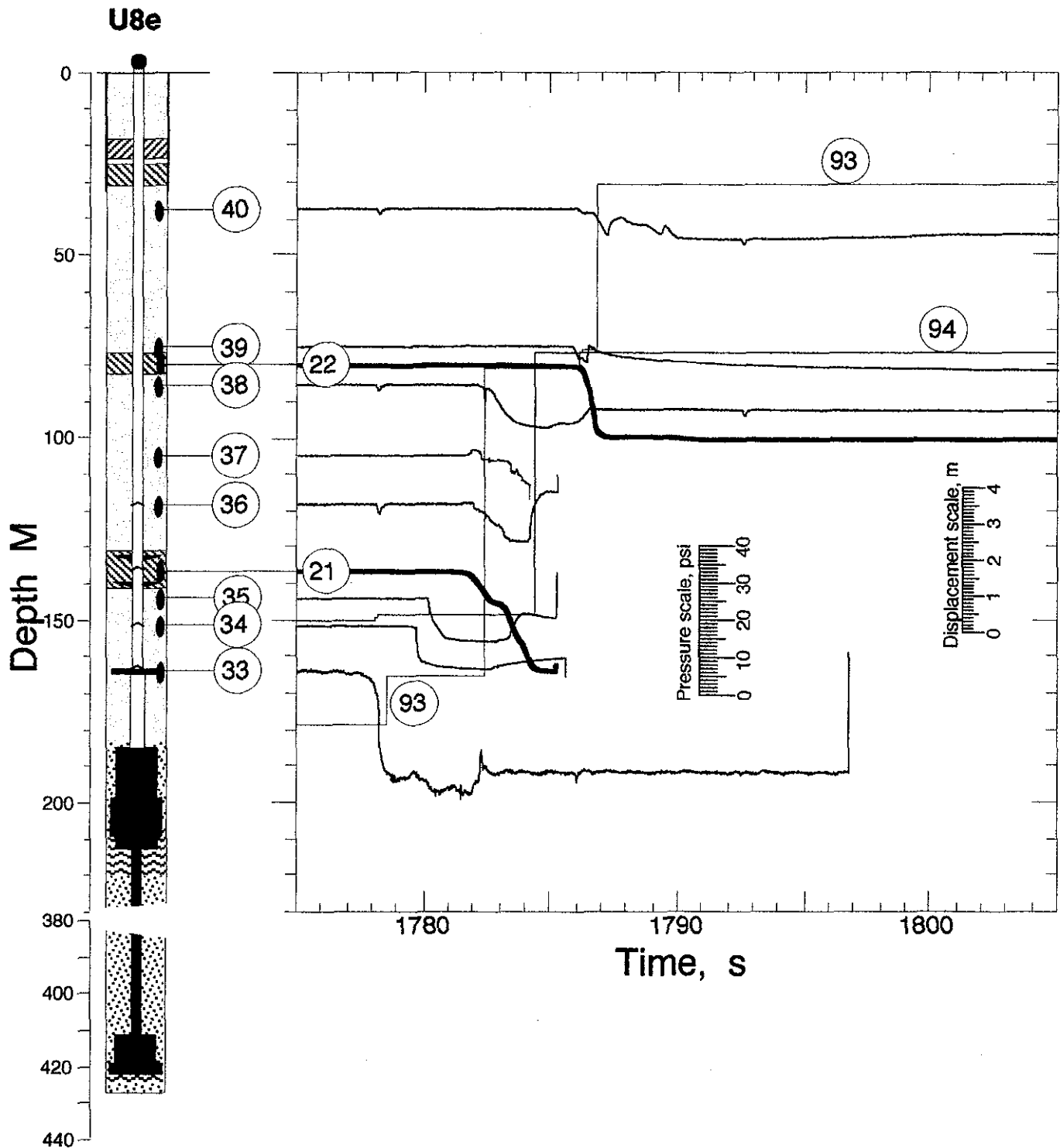


Figure 4.18 Composite of signals during collapse showing the progression of the collapse in the emplacement hole. Included are the wave forms of displacement of the rigid plugs and of pressure. Also shown are the positions of breaks in the CLIPER cables. Station 93 was attached to the emplacement pipe and 94 was emplaced on the instrumentation pendant. The heavy traces are the displacement wave forms of the plug displacement (stations 21 and 22).

5. Measurements in the Satellite Hole

The original plan for the satellite hole Ue8e was to instrument for a higher yield experiment with its explosion point at or below the elevation of the deepest station in hole Ue8e. Transducers were set, in the laboratory, to capture the data from such a device, emplaced in the hole and grouted in place. Subsequently, the original high-yield experiment was replaced with a multiple, lower yield test, CREMINO/CAERPHILLY which was buried at a shallower depth in the main hole.

In addition to the motion transducers fielded in the satellite hole, figure 1.5 indicates the presence of three soil stress gauges and two CLIPER cables. The soil stress transducers were fielded as part of this experiment but the data were collected by Sandia and are not reported here. The location of the satellite hole is 60.9 m from the emplacement hole which is more than two expected CREMINO cavity radii away and was thus not involved in the collapse so the CLIPERs did not record any activity.

Wave forms of the first 3 seconds of motion derived from the satellite hole Ue8e are shown in figures 5.1 - 5.20. Also included, as inserts in each of the plots, are the first 200 ms of the same data for greater time and amplitude definition. Arrivals and peak values of the motion are given in table 5.1 with the transducer characteristics given in tables 5.2 and 5.3. The deepest two stations each contained a triaxial complement of transducers while the remainder were instrumented for vertical motion only. The deepest five stations also included transducers of higher sensitivity than standard and are identified by "X" appended to the name. Since the system was originally designed to capture much higher amplitude signals, the data returned were expected to, and do, contain a very high system noise content.

Signals from stations 41 - 44 (figures 5.1 - 5.14) include a pulse of energy which smoothly offsets the baseline beginning at around 0.2 s and invalidates the records thereafter.

Stations 45 - 49 (figures 5.15 - 5.20) all include vertical data from both an accelerometer and velocimeter as cross-checks. Furthermore, These stations are closer to the higher yield device CREMINO so should be subject to lower system noise.

Station 49 (figure 5.20) includes "noise" in the acceleration history at about 270 ms that tends to integrate to insignificance in the velocity and displacement records. This is likely to be the signature of stress relief of the fiber glass pipe on which the instrumentation string was hung prior to being grouted in place. This is often seen in a grouted satellite hole when the ground goes into dilatation following reflection of the detonation wave from the free surface.

The data wave forms are presented as measured and not corrected for the expected direction of propagation of the wave front. The following table presents the slant range and the angle from horizontal of the geometrically shortest path from explosion point to the station. Ranges are measured from the reference depths.

| Station | from CAERPHILLY | | from CREMINO | |
|---------|-----------------|-------------|-----------------|-------------|
| | slant range (m) | angle (deg) | slant range (m) | angle (deg) |
| 41 | 75.1 | -34.8 | 261.2 | -76.5 |
| 42 | 65.0 | -20.4 | 240.5 | -75.3 |
| 43 | 60.9 | -1.2 | 220.0 | -73.9 |
| 44 | 68.9 | 37.9 | 188.0 | -71.1 |
| 45 | 98.9 | 52.0 | 145.5 | -65.3 |
| 46 | 143.1 | 64.8 | 101.0 | -52.9 |
| 47 | 244.1 | 75.6 | 66.4 | 23.4 |
| 48 | 306.6 | 78.4 | 106.5 | 55.1 |
| 49 | 354.6 | 86.1 | 152.0 | 66.4 |

Table 5.1 Summary of Free-Field Motion

| Gauge | Arrival Time (ms) | Acceleration Peak (g) | Velocity Peak (m/s) | Displacement Peak (cm) | Displacement Residual (cm) |
|---------------------|-------------------|-----------------------|---------------------|------------------------|----------------------------|
| 41ar | 33 | 2.2 | 0.15 | (a) | (a) |
| 41arX | 33 | 2.7 | 0.18 | (a) | (a) |
| 41uv | | - | -0.14 | -0.13 | (a) |
| 41uvX | | - | -0.21 | -0.17 | (a) |
| 41uh | | - | -0.19 | -0.17 | (a) |
| 42ar | 29 | 5.0 | 0.30 | (a) | (a) |
| 42arX | 28 | 9.0 | 0.62 | (a) | (a) |
| 42uv | | - | -0.15 | -0.12 | (a) |
| 42uvX | | - | -0.13 | -0.11 | (a) |
| 42uh | | - | 0.28 | 0.24 | (a) |
| 43av ^(b) | - | - | - | - | - |
| 43uv | 37 | - | -0.6 | -1.0 | (a) |
| 43uvX | | - | -0.05 | -0.03 | (a) |
| 44av | 33 | 3.8 | 0.15 | 0.13, -1.2 | 2.3 |
| 44uv | | - | 0.15 | 0.10, -1.8 | 2.2 |
| 44uvX | | - | 0.15 | 0.12, -1.7 | 1.0 |
| 45av | 46 | 3.3 | 0.15 | 0.20 | 0.9 ^(c) |
| 45uv | | - | 0.20 | 0.10 | -2.9 |
| 45uvX | | - | 0.12 | -0.1 | 0.3 |
| 46av | 42 | -1.4 | -0.41 | -2.6 | 0.7 ^(c) |
| 46uv | | - | -0.41 | -2.4 | 0.2 |
| 47av | 32 | 2.0 | 0.84 | 5.0 | g ^(c) |
| 47uv | | - | 0.5 | 2.8 | 0 |
| 48av | 51 | 0.97 | 0.26 | 2.1 | (a) |
| 48uv | | - | 0.24 | 1.8 | 0.5 |
| 49av | 82 | 0.76 | 0.24 | 2.4 | 1.9 |
| 49uv | | - | 0.15 | 1.4 | 0.6 |

(a) Channel questionable before this value attained.

(b) Channel lost before data arrival.

(c) Approximate.

Table 5.2 Containment-Related Accelerometer Characteristics

| <u>Gauge</u> | <u>Natural Frequency (Hz)</u> | <u>Damping Ratio</u> | <u>System Range (g's)</u> |
|--------------|-----------------------------------|----------------------|-------------------------------|
| 41ar | 1500 | 0.63 | 1000 |
| 41arX | 1300 | 0.70 | 500 |
| 42ar | 1630 | 0.65 | 1000 |
| 42arX | 1500 | 0.65 | 500 |
| 43av | 1275 | 0.70 | 500 |
| 44av | 750 | 0.65 | 100 |
| 45av | 420 | 0.55 | 20 |
| 46av | 350 | 0.65 | 20 |
| 47av | 380 | 0.60 | 20 |
| 48av | 375 | 0.55 | 20 |
| 49av | 420 | 0.55 | 20 |

Table 5.3 Containment-Related Velocimeter Characteristics

| Gauge | Natural Frequency (Hz) | Time to 0.5 Amplitude (s) | Calibration Temperature (°F) | Operate Temperature (°C) | Stop-Stop Range (m/s) | System Range (m/s) |
|-------|------------------------|---------------------------|------------------------------|--------------------------|-----------------------|--------------------|
| 41uv | 3.57 | 86.6 | 71.7 | 76.6 | 539 | 25 |
| 41uvX | 3.68 | 27.3 | 76.6 | 76.6 | 173 | 15 |
| 41uh | 2.95 | 89.0 | 76.2 | 76.6 | 485 | 16 |
| 42uv | 3.80 | 60.0 | 77.0 | 75.8 | 484 | 20 |
| 42uvX | 3.60 | 28.0 | 72.5 | 75.8 | 187 | 14 |
| 42uh | 2.78 | 33.5 | 74.5 | 75.8 | 190 | 23 |
| 43uv | 3.62 | 30.0 | 73.5 | 74.9 | 190 | 23 |
| 43uvX | 2.94 | 17.5 | 77.0 | 74.9 | 89 | 8 |
| 44uv | 3.60 | 25.5 | 75.2 | 72.8 | 204 | 16 |
| 44uvX | 2.90 | 24.0 | 81.8 | 72.8 | 63 | 5 |
| 45uv | 2.90 | 21.3 | 75.2 | 67.8 | 61 | 4.5 |
| 45uvX | 2.86 | 27.0 | 76.2 | 67.8 | 59 | 2 |
| 46uv | 2.94 | 18.2 | 76.6 | 68.7 | 59 | 5 |
| 47uv | 3.00 | 20.6 | 76.4 | 65.1 | 59 | 15 |
| 48uv | 3.06 | 20.0 | 76.2 | 64.0 | 62 | 5 |
| 49uv | 3.06 | 16.6 | 76.3 | 62.9 | 69 | 6 |

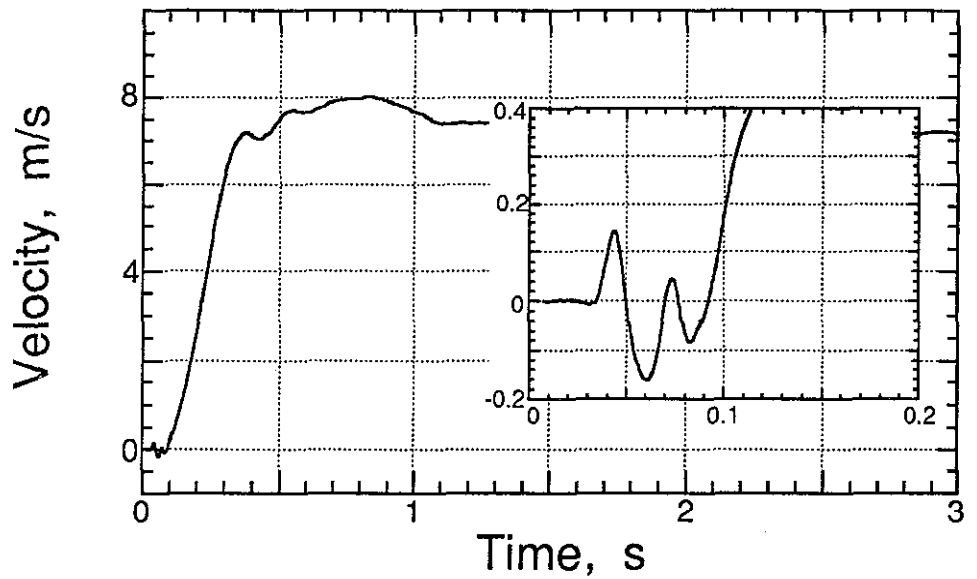
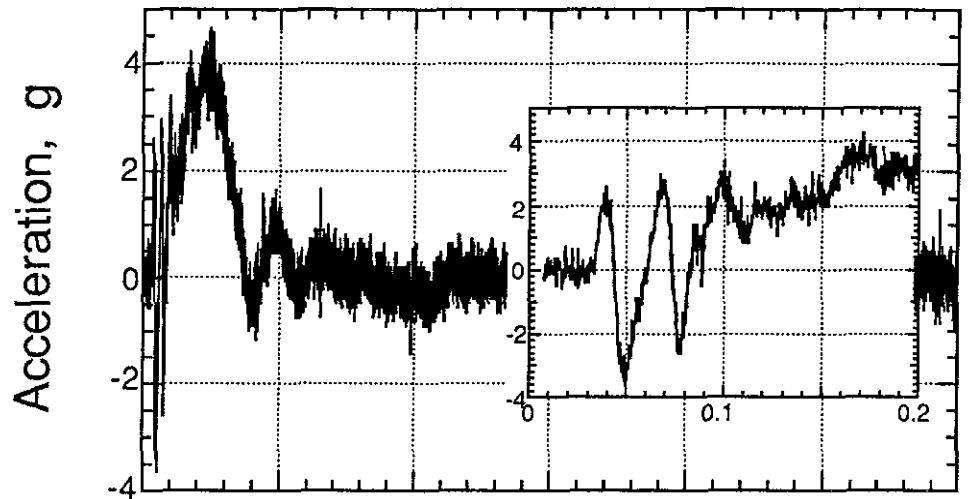
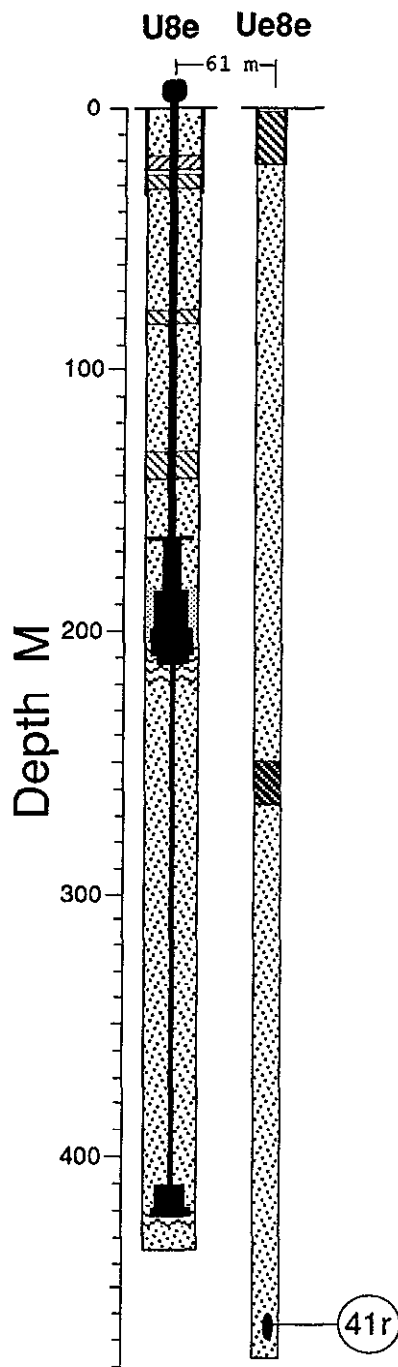


Figure 5.1 Radial motion measured in the satellite hole Ue8e at a depth of 463.3 m (station 41).

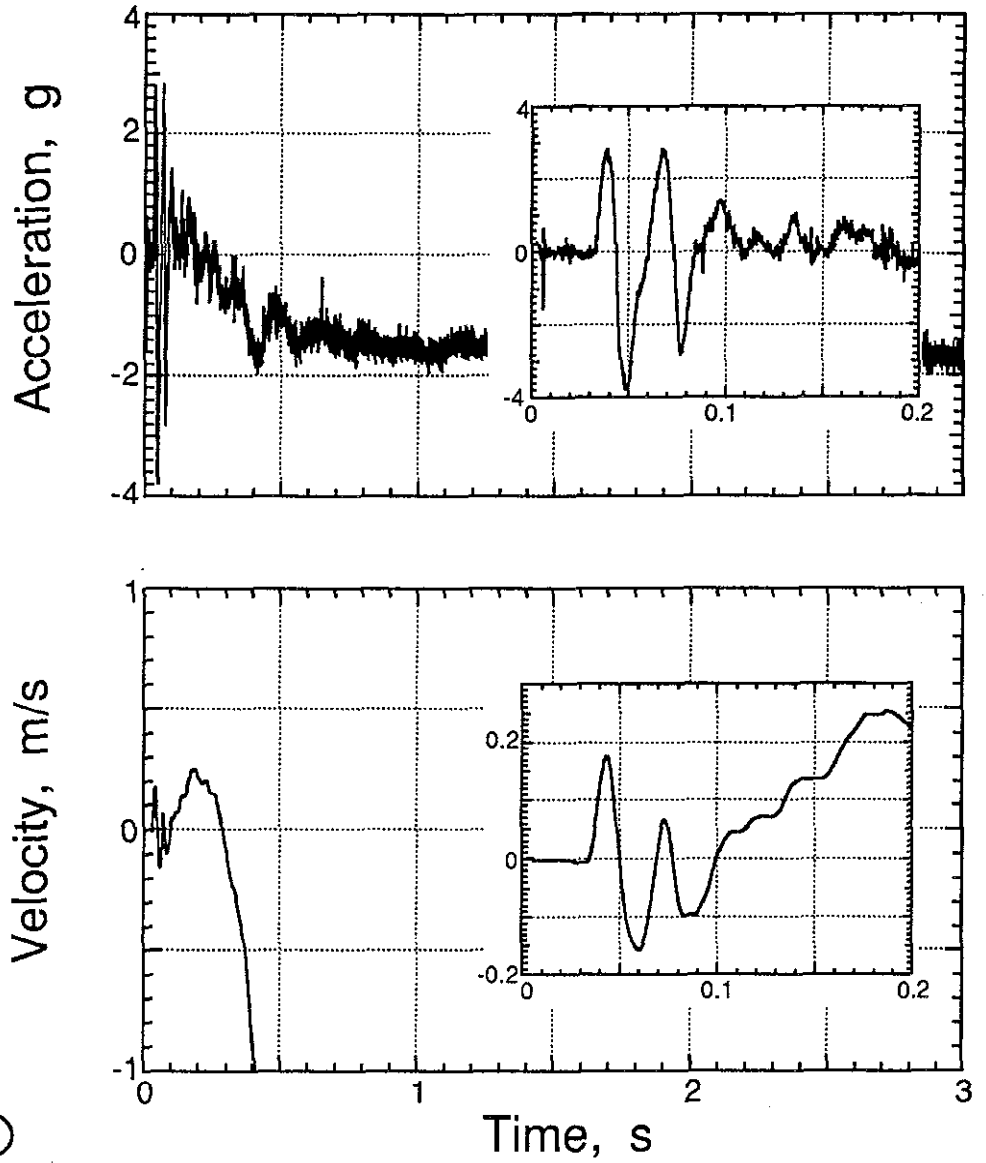
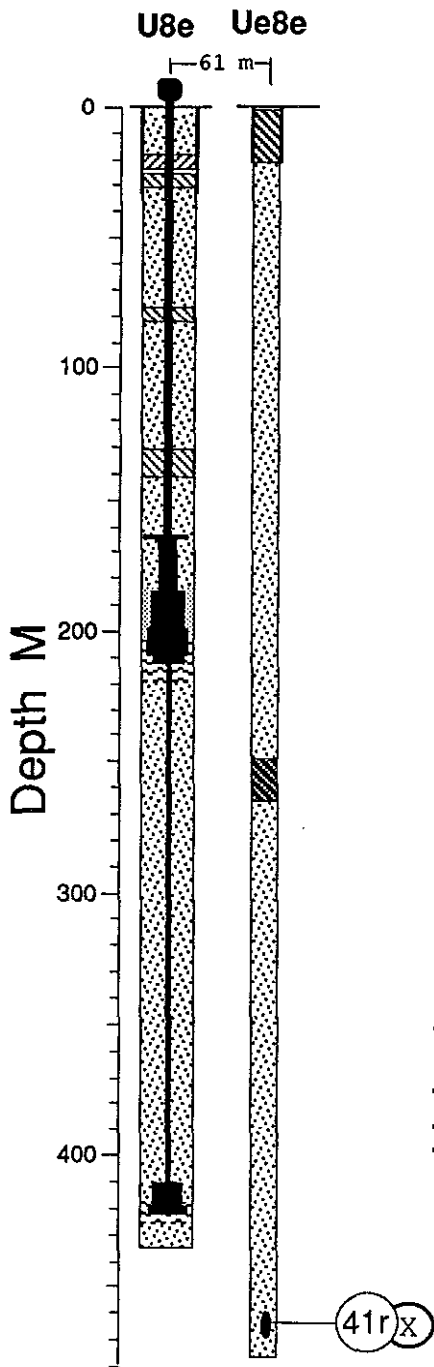


Figure 5.2 Radial motion measured in the satellite hole Ue8e at a depth of 463.3 m (station 41). Sensitive transducer employed.

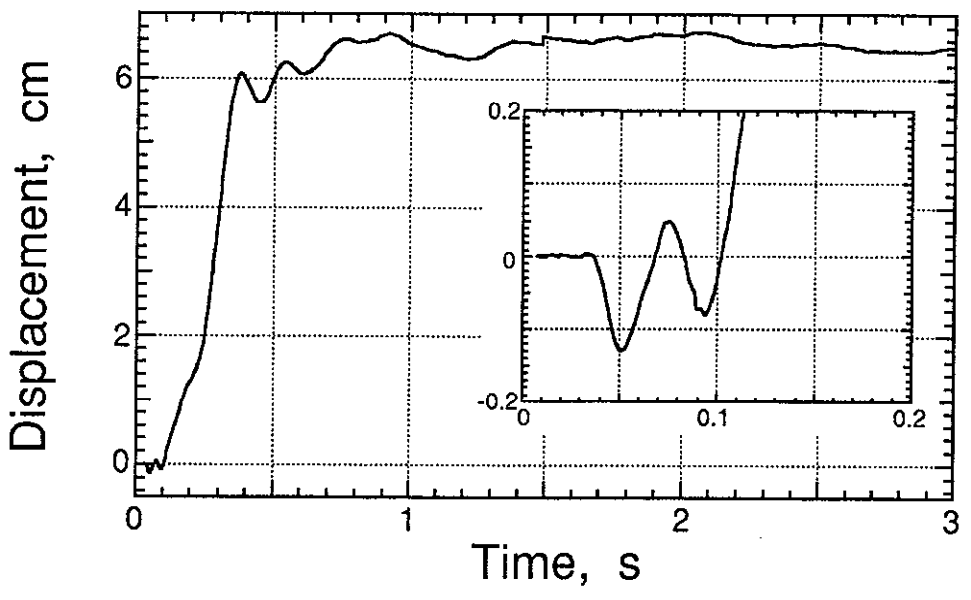
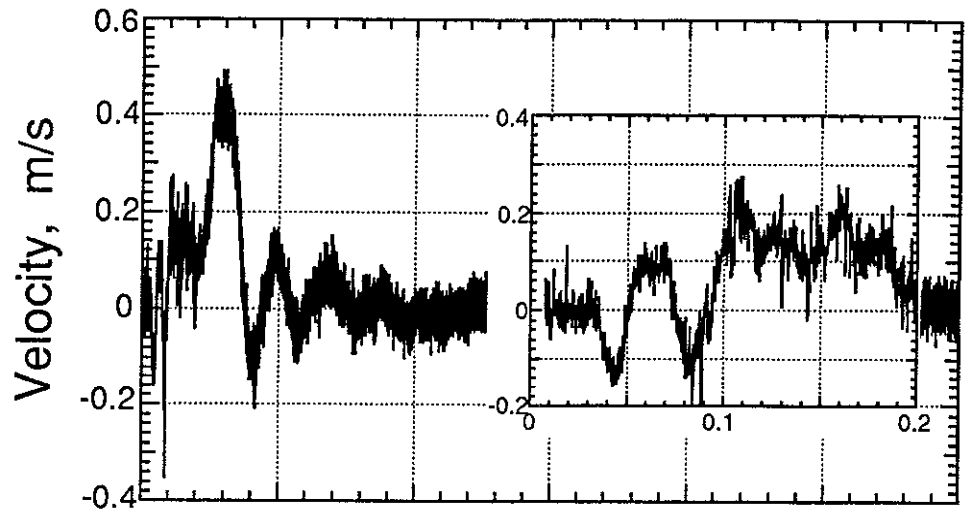
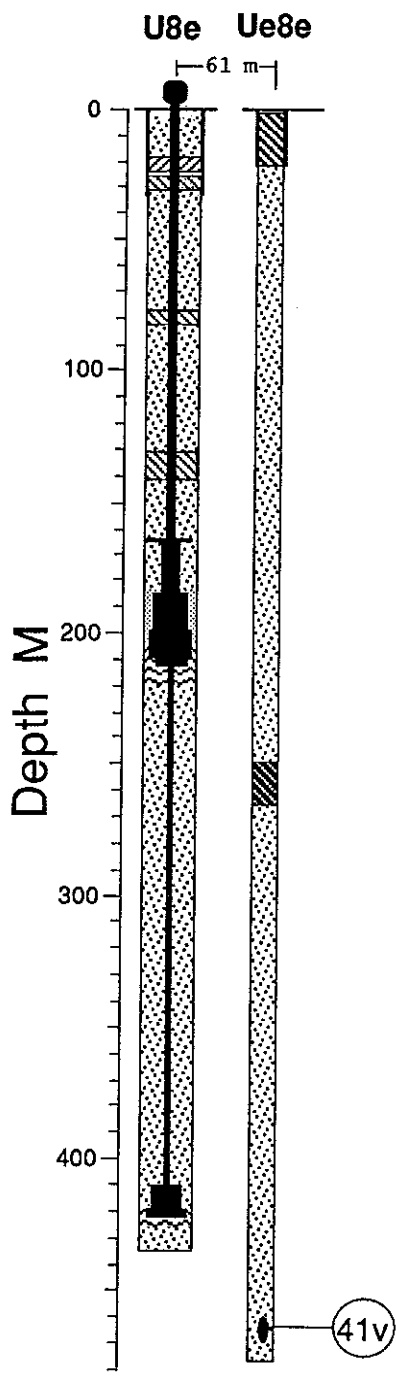


Figure 5.3 Vertical motion measured in the satellite hole Ue8e at a depth of 463.3 m (station 41).

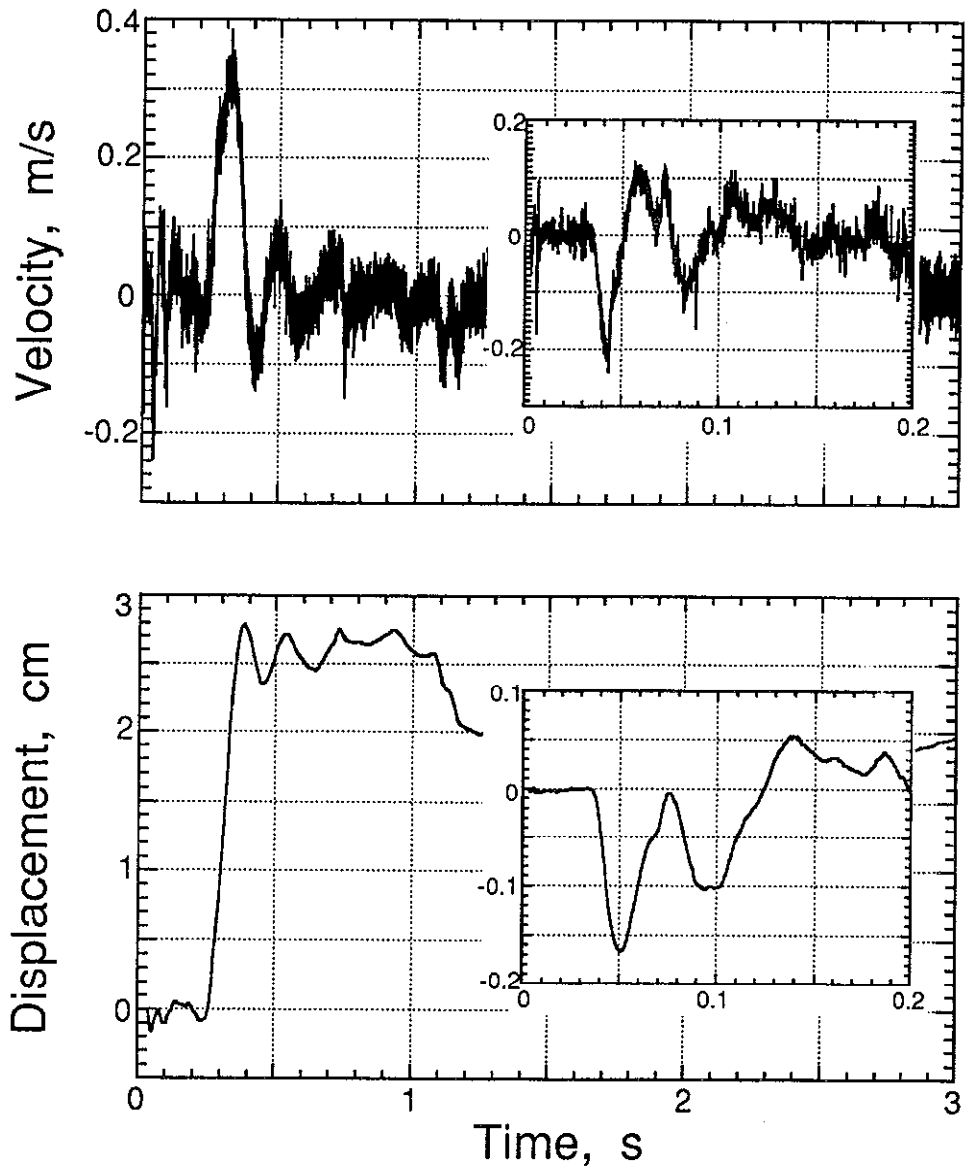
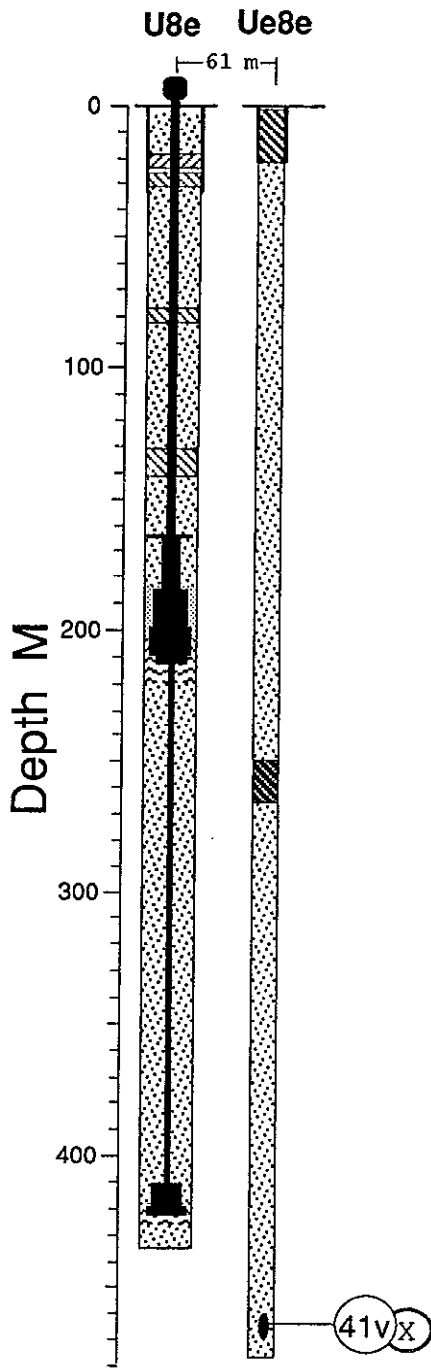


Figure 5.4 Vertical motion measured in the satellite hole Ue8e at a depth of 463.3 m (station 41). Sensitive transducer employed.

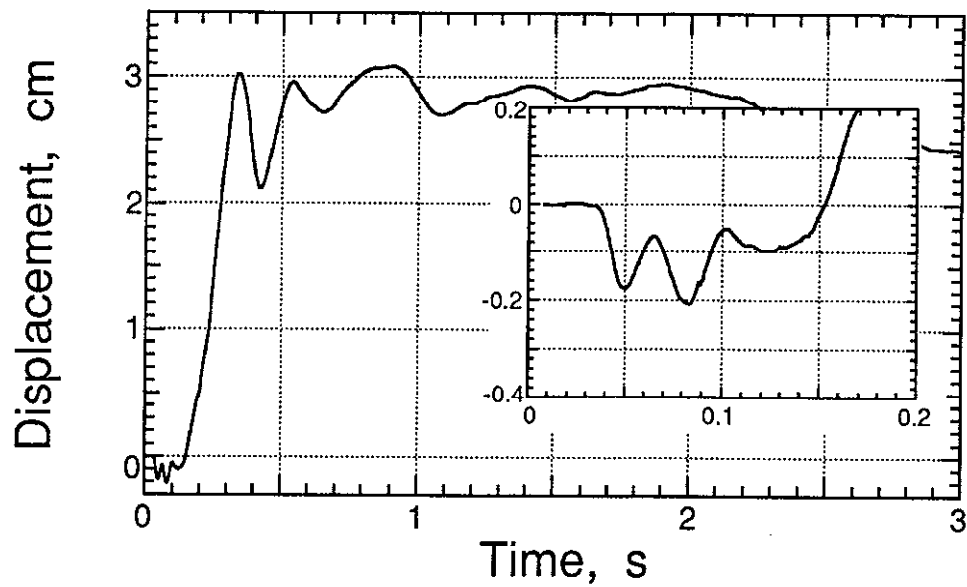
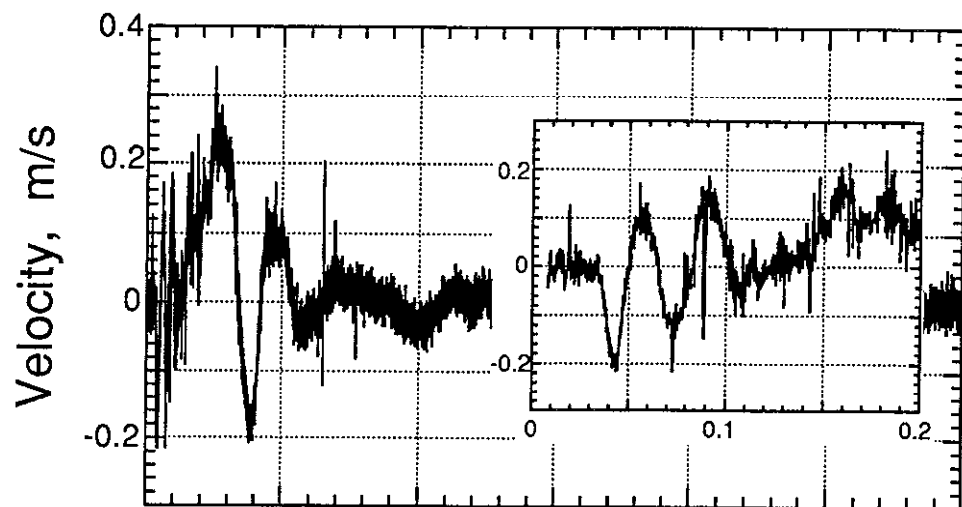
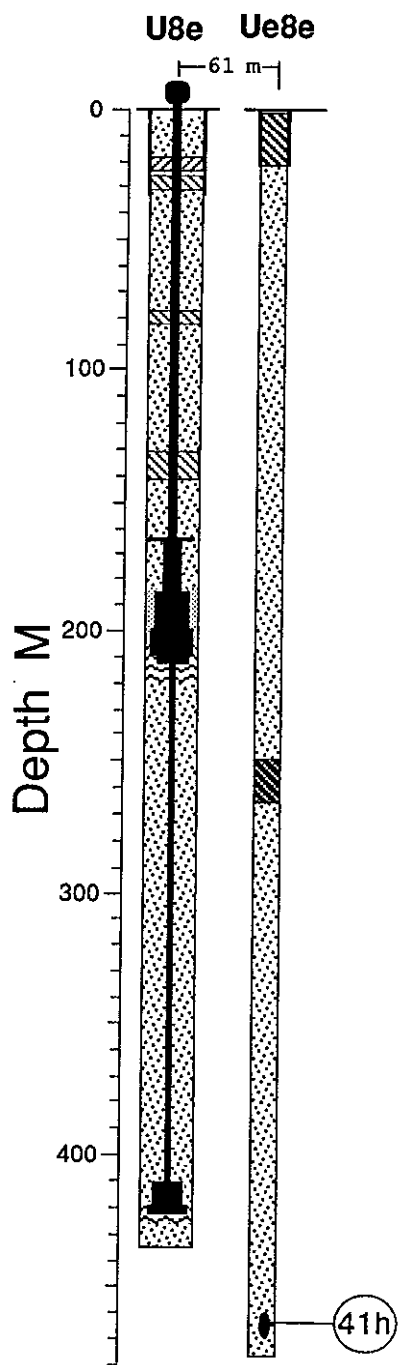


Figure 5.5 Horizontal motion measured in the satellite hole Ue8e at a depth of 463.3 m (station 41).

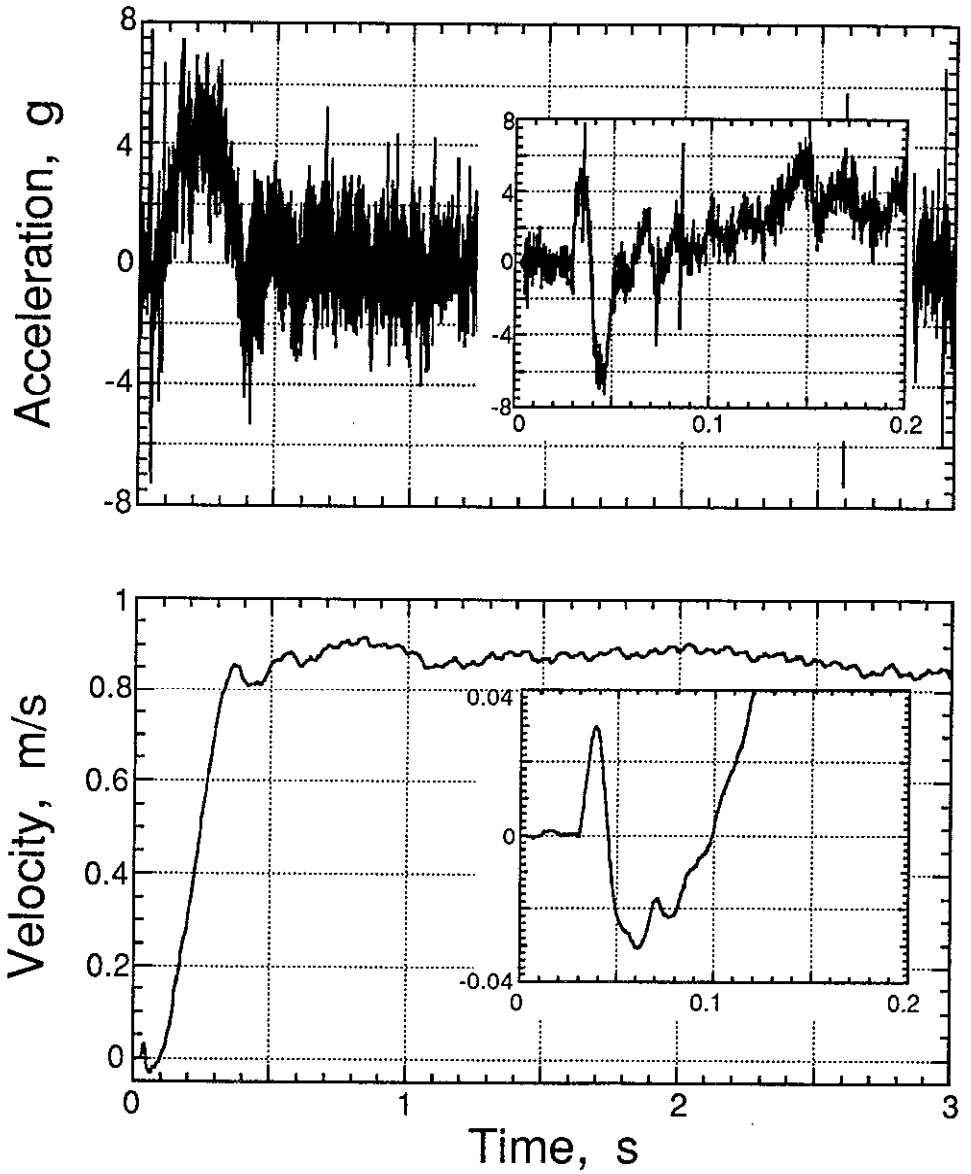
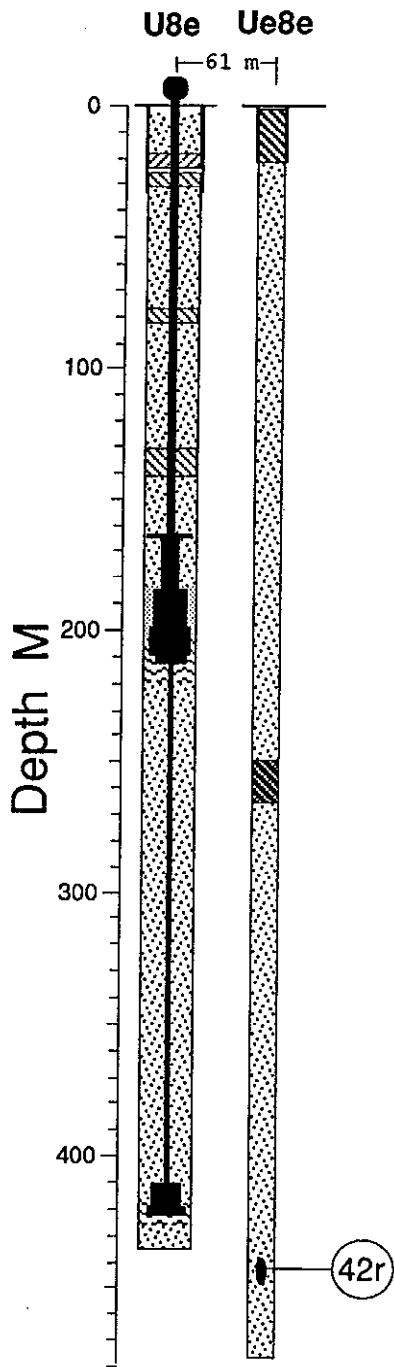


Figure 5.6 Radial motion measured in the satellite hole Ue8e at a depth of 442.0 m (station 42).

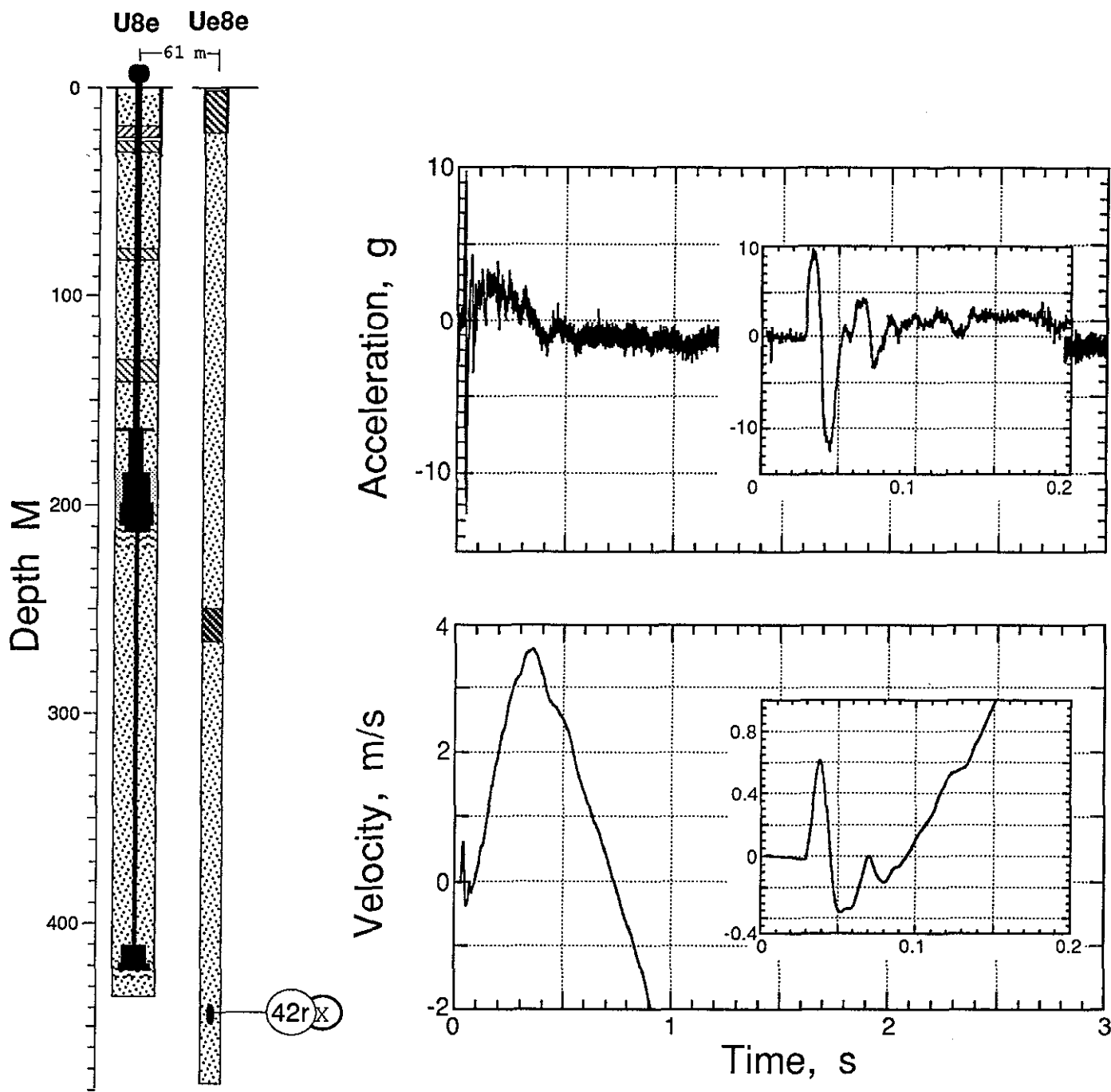


Figure 5.7 Radial motion measured in the satellite hole Ue8e at a depth of 442.0 m (station 42). Sensitive transducer employed.

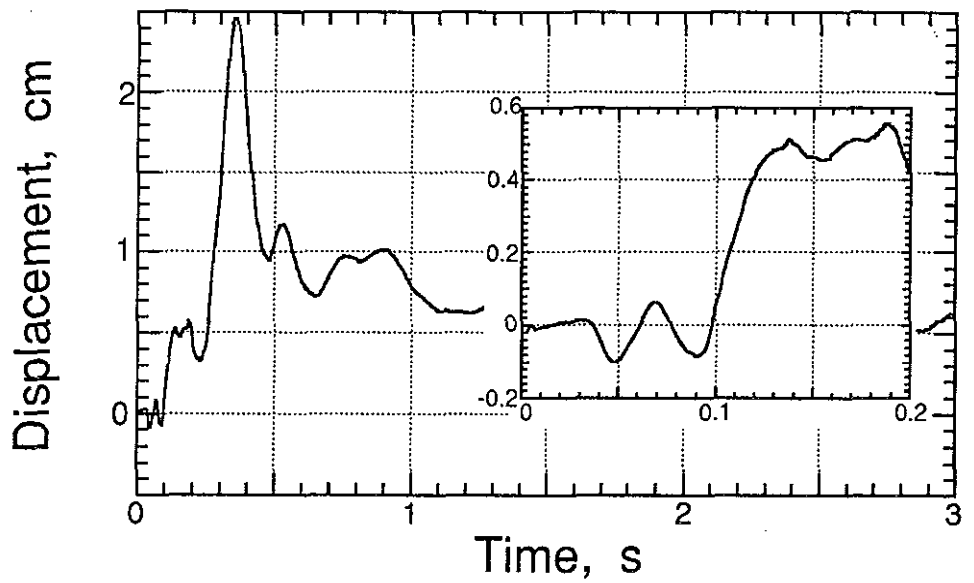
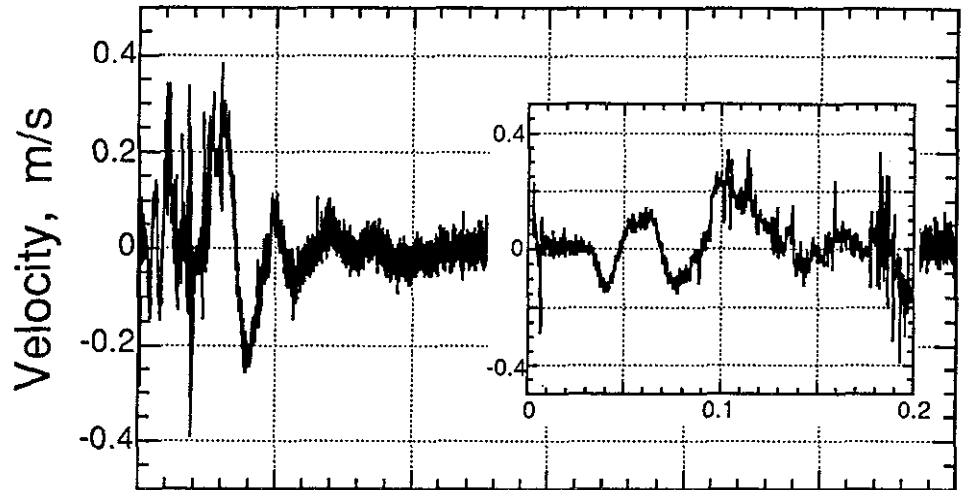
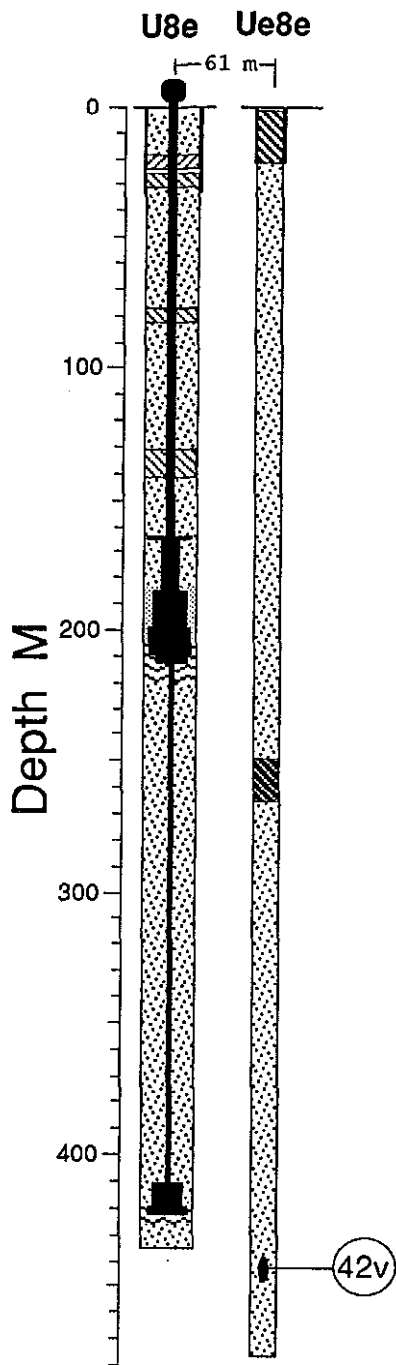


Figure 5.8 Vertical motion measured in the satellite hole Ue8e at a depth of 442.0 m (station 42).

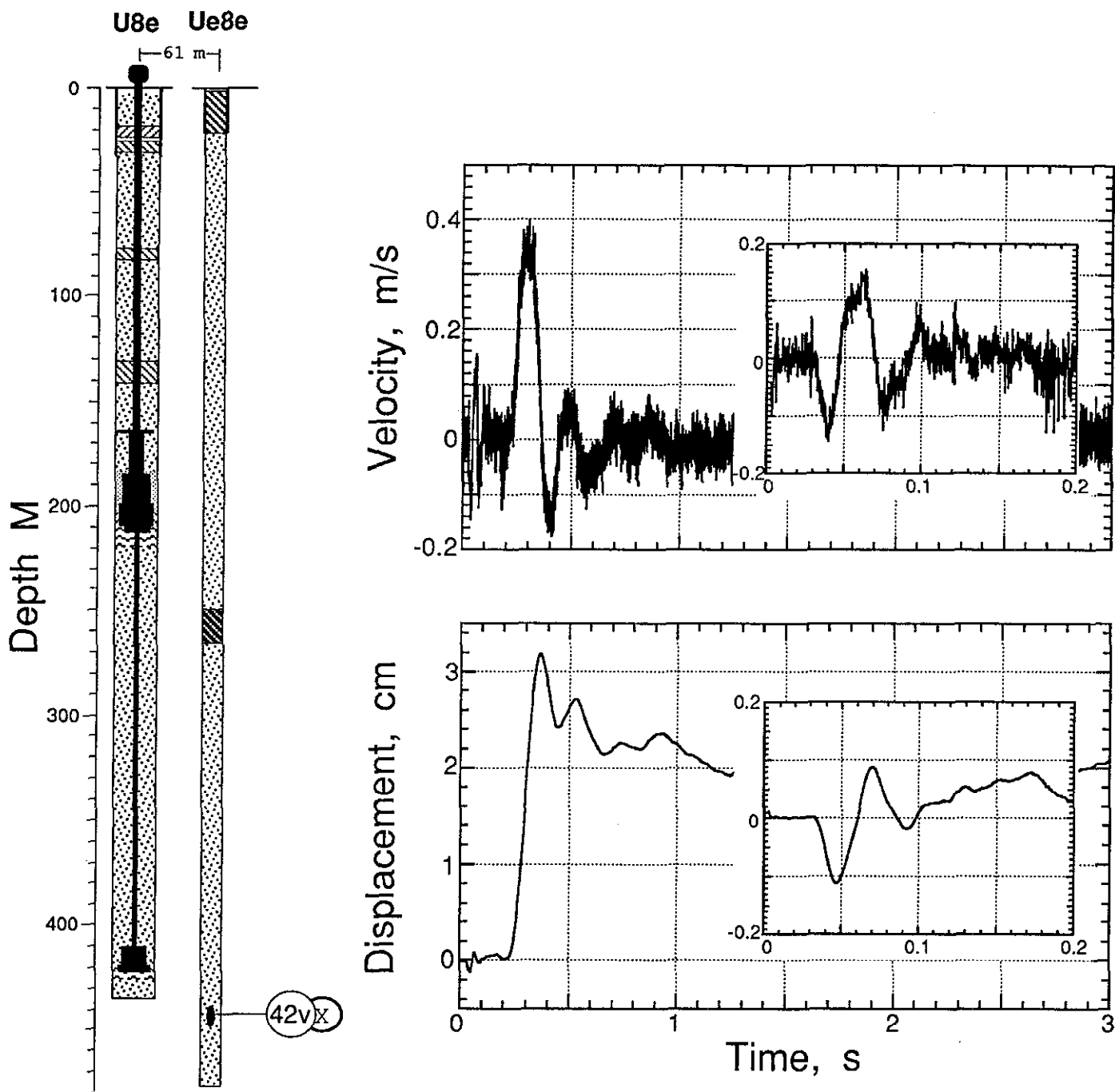


Figure 5.9 Vertical motion measured in the satellite hole Ue8e at a depth of 442.0 m (station 42). Sensitive transducer employed.

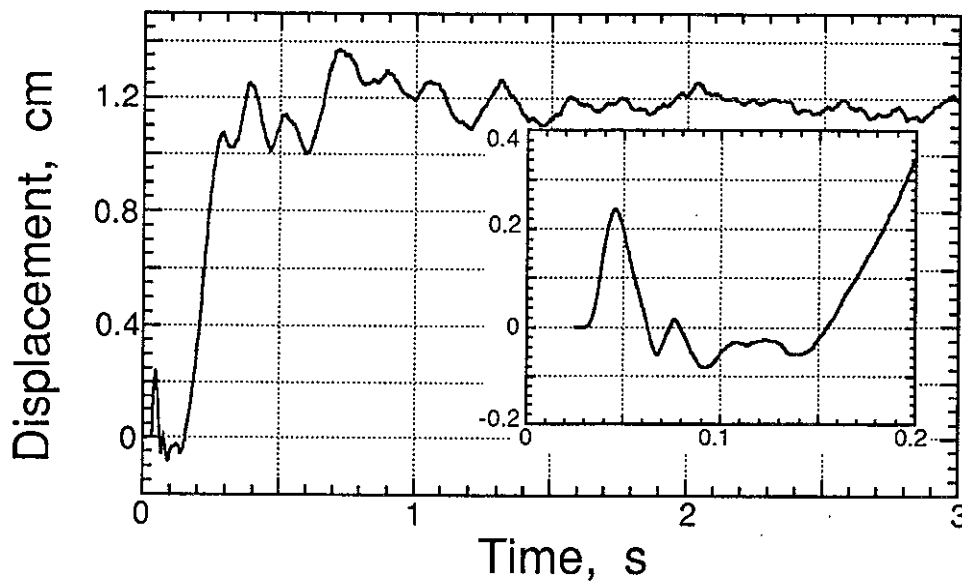
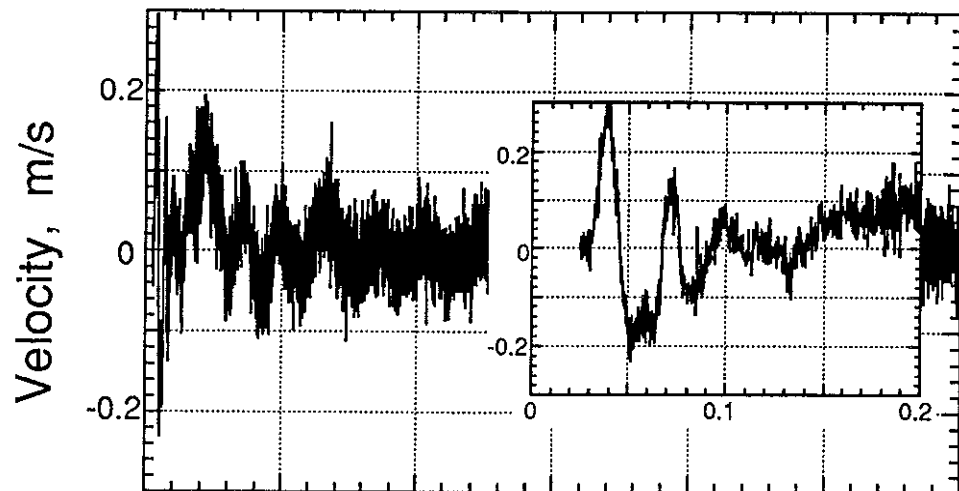


Figure 5.10 Horizontal motion measured in the satellite hole Ue8e at a depth of 442.0 m (station 42).

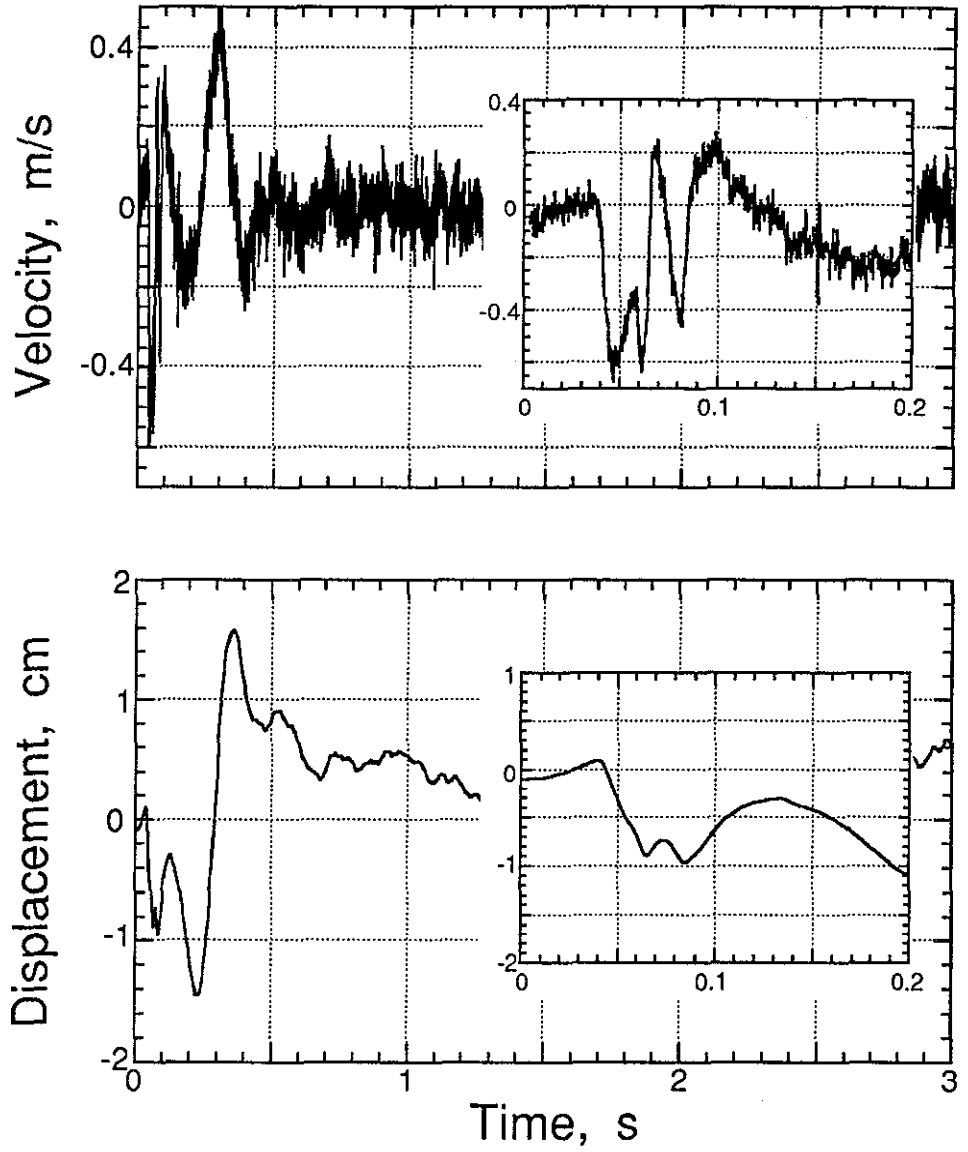
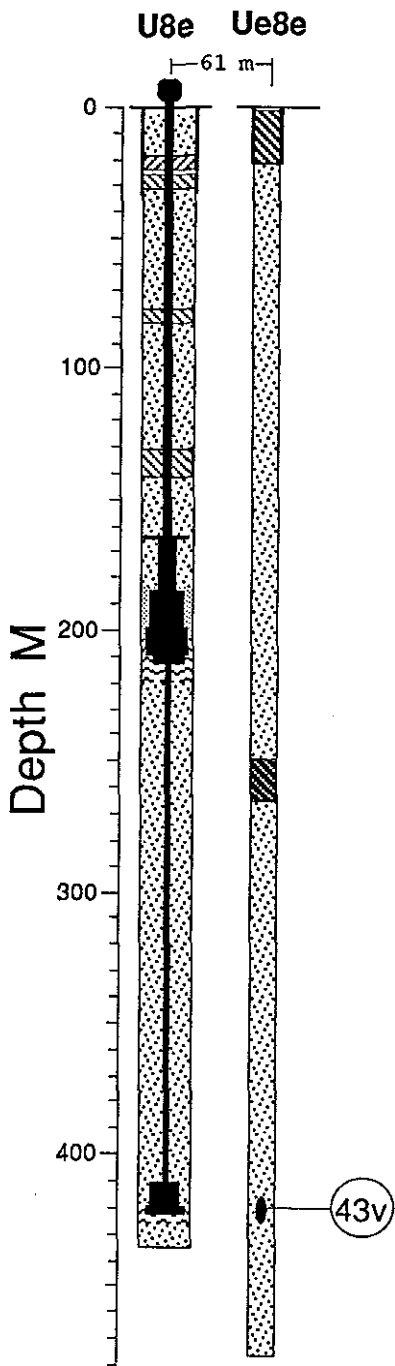


Figure 5.11 Vertical motion measured in the satellite hole Ue8e at a depth of 420.6 m (station 43).

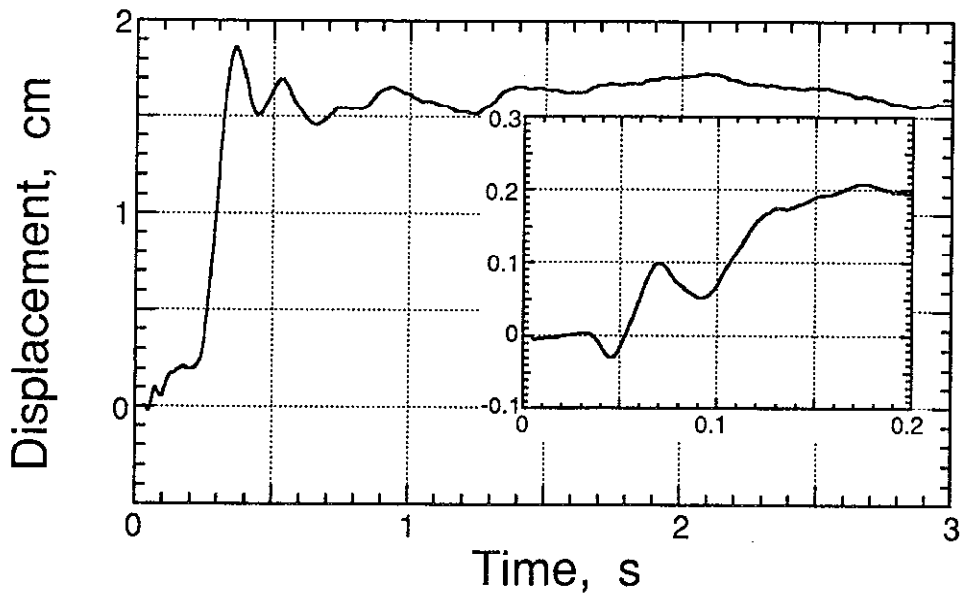
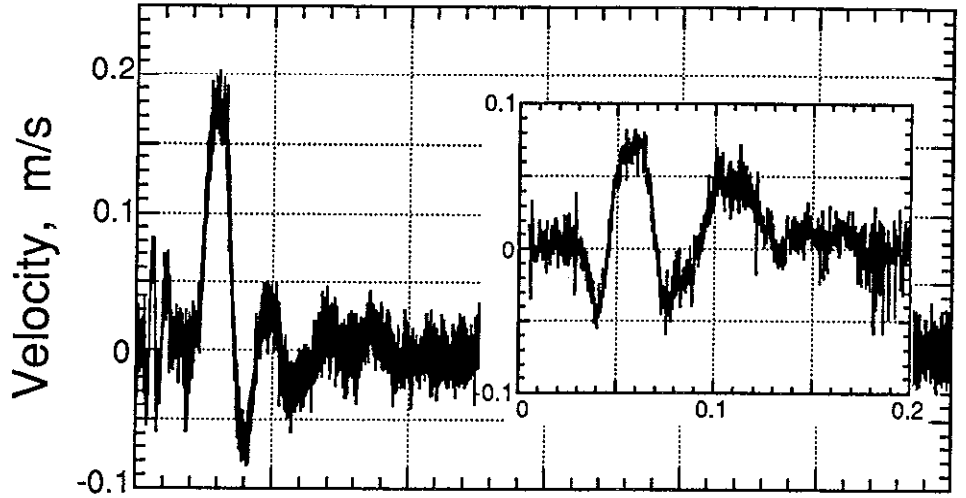
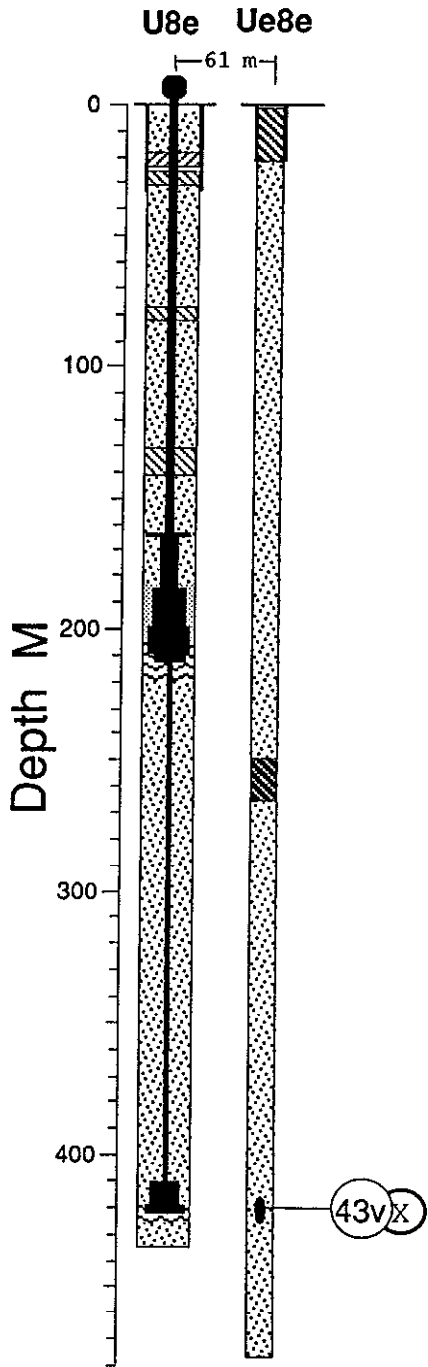


Figure 5.12 Vertical motion measured in the satellite hole Ue8e at a depth of 420.6 m (station 43). Sensitive transducer employed.

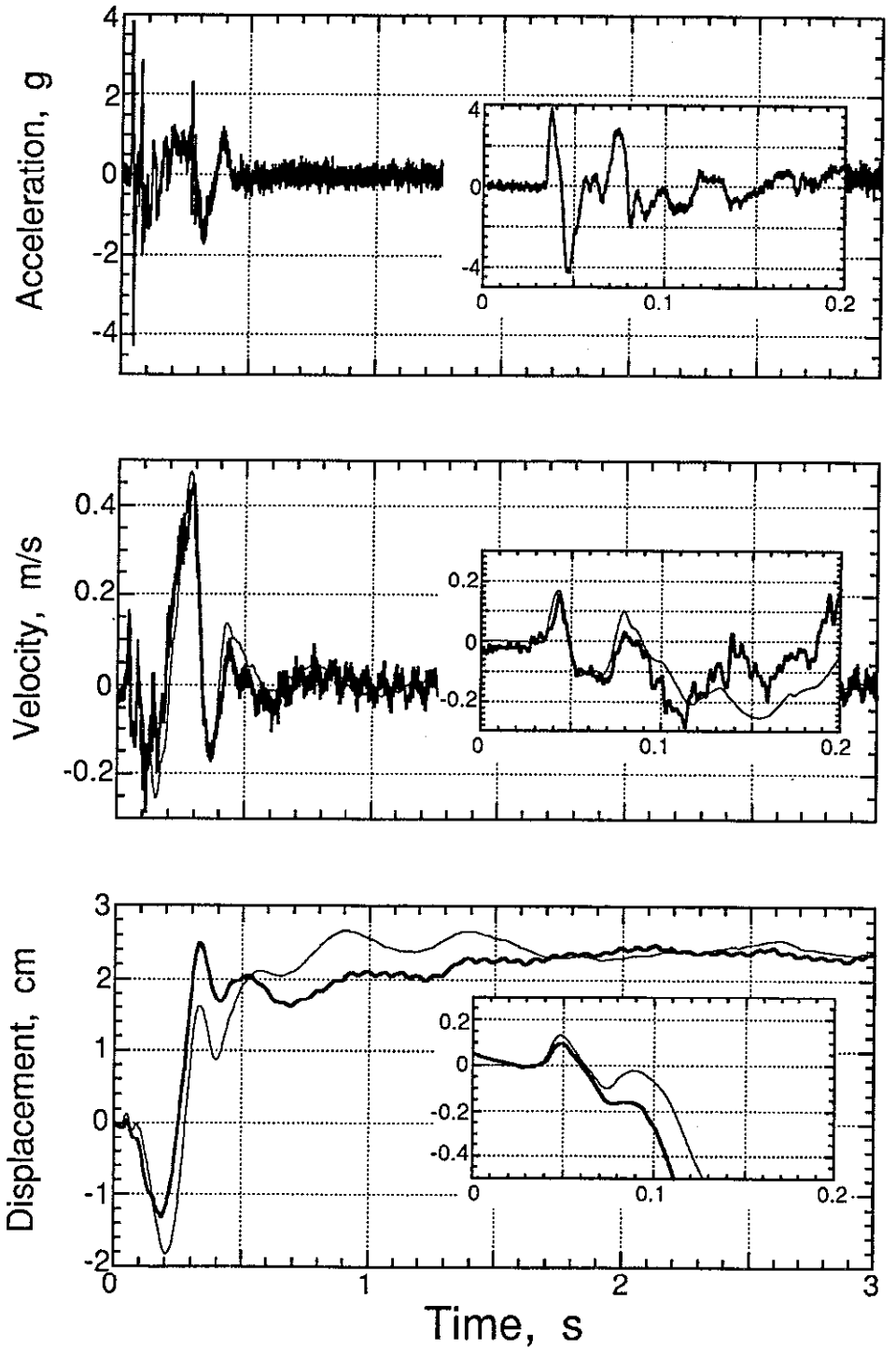
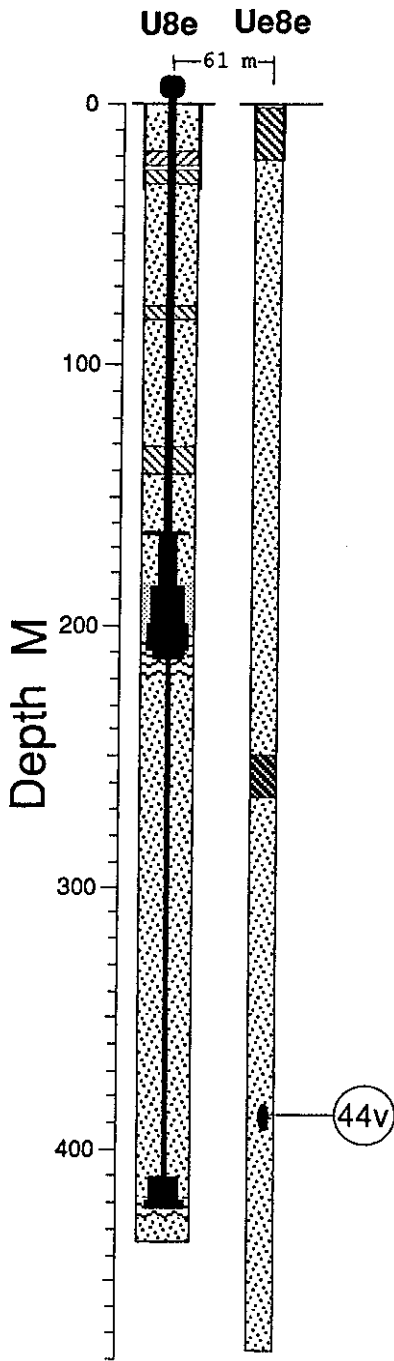


Figure 5.13 Vertical motion measured in the satellite hole Ue8e at a depth of 387.1 m (station 44). When there is more than one trace on a plot, the heavier is derived from the velocimeter.

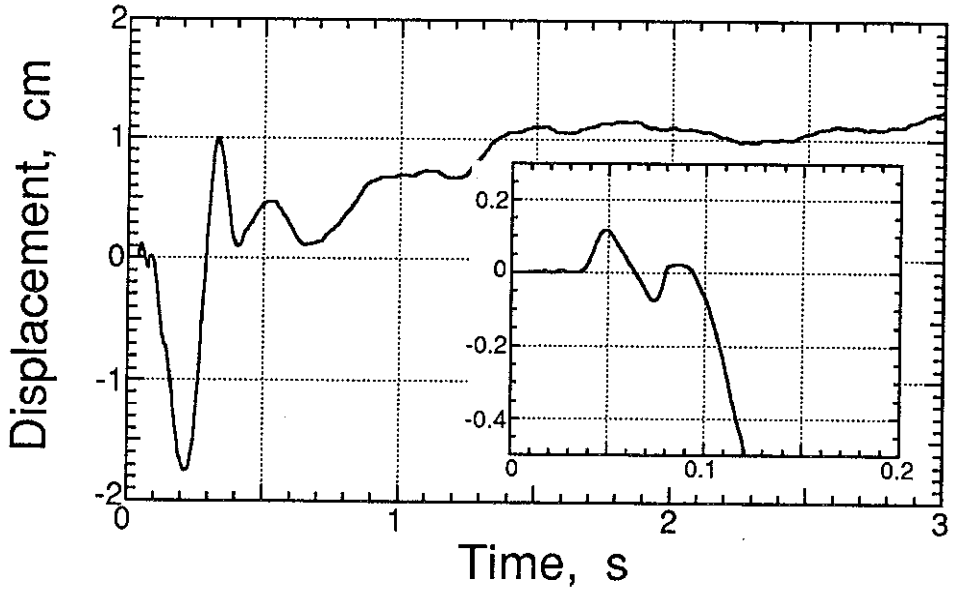
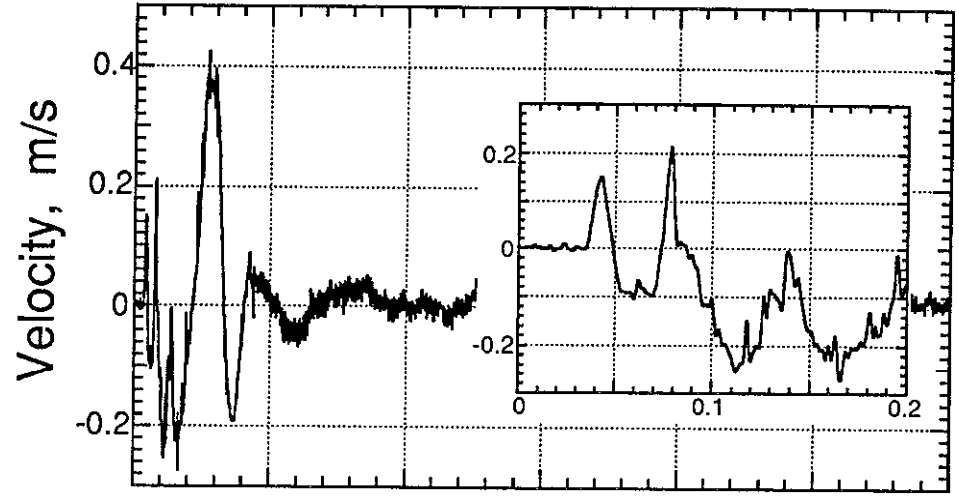
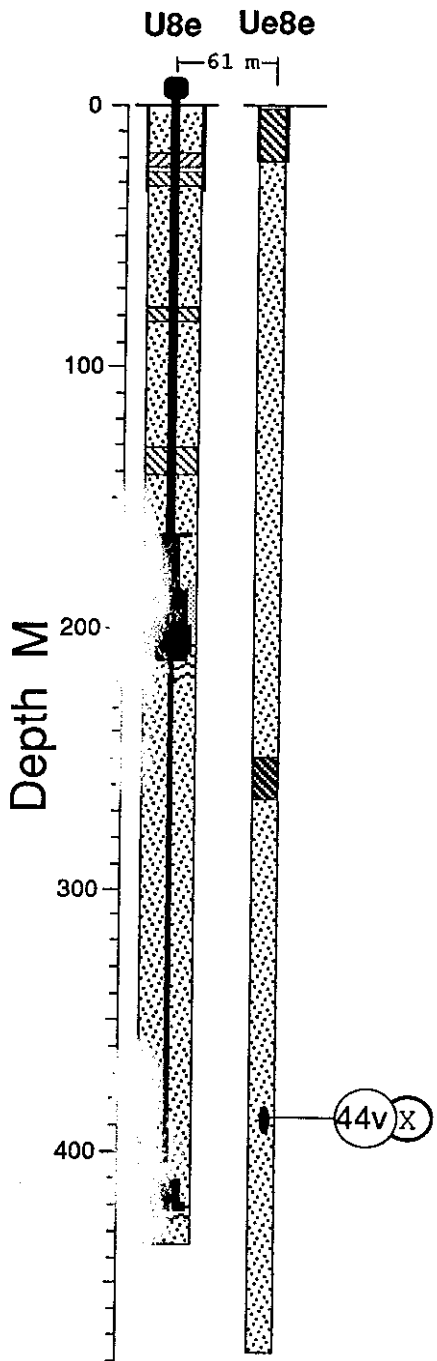


Figure 5.14 Vertical motion measured in the satellite hole Ue8e at a depth of 387.1 m (station 44). Sensitive transducer employed.

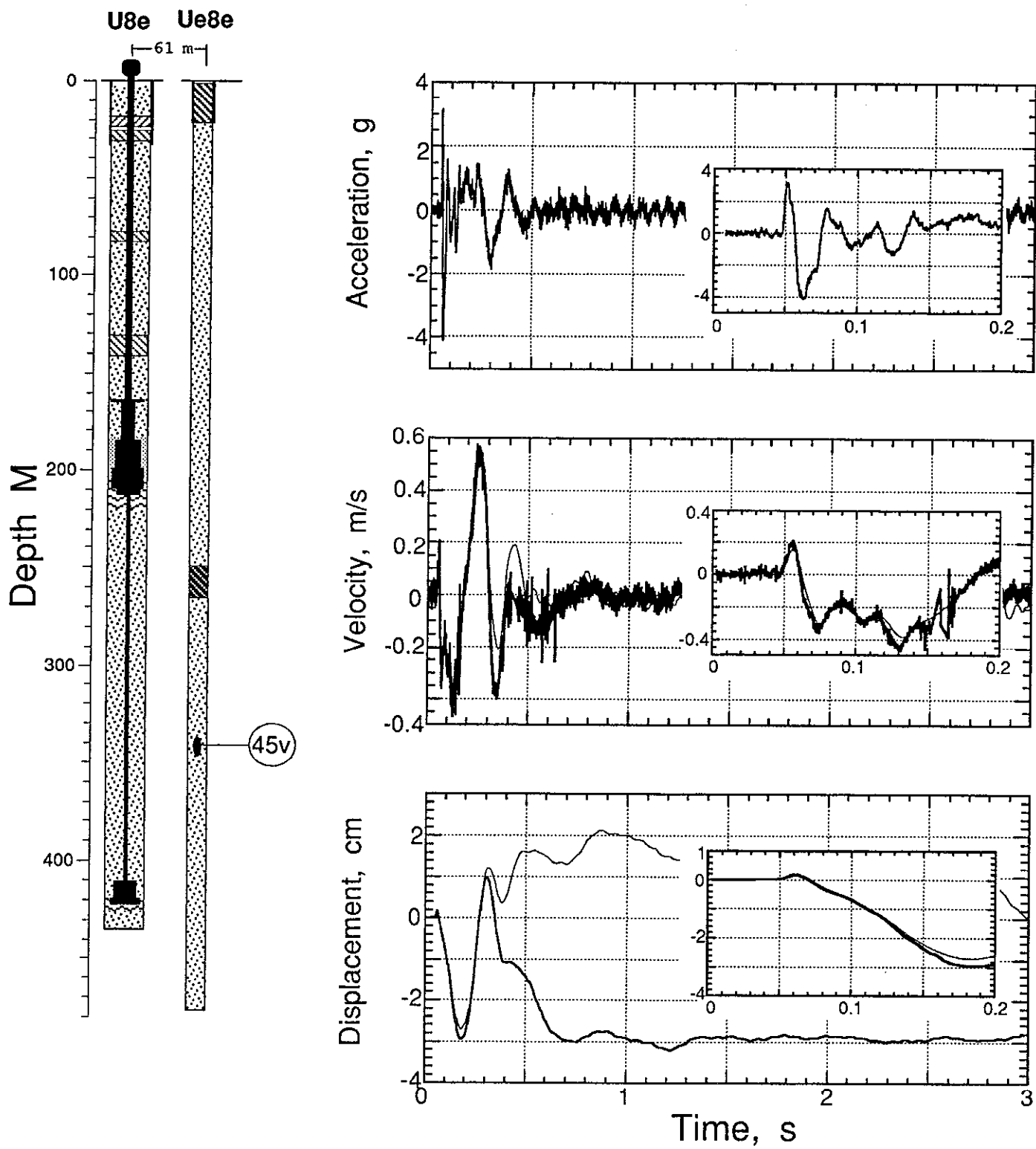


Figure 5.15 Vertical motion measured in the satellite hole Ue8e at a depth of 341.4 m (station 45). When there is more than one trace on a plot, the heavier is derived from the velocimeter.

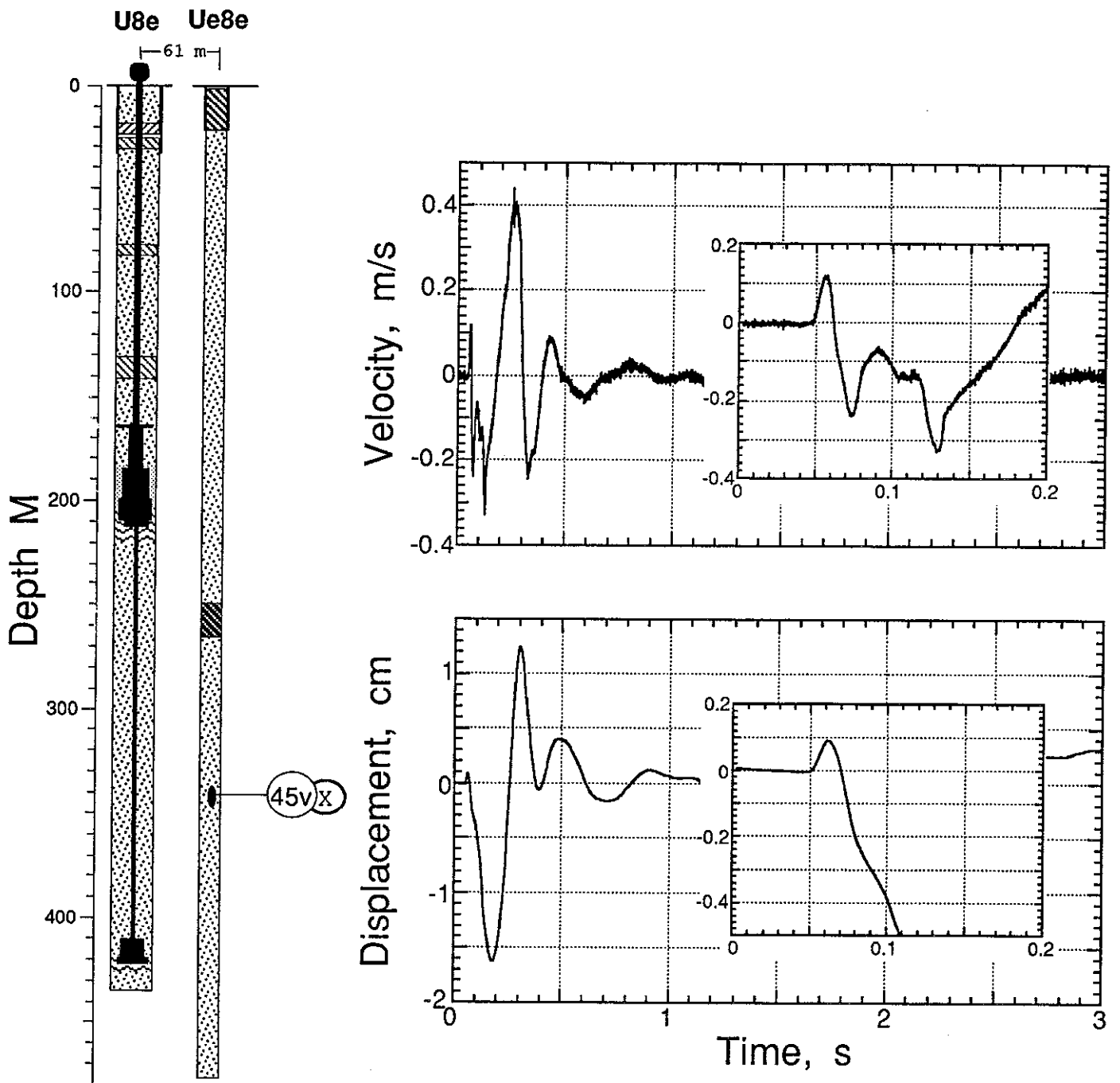


Figure 5.16 Vertical motion measured in the satellite hole Ue8e at a depth of 341.4 m (station 45). Sensitive transducer employed.

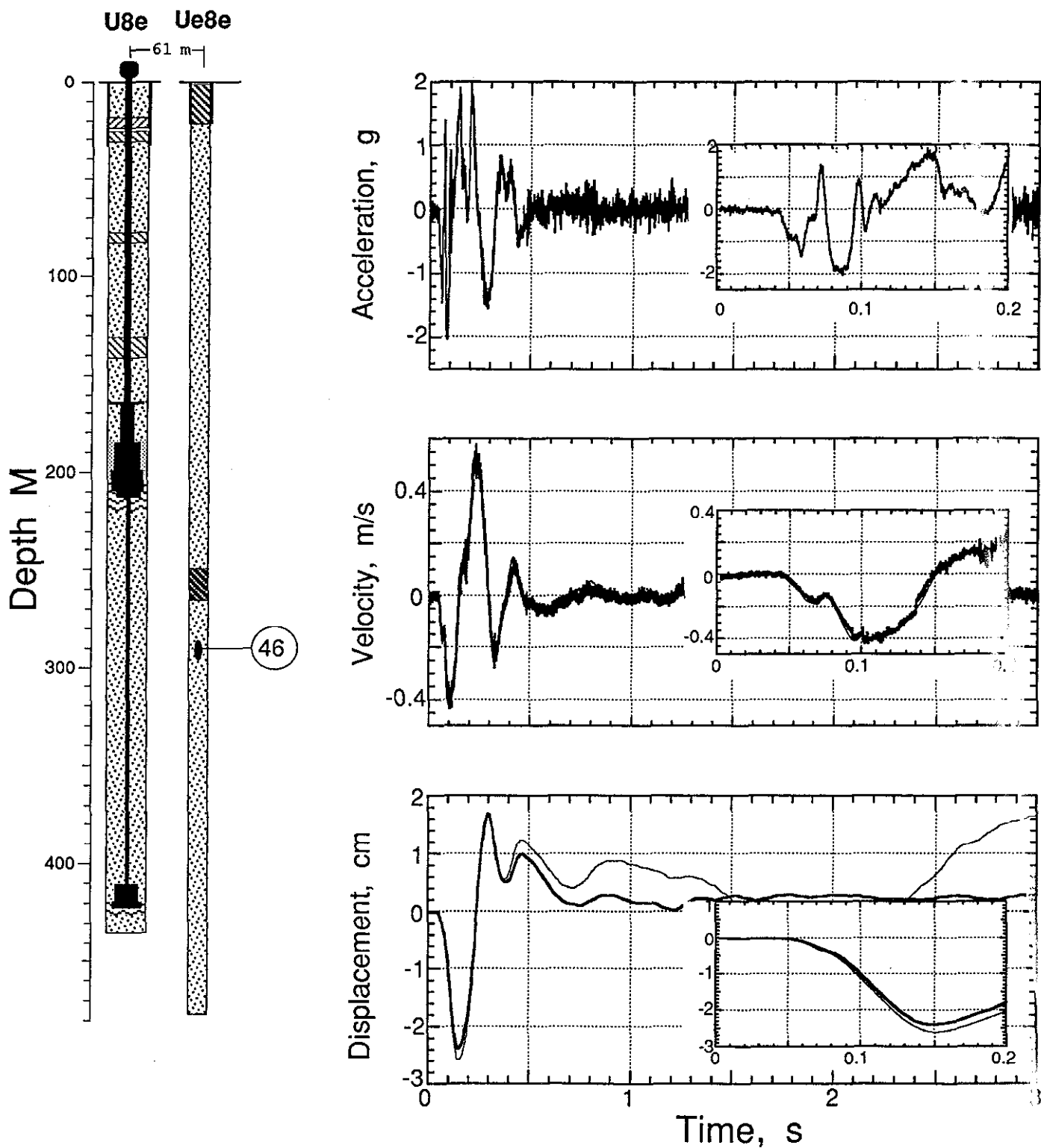


Figure 5.17 Vertical motion measured in the satellite hole Ue8e at a depth of 289.9 m (station 46). When there is more than one trace on a plot, the heavier is derived from the velocimeter.

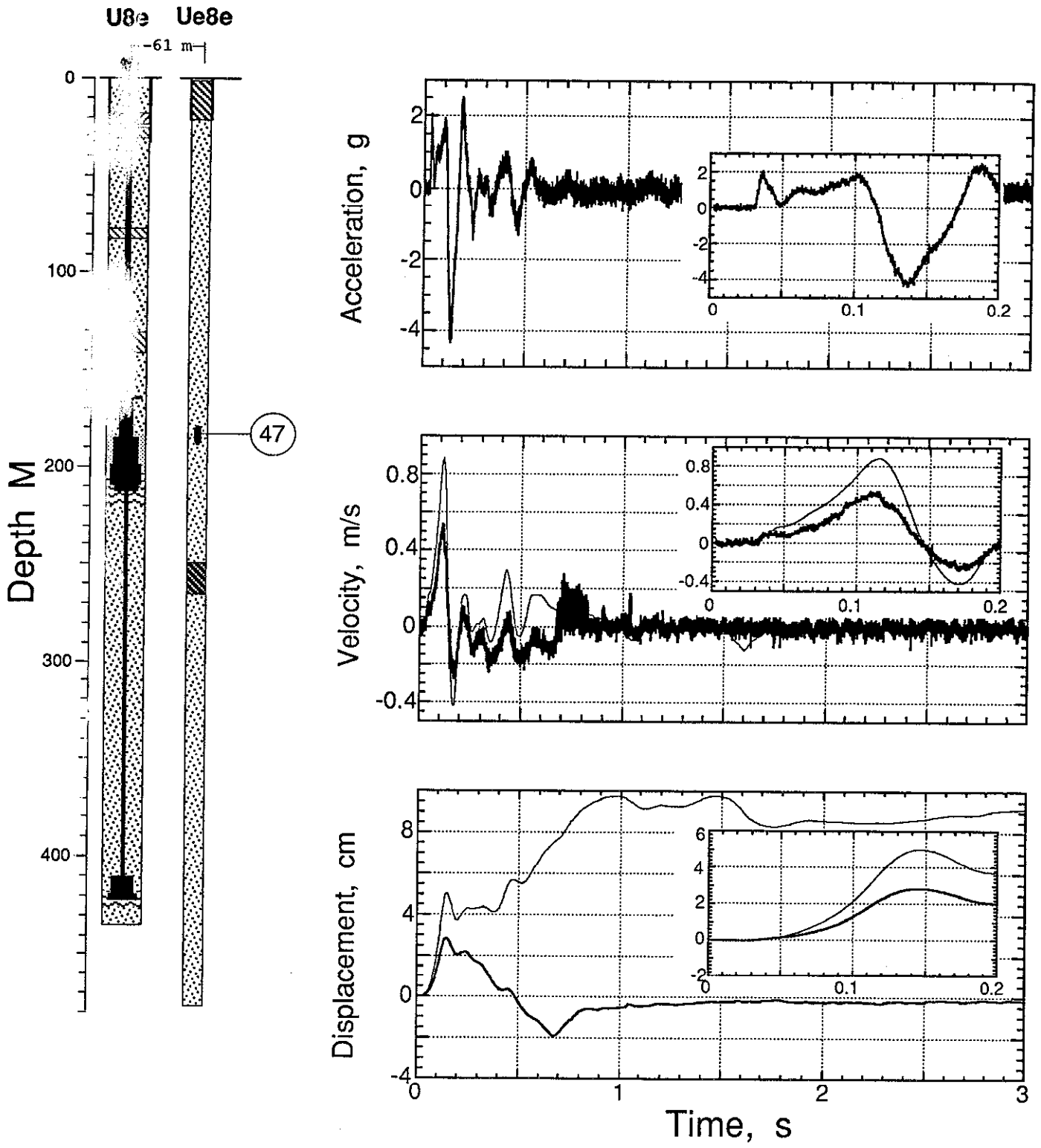


Figure 5.18 Vertical motion measured in the satellite hole Ue8e at a depth of 182.9 m (station 47). When there is more than one trace on a plot, the heavier is derived from the velocimeter.

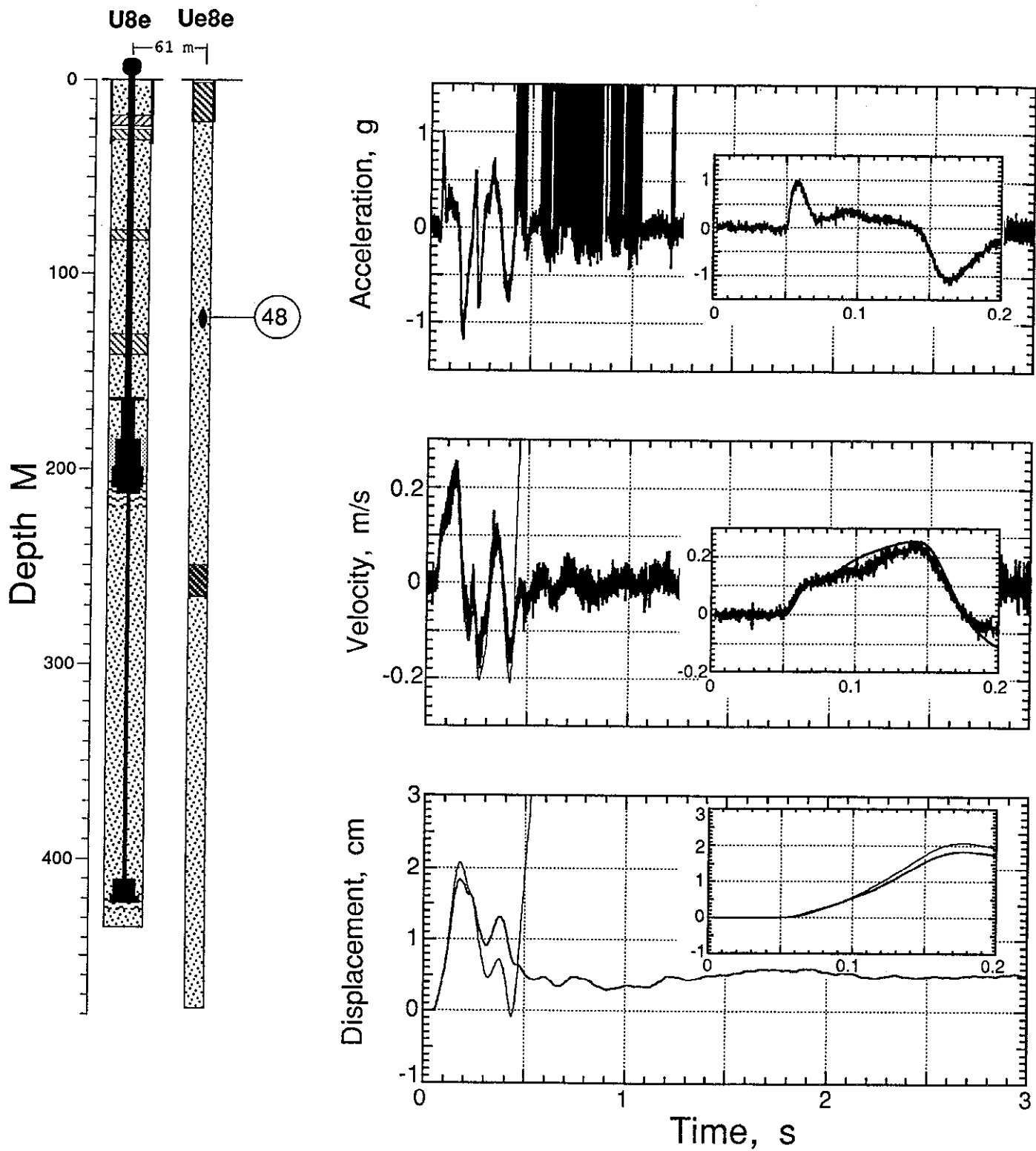


Figure 5.19 Vertical motion measured in the satellite hole Ue8e at a depth of 121.9 m (station 48). When there is more than one trace on a plot, the heavier is derived from the velocimeter.

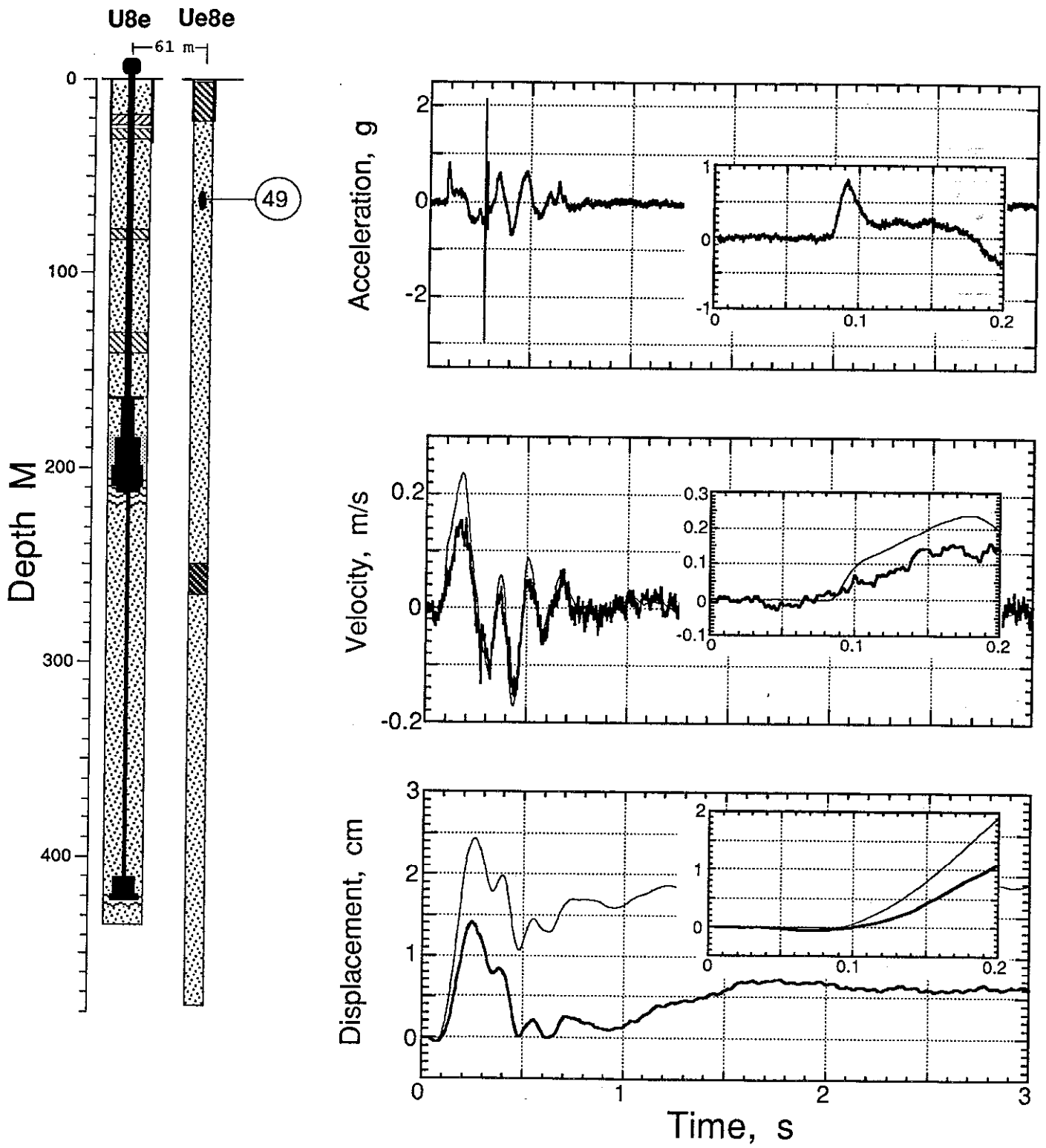


Figure 5.20 Vertical motion measured in the satellite hole Ue8e at a depth of 61.0 m (station 49). When there is more than one trace on a plot, the heavier is derived from the velocimeter.

References

1. Nancy W. Howard, Larry McKague and Richard Carlson, "U8e Site Characteristics Summary", AGTG 77-109, Lawrence Livermore National Laboratory, Livermore, CA, December 12, 1977.
2. George W. Kronsbein for William J. Mayer, "Containment Report for U8e," Holmes & Narver, NTS:A2:78-87, September 22, 1978.
3. LLNL contacts for additional information: R. A. Heinle (CORTEX and SLIFER data)
4. William G. Webb, "Special Measurements Final Engineering Report for CREMINO, U8e ", EG&G, Energy Measurements, Las Vegas, NV, SM:78E-64-35, 5 October, 1978.
5. William G. Webb, "Special Measurements Physics/Instrumentation Package for CREMINO, U8e", EG&G, Energy Measurements, Las Vegas, NV, SM:78E-64-37,8 November, 1978.

Appendix A. High Resolution Pressure and Temperature in Emplacement Pipe

Shortly after the event, in 1978, the CREMINO/CAERPHILLY data were digitized and first reports were generated, primarily by C. W. Olsen. To the best of our knowledge, these early digital data were not preserved except in the paper report form. The analog tapes were redigitized in 1993 to preserve the data in electronic form, however, some of the magnetic tapes of that era had a binder defect producing "sticky" tape that degraded the signal and the high time-resolution required for the reproduction of the wave forms of stations 2, 3, and 4 was not possible.

Figures A1-A4 are reproductions of the figures of the early report. Pressure units are bars, temperature units are degrees centigrade, and times are in milliseconds. Note the exponential notation on each of the axes.

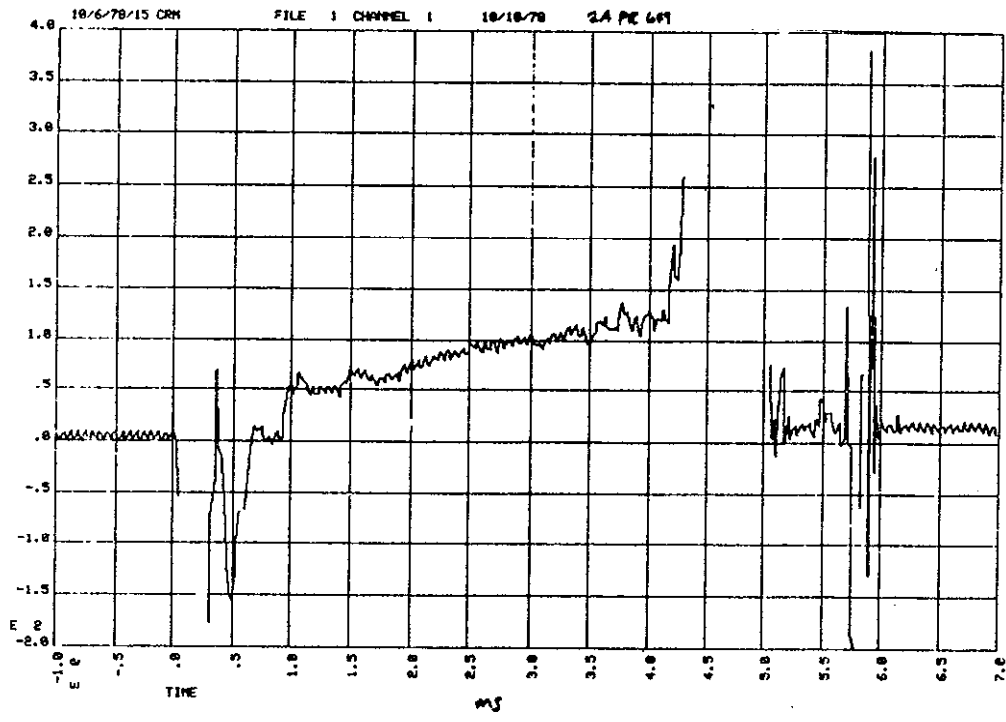


Figure A.1 Pressure in the emplacement pipe at station 2A. Data were reduced in 1978. Compare to figure 3.1. No pressure data were reported for station 2B. Units are bars and milliseconds. The maximum time displayed is 7 ms.

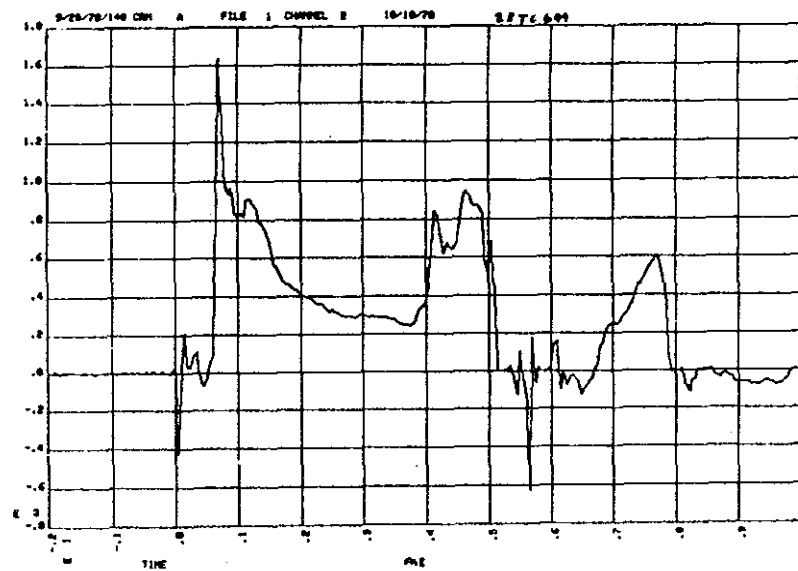
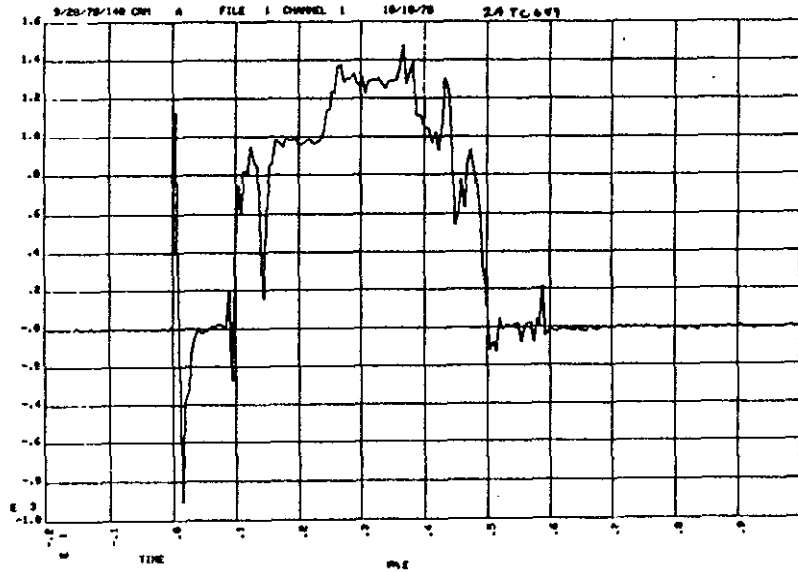


Figure A.2 Temperature in the emplacement pipe at stations 2A and 2B. Data were reduced in 1978. Compare to figure 3.1. Units are degrees centigrade and milliseconds. The maximum time displayed is 10 ms.

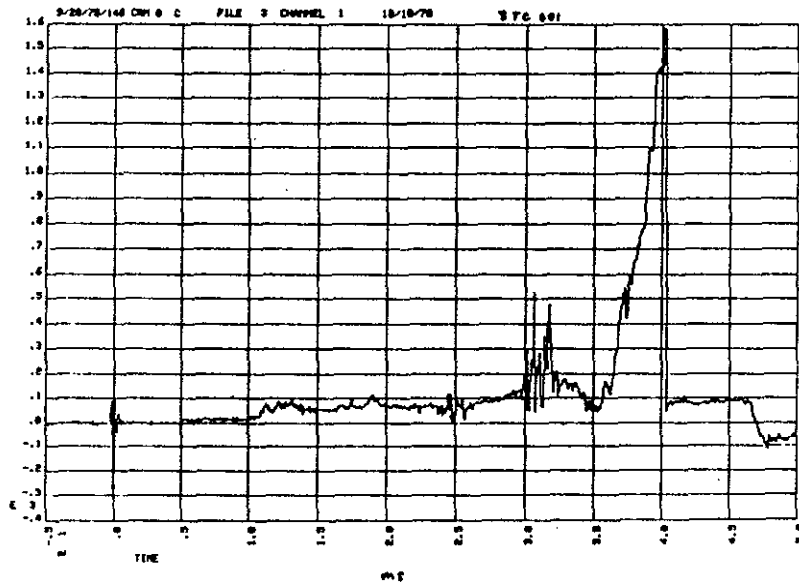
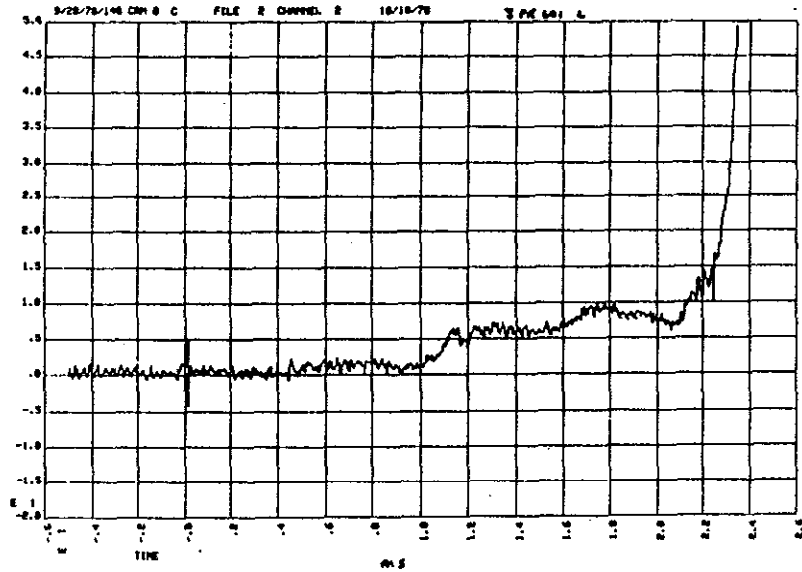


Figure A.3 Pressure and temperature in the emplacement pipe at station 3. Data were reduced in 1978. Pressure data compare to figure 3.2, upper plot. Units are bars, degrees centigrade, and milliseconds. The maximum time displayed is 50 ms.

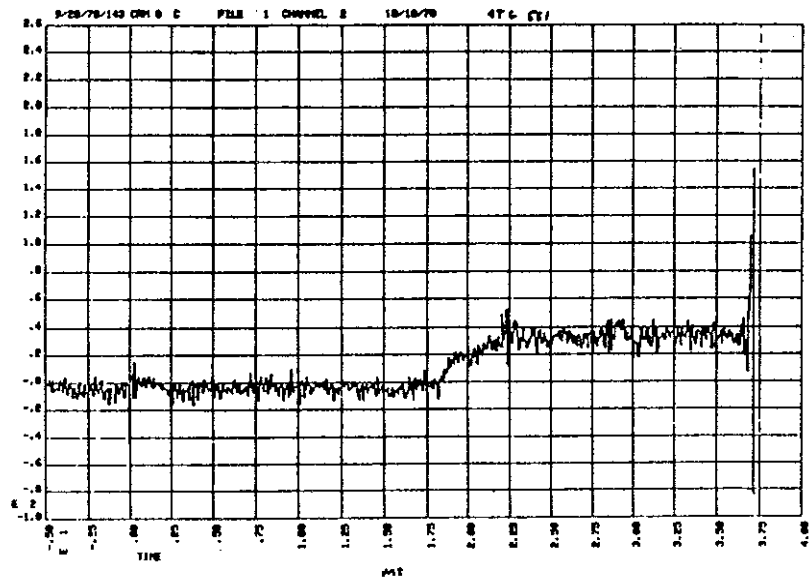
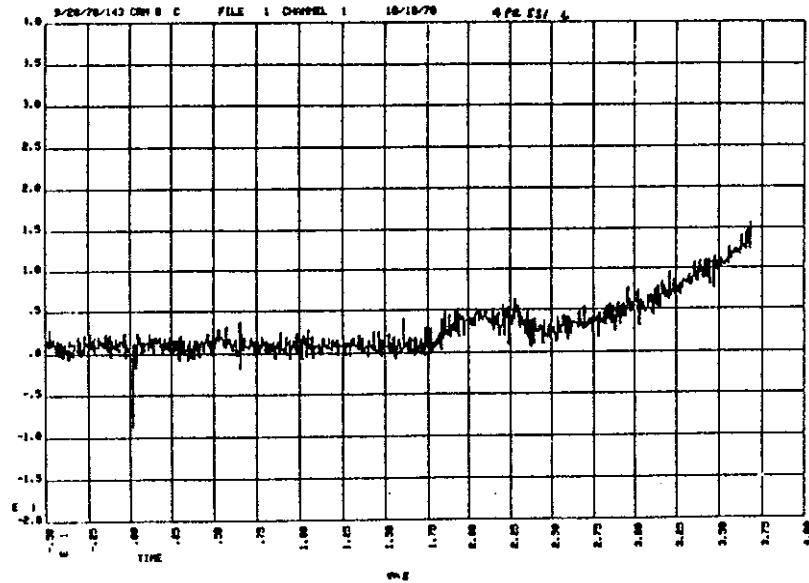


Figure A.4 Pressure and temperature in the emplacement pipe at station 4. Data were reduced in 1978. Pressure data compare to figure 3.3, low-range transducer. Units are bars, degrees centigrade, and milliseconds. The maximum time displayed is 40 ms.